Norwegian University
of Life Sciences

**Master's Thesis 2021 30 ECTS**
Faculty of Chemistry, Biotechnology and Food Science

# Cocoons from *Hermetia illucens* as photosensitizer for photobiocatalytic LPMO reactions

Fredrikke Sæther
Chemistry and Biotechnology

## Acknowledgment

The present work was carried out at the Protein Engineering and Proteomics (PEP) group at the Faculty of Chemistry, Biotechnology and Food Science at the Norwegian University of Life Sciences, with Professor Vincent G. H. Eijsink as a supervisor and Eirik G. Kommedal as a co-supervisor.

I would like to express my gratitude to Professor Vincent G. H. Eijsink for giving me this opportunity, and for his guidance and comments on my work. A tremendous, big thank you to my co-supervisor Eirik G. Kommedal for always being available to answer and discuss all kinds of questions and for commenting during the writing process of this research.

In addition, I would like to thank the rest of the PEP group for being helpful and eager to share their knowledge.

Last but not least, I would like to thank my dear boyfriend, family and friends for their support during this weird and isolating corona situation. I could not have done this without you.

Thanks for seven fun and memorable years here at NMBU, it has been a blast!

Ås, August 2021

Fredrikke Sæther

## Abstract

An increasing global focus on reducing fossil fuel-derived emissions, has led to a demand for environmentally friendly and renewable alternatives. Cellulose and chitin, two of the most abundant biopolymers in Nature, have proven to be valuable biomaterials that can replace crude oil in the production of fuels, chemicals, and other materials. However, these biopolymers are crystalline and very demanding to degrade. The discovery of LPMOs in 2010 has revolutionized the understanding of how these crystalline materials are degraded by oxidative enzymes in cooperation with glycoside hydrolases. LPMOs are Cu-dependent oxidoreductases that depend on a reduced copper in the active site and $O_2$ or $H_2O_2$ as a co-substrate. Previous studies have shown the ability of a photosensitizer, i.e., chlorophyllin, or an inorganic photocatalyst, vanadium doped $TiO_2$, to generate reducing equivalents and $H_2O_2$ for LPMO catalysis. The research presented in this thesis aimed to investigate the photosensitizing abilities of a natural material that LPMOs may encounter in Nature, namely pupal exuviae from an insect, *Hermetia illucens*.

The pupal exuviae from *Hermetia illucens* used in the research described in this thesis were provided by Dr. Thomas Hahn at the Fraunhofer Institute. Prior to the research, the raw material of these pupae were analyzed for their content of chitin (23-25%) and catechols (10%). Insoluble catechols are aromatic components with phenolic groups and have a chemical structure comparable to lignin, which is a known activator of LPMO catalysis. Here, we analyzed whether light-exposed fine-milled cocoon powder of *Hermetia illucens* (FMC), with its content of insoluble catechols, can provide a cellulose-active LPMO, *Sc*AA10C, with reducing equivalents and co-substrate ($H_2O_2$) to catalyze the depolymerization of microcrystalline cellulose, Avicel. Activity assays were performed with different amounts of FMC, LPMO, Avicel and different light intensities to address the effects of these variables on LPMO activity. To assess the role of superoxide in the photobiocatalytic system, experiments with superoxide dismutase were carried out. Furthermore, the amplex red assay was used to measure the accumulation of $H_2O_2$. Finally, we assessed whether chitin in the FMC and β-chitin could be degraded by a chitin-active LPMO, *Sm*AA10A, using FMC as photosensitizer.

The results showed that light-exposed FMC acts as an excellent photosensitizer to sustain *Sc*AA10C and *Sm*AA10A activity. The observations showed that increasing the FMC concentration and the light intensity led to increased progress curves and production of LPMO products (i.e., oxidized sugars). In contrast, the increase of LPMO concentrations did not show any effect, showing that the reactions were limited by the FMC/light system. The LPMO became less active at higher substrate concentrations which is likely due to the light attenuating properties of the substrate, limiting the

production of $H_2O_2$. The addition of superoxide dismutase to the reactions did not affect the production of oxidized products, indicating that reduction of $O_2$ to $H_2O_2$ happened in one step, and not via superoxide. Inactivation of *Sc*AA10C was observed in a reaction with high (10 g/L) amounts of FMC and light intensity corresponding to 10% of $I_{max}$, most likely due to overproduction and accumulation of $H_2O_2$, which results in futile $H_2O_2$-turnover by the LPMOs. Interestingly, reactions with *Sm*AA10A showed light-driven degradation of chitin in the FMC, meaning that the material can act as a photosensitizer for its own oxidative degradation reactions. Reactions with β-chitin showed light-driven FMC-catalyzed efficient degradation by *Sm*AA10A, conforming the potential of FMC as a general photosensitizer for promoting LPMO catalysis.

## Sammendrag

Et økt globalt fokus på å redusere utslipp av fossilt brennstoff, har ført til krav om å finne mer miljøvennlige og fornybare alternativer. Cellulose og kitin, to av de mest utbredte biopolymerene i Naturen, har vist seg å være verdifulle biomaterialer som kan erstatte råolje i produksjon av drivstoff, kjemikalier og andre materialer. Disse biopolymerene er krystallinske og svært krevende å bryte ned. Oppdagelsen av LPMOer i 2010 har revolusjonert forståelsen av hvordan disse krystallinske materialene brytes ned av oksidative enzymer i samarbeid med glykosidhydrolaser. LPMOer er Cu-avhengige oksidoreduktaser som er avhengige av et redusert kobber i det aktive setet samt tilgang på enten $O_2$ eller $H_2O_2$ som kosubstrat. Tidligere studier har vist hvordan fotosensibiliserende stoffer som klorofyllin, og en uorganisk fotokatalysator, vanadium dopet $TiO_2$, kan generere reduserende ekvivalenter og $H_2O_2$ for å katalysere LPMO-aktivitet. Målet med denne oppgaven var å undersøke de fotosensibiliserende evnene til et naturlig materiale som LPMOer kan møte på i Naturen, nemlig pupperester fra et insekt, *Hermetia illucens*.

Rester av pupper fra *Hermetia illucens* benyttet i denne studien ble tilsendt fra Dr. Thomas Hahn ved Fraunhofer Institutt som et fotosensibiliserende stoff. Råmaterialet til disse puppene ble forut for studien analysert for sitt innhold av blant annet kitin (23-25%) og katekoler (10 %). Uløselige katekoler er aromatiske forbindelser med fenolgrupper bundet til seg og har en kjemisk struktur sammenlignbar med lignin, en kjent aktivator for LPMO-katalyse. I denne oppgaven undersøkes det om lyseksponert finmalt kokongpulver av *Hermetia illucens* (FMC), med sitt innhold av uløselige katekoler, kan bistå en celluloseaktiv LPMO, *Sc*AA10C, med reduserende ekvivalenter og kosubstrat ($H_2O_2$) for katalyse av enzymatisk nedbrytning av mikrokrystallinsk cellulose, Avicel. Aktivitetsanalyser ble gjennomført med ulik mengde FMC, LPMO, Avicel samt ulik lysintensitet for å adressere disse ulike variablenes effekt på LPMO-aktivitet. For å vurdere superoksids rolle innen det fotobiokatalytiske systemet, ble eksperimenter med superoksid dismutase gjennomført. Videre ble det foretatt amplex red analyser for å måle på akkumulert mengde $H_2O_2$. Til slutt ble nedbrytning av kitin i FMC og β-kitin demonstrert ved bruk av en kitinaktiv LPMO, *Sm*AA10A, fotokatalysert av FMC.

Resultatene viste at lyseksponert FMC er et utmerket fotosensibiliserende stoff for katalyse av *Sc*AA10C- og *Sm*AA10A-aktivitet. Observasjonene viste at ved økte FMC-konsentrasjoner og lysintensiteter, økte produksjonsraten og den totale produksjonen av LPMO produkter (dvs. oksiderte sukre). I motsetning, viste ikke økte LPMO-konsentrasjoner til noen effekt, hvilket vil si at LPMO aktiviteten i det gjeldene systemet var begrenset av FMC og lys. LPMOen ble mindre aktiv ved tilsetning av økte mengder substrat som mest sannsynlig forklares av substratets lysattenuerende

egenskaper, noe som begrenser produksjon av $H_2O_2$. Tilsetning av superoksid dismutase til reaksjonene påvirket ikke produksjonen av oksiderte produkter, noe som indikerer at reduksjon av $O_2$ til $H_2O_2$ skjer i ett trinn, og ikke via superoksid. Inaktivering av *Sc*AA10C ble observert i en reaksjon tilsatt høy (10 g/L) konsentrasjon av FMC eksponert med en lysintensitet tilsvarende 10 % av $I_{max}$. Denne inaktiveringen kan mest sannsynlig forklares av en overproduksjon og opphopning av $H_2O_2$ som ikke LPMOene klarer å omsette. I tillegg viste ScAA10A til lysdrevet nedbrytning av kitin i FMC, hvilket betyr at FMC kan fungere som en fotosensibilisator for sine egne oksidative nedbrytningsreaksjoner. Observasjoner viste til lysdrevet FMC-katalysert effekt ved nedbrytning av β-kitin i reaksjoner med SmAA10A, hvilket bekrefter potensialet om bruk av FMC som en generell fotosensibilisator til å fremme LPMO-katalyse.

## Abbreviations

| | |
|---|---|
| **$A_{280}$** | Absorbance of ultraviolet light at 280 nm |
| **AA** | Auxiliary Activity |
| **AscA** | Ascorbic Acid |
| **CAZy** | Carbohydrate-Active enZymes |
| **CBM** | Carbohydrate-binding module |
| **CBP21** | *Sm*AA10A, Chitin-binding protein |
| **CelS2** | *Sc*AA10C |
| **ChiA** | Chitinase A |
| **Chl** | Chlorophyllin |
| **CV** | Column Volume |
| **$dH_2O$** | Milli-Q® Sterile Water |
| **DOPET** | 3,4-Dihydroxylphenylethanol |
| ***E. coli*** | *Escherichia coli* |
| **EDTA** | Ethylenediaminetetraacetic acid |
| **EG** | Endoglucanase |
| **FMC** | Fine Milled Cocoons |
| **g** | Force of gravity |
| **GH** | Glycoside Hydrolase |
| **GlcNAc** | *N*-Acetylglucosamine |
| **HILIC** | High-Performance Interaction Liquid Chromatography |
| **His** | Histidine |
| **HPAEC** | High-Performance Anion-Exchange Chromatography |
| **HPLC** | High-Performance Liquid Chromatography |
| **HRP** | Horseradish Peroxidase |
| **ICS** | Ion Chromatography System |
| **IEX** | Ion Exchange Chromatography |
| **kDa** | Kilo Dalton |
| **LDS** | Lithium Dodecyl Sulfate |
| **LPMO** | Lytic Polysaccharide Monooxygenase |
| **NaOAc** | Sodium acetate |
| **NADA** | *N*-Acetyldopamine |
| **NAG** | *N*-Acetylglucosamine |

| | |
|---|---|
| **NBAD** | *N*-β-Alanyldopamine |
| **PAD** | Pulsed Amperometric Detection |
| **PASC** | Phosphoric Acid Swollen Cellulose |
| **pI** | Isoelectric point |
| **PPE** | Periplasmic Extract |
| **rpm** | Revolutions per minute |
| **RSLC** | Rapid Separation Liquid Chromatography |
| **ROS** | Reactive Oxygen Species |
| **LDS-PAGE** | Lithium Dodecyl Sulfate Polyacrylamide Gel Electrophoresis |
| **SEC** | Size Exclusion Chromatography |
| **SOD** | Superoxide Dismutase |
| **TGS** | Tris-Glycine-SDS |
| **w/v** | Weight / volume |
| **w/w** | Weight / weight |

# Table of content

# 1. Introduction

## 1.1 Renewable biomass

Renewable biomass has received much attention during this century due to higher demands on sustainable energy sources as a result of global climate change. Climate change has led to an aim for biofuels to account for 25% of all transport fuel by 2030 within the E.U. By the same year, the U.S. Department of Energy wants 30% of all gasoline needs to be covered by biofuels (Himmel et al., 2007). For this to become a reality, degradation of biomass, including recalcitrant polysaccharides such as cellulose and chitin, is required. Using plant biomass instead of crude oil to produce fuels and fine chemicals is considered a key technology in the 21$^{st}$ century and the characteristics of a (plant-based) biorefinery are similar to those of an oil refinery (Hülsey, 2018). As crude oil is fractionated to gasoline, petroleum gas and tar and further processed into fuel, chemicals and plastic materials. Likewise, plant biomass is fractionated to sugars, lignin and fats, which can be used to produce the similar products (**Figure 1**) (Hüsley, 2018). However, there is one important difference between using crude oil and plant biomass as a resource. When using crude oil, all produced $CO_2$ is directly emitted to the atmosphere. Unlike crude oil, plants are able to take up the same amount of $CO_2$ as they produce and are thereby part of a cycle (**Figure 1**). Therefore, use of cellulose, the world's most abundant polymer and one of the main components in plants, offers a great potential for reduction of greenhouse gas emissions.

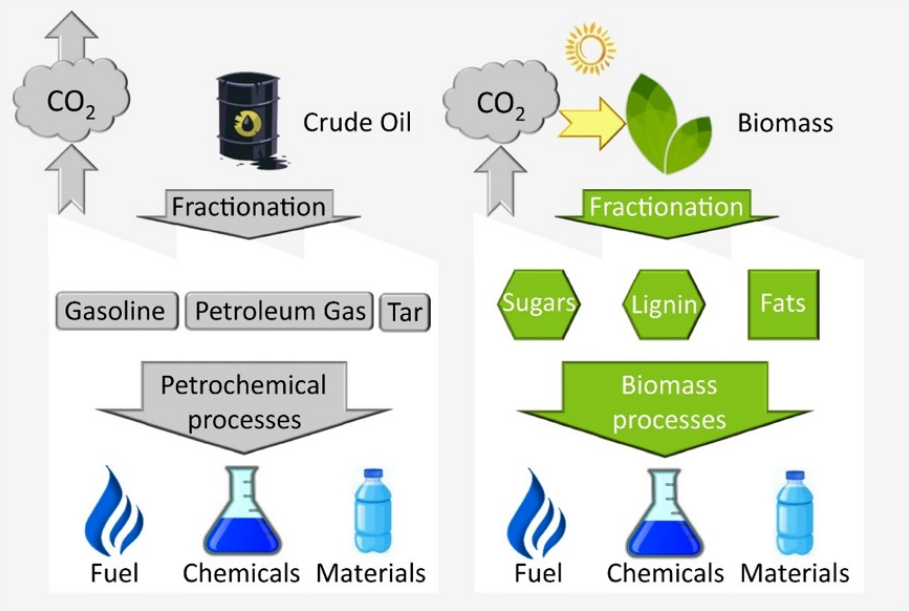


**Figure 1. Schematic comparison of petroleum oil and plant biomass refinery.** The figure illustrates the pathway from crude oil and plant biomass to various products and further how $CO_2$ is emitted to the atmosphere or taken up by plants. The figure is taken from Hülsey, 2018.

Besides plant-based biomass, other sources of biomass may be useful to achieve the demand for a greener economy. Chitin, which is the second most abundant polymer on Earth and the most abundant nitrogen-containing biopolymer, can be obtained from insect exoskeletons and fishery waste such as shrimps and crabs (Kramer et al., 1995; Li et al., 1992). By "shell biorefinery", chitin can be converted into nitrogen-rich chemicals for use as flocculating agents within water purification and for applications in the textile and medicine industry (Hüsley, 2018; Hahn et al., 2020).

### 1.1.1 Lignocellulosic biomass

Lignocellulose refers to the primary building blocks of plant cell walls (Lee et al., 2014). This primarily includes major polysaccharide polymers, cellulose (30-50%) and hemicellulose (20-30%), and an aromatic polymer, lignin (20-30%). Cross-links between the tree types of polymers contribute to stiffening the plant cell wall and mechanical protection against microbial attacks (Elumalai et al., 2018; Ezeilo et al., 2017; Lee et al., 2014).

Cellulose is the most abundant polymer on Earth, built up by D-glucose units linked together by β-1,4 glycosidic bonds where every second unit is rotated 180$^{o}$ relative to its neighbor. The repeating units of two D-glucose units are referred to as cellobiose (**Figure 2**) (Zhao et al., 2020). Hydrogen bonds between the hydroxyl groups lead to inter-chain interactions between the polymer-chains, which results in crystalline and amorphous regions. These regions make the cellulose insoluble in water and resistant to depolymerization (Lindman et al., 2010). There are seven different forms of cellulose, so-called polymorphs. Out of these, there are two which are common in nature, Iα and Iβ, also referred to as native cellulose. Iα is synthesized in bacteria, while Iβ is the polymorph mainly produced in plants. They have the same backbone conformation but differ in the way that the intermolecular hydrogen bonds are oriented. By various chemical treatments, cellulose I can be transformed into five other polymorphs, II, $III_1$, $III_{11}$, $IV_1$, and $IV_{11}$ (Goldberg et al., 2014; O'Sullivan, 1997).

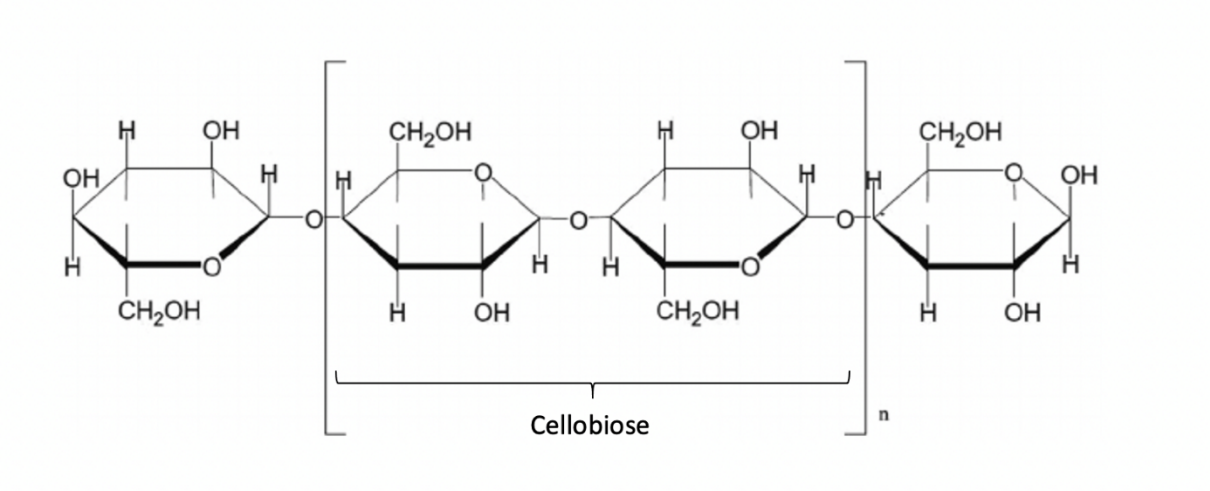


**Figure 2. Cellulose structure.** The figure illustrates how D-glucose units are linked together by β-1,4 glycosidic bonds and rotated 180$^{o}$ relative to each other. Two D-glucose units linked together form the cellobiose units, which is repeated n times to form a polymer-chain. The figure was taken from Akil et al., 2011, and modified for the purpose of this thesis.

The term hemicellulose refers to a wide variety of non-cellulosic plant polysaccharides consisting of various pentose and hexose monomers. Hemicelluloses have backbones composed of D-xylose, D-mannose, D-glucose and/or D-galactose that may be substituted with a variety of sugars, including D-xylose, D-galactose, L-arabinose and 4-O-methyl-D-glucoronic acid (Elumalai et al., 2017). Together with lignin, hemicellulose forms a matrix that embraces cellulose fibers and contributes to the compact and rigid structure of the plant cell wall (Hasanov et al., 2020).

The mechanical rigidity and strength of the plant is mainly provided by lignin. The hydrophobic properties of lignin prevents transportation of water and nutrients through the plant cell wall (Elumalai et al., 2017). Lignin is built up by three precursor monolignols which are derivatives of benzene with various degrees of methoxylation: p-coumaryl alcohol, coniferyl alcohol, and sinapyl alcohol (**Figure 3**). The chemical properties of lignin depend on the composition of the three monolignols and how they are bound together by either ether or ester bonds. The relative amount of each monolignol incorporated in lignin depends on the lignin source (Horn et al., 2012). For example, softwood lignin consists almost exclusively of coniferyl alcohol, while hardwood lignin contains both coniferyl alcohol and sinapyl alcohol. Grass lignin, on the other hand, consists of all three types of monolignols (Hasanov et al., 2020).

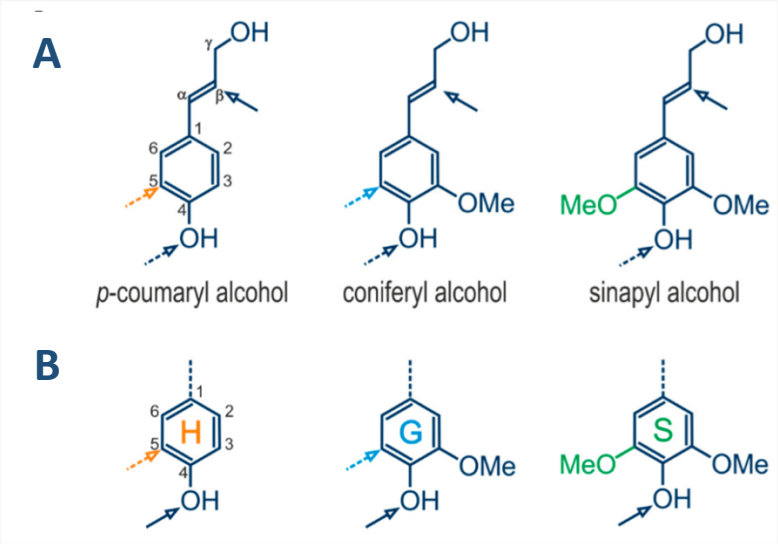


**Figure 3. Chemical structures of different lignin units. A:** Shows the structures of p-coumaryl alcohol, coniferyl alcohol and sinapyl alcohol. **B**: shows the corresponding p-coumaryl, coniferyl, and sinapyl units. Colors help identify the unit-specific structures, while arrows are pointing at sites that are involved in radical coupling during lignification. Dashed arrows point at sites that are less prevalent than the sites that are pointed by undashed arrows. The figure is taken from Hasanov et al., 2020.

### 1.1.2 Insect biomass

In addition to fishery waste of shrimps and crabs, insect biomass has become a relevant source of chitin as reports have shown a chitin content of up to 40% of the insects' wet weight (Kramer et al., 1995). Other than chitin, the insects consist of up to 30% catechols in addition to proteins and minerals (Kramer et al., 1995).

Chitin is a polysaccharide made of repeating *N*-acetyl-D-glucosamine units linked together by β-1,4 glycosidic bonds and rotated 180° relative to the neighboring unit. In the *N*-acetyl-D-glucosamine units, the second carbon (C2) of the glucose unit contains an *N*-acetyl group (**Figure 4**) (Jang et al., 2004). Chitin occurs in different polymorphs, α-, β- and γ-chitin. α-chitin is mainly found in hard structures such as arthropod cuticles (Roberts, 1992) and exoskeletons of crustaceans (Hajji et al., 2014; Rinaudo, 2006). β-chitin can be isolated from squid pen, and the rare variant γ-chitin has been detected in insects such as *Lucanidae* beetles and the cell wall of fungi (Jang et al., 2004). The three polymorphs differ in the arrangement of the sugar chains. α-chitin has an anti-parallel chain orientation, which leads to a more compact and less water-accessible structure as inter-chain hydrogen bonds are favored. In contrast, β-chitin has its sugar chains oriented parallel to each other, which leads to fewer inter-chain interactions (Hajji et al., 2014). The combination of anti-parallel and parallel orientations of the polymer-chains describes the last polymorph, γ-chitin. As both β- and γ-chitin can be converted to α-chitin, α-chitin is considered the most stable polymorph (Roberts, 1992).

Chitin can be converted to chitosan by deacetylation. Chitosan has an $NH_2$-group available for protonation and is soluble in acidic media (Rinaudo, 2006). Chitin is considered to be converted to chitosan when the degree of deacetylation exceeds 50% (Rinaudo, 2006).

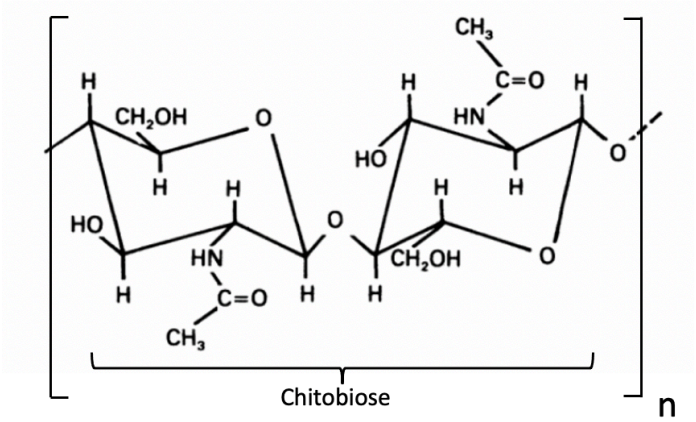


**Figure 4. Chitin structure.** The figure illustrates how N-acetyl-D-glucosamine units are linked together by β-1,4 glycosidic bonds and rotated 180° relative to each other. Two N-acetyl-D-glucosamine units linked together form the chitobiose units, which is repeated n times to form a polymer-chain. The figure was taken from Rinaudo, 2006, and modified for the purpose of this thesis.

Catechols are aromatic compounds with two neighboring hydroxyl groups that are abundant in insect exoskeletons. Insect metamorphosis includes four life stages: egg, larva, pupa, and adult. As a black solider fly (*Hermetia illucens*) develops from the pupa stage to the adult stage, the pupal exoskeleton is shed. During the life cycle of the black soldier fly, the insect cuticle of the adult fly undergoes sclerotization at which point protein molecules cross-link with chitin and catechols to form the insect's rigid exoskeleton (Kramer et al., 2000). The sclerotization process involves various catechols such as *N*-acetyldopamine (NADA), *N*-β-alanyldopamine (NBAD), and 3,4-dihydroxylphenylethanol (DOPET) (**Figure 5**) which become covalently bound to side-chain functional groups of amino acids from insect proteins, mostly histidine (Kramer et al., 2000). Due to interactions between the catechols and proteins, the exoskeleton becomes increasingly hydrophobic and insoluble (Kramer et al., 2000). The composition of chitin, catechols, and proteins depends on the region and functionality properties of the cuticle, but how these differences are obtained has not yet been described (Andersen, 2010).

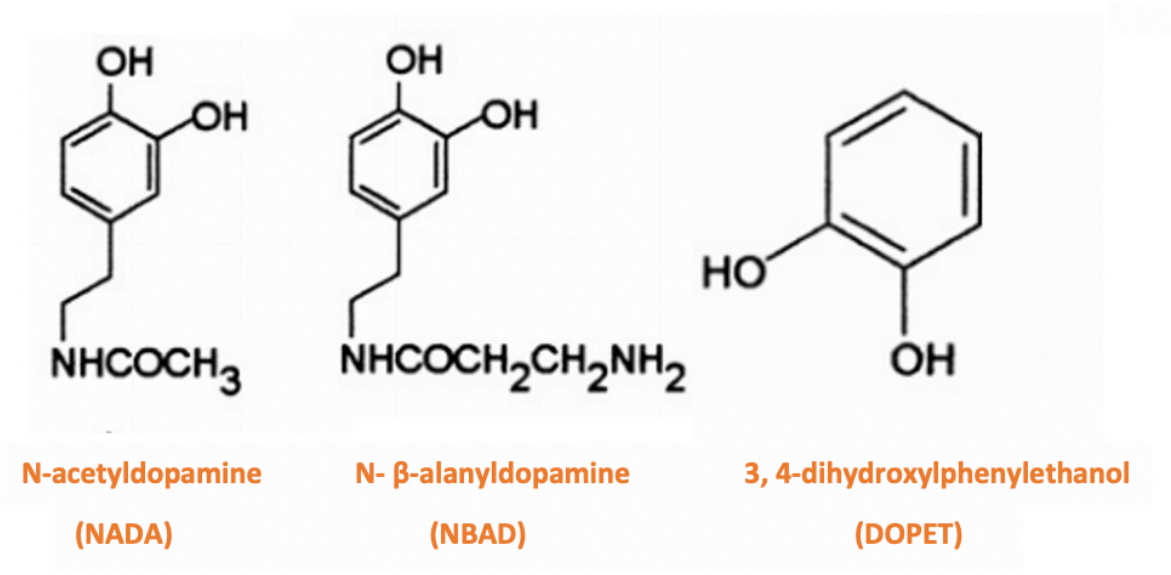


**Figure 5. Chemical structures of different catechols.** The figure shows the chemical structures of *N*-acetyldopamine (NADA), *N*-β-alanyldopamine (NBAD), and 3,4-dihydroxylphenylethanol (DOPET). These structures are typically found in insect exoskeleton. The figure is taken from Andersen, 2010, and modified for the purpose of this thesis.

## 1.2 Enzymatic degradation of recalcitrant polysaccharides

The CAZy database was created in 1998 to categorize the variety of enzymes involved in the degradation or modification of complex carbohydrates based on their sequence and structure (Levasseur et al., 2013). The CAZy database includes glycoside hydrolases (GHs), glycosyltransferases (GTs), polysaccharide lyases (PLs), carbohydrate esterases (CEs), carbohydrate-binding modules (CBMs), and auxiliary activities (AAs). Glycoside hydrolases (GHs) represent the most abundant group of enzymes in the CAZy database with 128 different families that are distinguished based on amino acid sequence similarities (Cantarel et al., 2009). For example, families GH5 and GH6 contain hydrolases that specifically break down cellulose, also referred to as cellulases, while families GH18 and GH19 include chitinases, GHs that breaks down chitin. GHs cleave glycosidic bonds by a hydrolytic reaction mechanism and when acting on polymers such as cellulose and chitin, they may either randomly cleave internal bonds or attack the reducing or non-reducing chain ends (Horn et al., 2012). The enzymatic activity of GHs on polymers is limited by the accessibility of the sugar chains and will normally be highest for soluble substrates. GH domains may be appended to a carbohydrate-binding modules (CBM), which are non-catalytic domains. They have carbohydrate-binding activity and contribute as modules for larger enzymes to better attach to carbohydrates (Shoseyov et al., 2006).

The CAZy database is continuously updated, and after the revolutionary discovery of lytic polysaccharide monooxygenases (LPMOs) by Vaaje-Kolstad et al. in 2010, a new group of enzyme families, referred to as auxiliary activity (AA), was introduced (Levasseur et al., 2013). The AA families comprise 17 families where 7 of them include LPMOs. LPMOs are copper-dependent enzymes that catalyze oxidative cleavage of the glycosidic bonds in recalcitrant polysaccharides such as cellulose and chitin. The oxidative cleavages make the polysaccharide less crystalline and more available for GHs to bind to further hydrolyze the polymer (Vaaje-Kolstad et al., 2005b).

### 1.2.1 Cellulose degradation

Enzymatic degradation of cellulose was, until recently, thought to accomplished through the synergetic action of three enzyme types, all classified as glycoside hydrolases: Endo-1,4-β-glucanases, Exo-1,4-β-glucanases, and β-glucosidases (Horn et al., 2012). Endo-1,4-β-glucanases, or endoglucanases (EGs), hydrolyze glycosidic bonds randomly in the cellulose chain, which leads to more reducing and non-reducing polysaccharide chain ends and more accessible sites for exo-1,4-β-glucanases, also referred to as cellobiohydrolases. The cellobiohydrolases attack glycosidic bonds in these reducing or non-reducing ends of the polysaccharide chains depending on enzyme specificity. The activity of endo- and exo-glucanases results in oligosaccharides and disaccharides, respectively. β-glucosidases act on these oligo- and disaccharides converting them into sugar monomers (**Figure 6**) (Arantes et al., 2010). It is worth noting that different types of endo- and exo-hydrolases acts to degrade the various polymorphs of cellulose.

The discovery of LPMOs represents a paradigm shift in the enzymatic deconstruction of recalcitrant polysaccharides. LPMOs cut directly on the crystalline surface of polysaccharides to generate new chain ends for the classical hydrolytic enzymes (Horn et al., 2012). LPMOs employ redox chemistry to oxidize glycosidic bonds using $O_2$ or $H_2O_2$ as co-substrate (see more details in section 1.3.3). To become catalytically active, LPMOs require delivery of reducing equivalents and depend on other enzymes or molecules to provide them reducing power and, if $H_2O_2$ is being used, the co-substrate (Bissaro et al., 2018). Commercial production of energy and biofuels from insoluble polysaccharides has been hampered due to the inefficient conversion of insoluble polysaccharides to soluble, fermentable sugars, but the use of LPMOs has improved this conversion process (Horn et al., 2012; Costa et al., 2020).

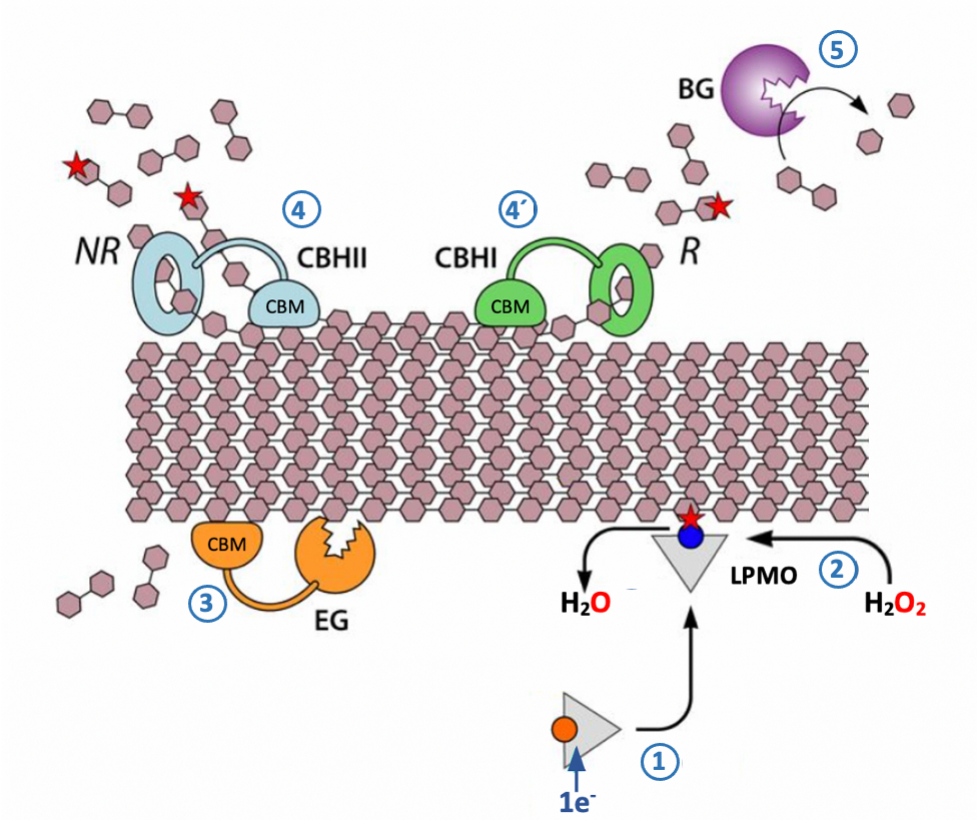


**Figure 6. The synergy of LPMOs and cellulases degrading cellulose.** The figure Illustrates how insoluble cellulose chains are oxidized by LPMOs and further hydrolyzed step by step by the synergy of various glycoside hydrolases. The reduction of the LPMO active site **(1)** activates the enzyme to oxidatively cleave crystalline cellulose using $H_2O_2$ as a co-substrate **(2)**. Endoglucanases (EG) randomly cleave the more accessible parts of cellulose **(3)**, while cellobiohydrolases (CBHI and CBHII) cuts the chain from the reducing **(4')** or the non-reducing end **(4)**. Finally, β-glucosidases (BG) splits the oligomers into monomers **(5)**. The endo- and exo-glucanases may contain a carbohydrate-binding module (CBM) to promote the hydrolase activity. **NR** and **R** indicate the non-reducing and the reducing chain end, respectively. Possible sources of $H_2O_2$ are discussed in section 1.3.5. The figure was taken from Bissaro et al., 2018, and modified for the purpose of this thesis.

### 1.2.2 Chitin degradation

Chitin degradation is carried out by a mix of various enzymes. Among them are chitinases found in the GH18 and GH19 families and LPMOs. The GH18 family includes well-studied powerful enzymes such as ChiA, ChiB, and ChiC isolated from the same gram-negative bacterium, *Serratia marcescens*. ChiA and ChiB are both considered exo-chitinases and attacks the reducing and non-reducing chain ends, respectively, producing chitobiose units (Vaaje-Kolstad et al., 2013). To provide continuous access to new reducing and non-reducing chain ends, ChiC catalyzes random cleavage in the more amorphous regions of the chitin surface. Chitobiases act on the chitobiose units produced by ChiA and ChiB converting them into sugar monomers (**Figure 7**) (Beier et al., 2013). LPMOs provide more access point for chitinases to bind by oxidatively cleaving the most recalcitrant parts of chitin. These enzymes are discussed in section 1.3.

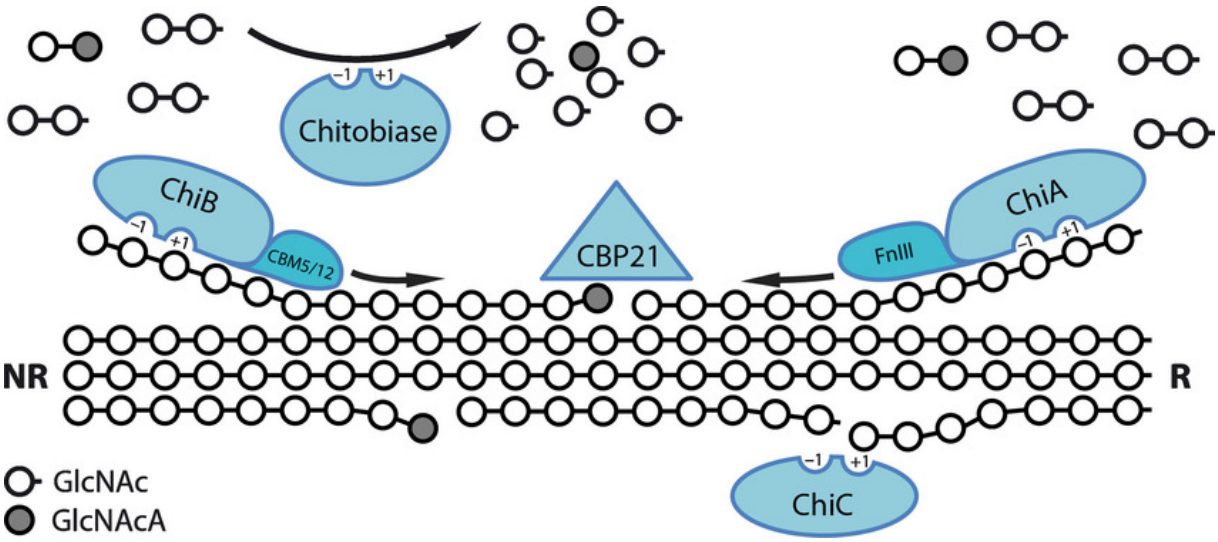


**Figure 7. Synergy of LPMOs and chitinases when degrading chitin.** The figure Illustrates how insoluble chitin chains are oxidized by LPMOs (here exemplified by CBP21) and further hydrolyzed step by step by the synergy of various glycoside hydrolases. The LPMOs oxidatively cleave the crystalline structure of chitin resulting in C1-oxidized products which are converted into GlcNAcA (grey circles). ChiC randomly cleaves in amorphous regions of the substrate, while ChiA and ChiB cleaves chains into chitobiose units from the reducing (**R**) and the non-reducing (**NR**) end, respectively. Finally, a chitobiase cleaves the chitobiose units into GlcNAc monomers (white circles). The figure was taken from Vaaje-Kolstad et al., 2013.

## 1.3 Lytic Polysaccharide Monooxygenases

### 1.3.1 Discovery

Before LPMOs were discovered, the classical view on enzymatic cellulose degradation was that hydrolytic enzymes were responsible for depolymerizing cellulose (Horn et al., 2012). However, the presence of an enzyme capable of converting native cellulose into a form that would be more accessible for these hydrolytic enzymes was hypothesized in 1950 (Reese et al., 1950). The first demonstration of surface disruption in an insoluble carbohydrate by a protein came in 2005, when it was shown that a small chitin-binding protein from family 33 of carbohydrate-binding modules (CBM33), CBP21 (today also referred to as *Sm*AA10A), is essential for the ability of *S. marcescens* to efficiently degrade chitin (Vaaje-Kolstad et al., 2005b). CBP21 was shown to bind to chitin, causing structural changes in the chitin, leading to improved chitin depolymerization by chitinases (Vaaje-Kolstad et al., 2005b). Although CBP21 was first described as a chitin-binding protein without catalytic activity, Vaaje-Kolstad et al. showed in 2010 that CBP21 is capable to oxidatively cleave β-1,4-glycosidic bonds in crystalline chitin using experiments with isotope labeled $^{18}O_2$ and $H_2{}^{18}O$. Vaaje-Kolstad and colleagues noted the structural similarities between CBM33 and a fungal protein

at the time referred to as GH61 and hypothesized that GH61 most likely would have equivalent oxidizing properties. This hypothesis was confirmed one year later by an experiment showing that a GH61 oxidatively cleaved glycosidic bonds in cellulose (Quinlan et al., 2011). The latter study also showed that the function of GH61 depends on Cu(II) and that the LPMO reaction requires molecular oxygen as a co-substrate, as well as an electron from a reducing agent (Quinlan et al., 2011). The same year, a CBM33 protein isolated from *Streptomyces coelicolor,* CelS2, was demonstrated to oxidative cleavage glycosidic bonds in cellulose (Forsberg et al., 2011). Following these discoveries, proteins in the CBM33 and GH61 families were renamed as "Lytic Polysaccharide Monooxygenase" (LPMO; Horn et al., 2012), and they were incorporated into the CAZy database, as Auxiliary Activities (AA). GH61 and CBM33 thus became AA9 and AA10, respectively (Levasseur et al., 2013). Later, novel LPMO families were discovered and the LPMO are currently divided into seven AA families, AA9-11 and AA13-16, based on sequence similarity (Vaaje-Kolstad et al., 2017).

### 1.3.2 Structure

The various LPMOs consist of varied sequences and are often substrate specific. Despite these variations, structural similarities have been observed in the catalytic domains. These domains typically consist of seven to nine β-strands oriented to form a β-sandwich, where varying loops and helices connect the strands. The substrate specificity is thought to be determined in part by a "flat" area between β-strands 1 and 2 in LPMOs in the AA9 family and between β-strands 1 and 3 for LPMOs in the AA10 family (The red areas in **Figure 8,** labeled as L2), as this is the area that interacts with the substrates (Zhou et al., 2020; Vaaje-Kolstad et al., 2017). This is also the area with the biggest variation among the LPMOs, both in length and structurally (Dimarogona et al., 2012).

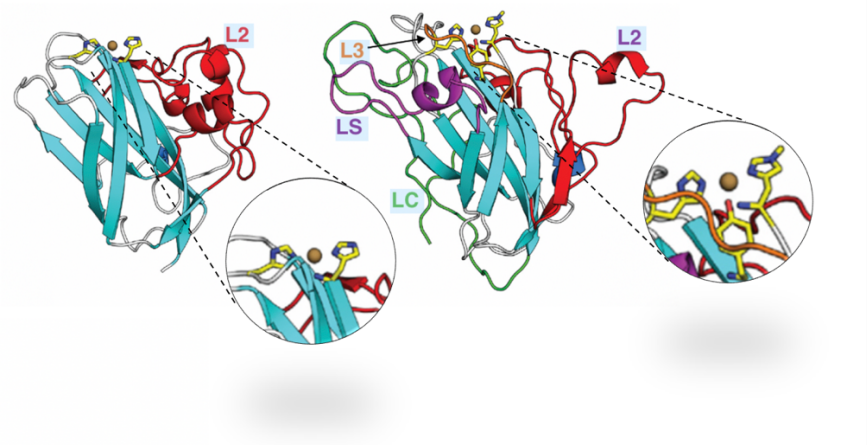


**Figure 8. LPMOs structural fold and active site.** The figure shows the typical structural folds and the active site of LPMOs from families AA10, to the left, and AA9, to the right. Loops that vary and that may determine the binding specificity (L2) and the shape of the LPMO (L3, LS, and LC) are indicated. Note that for the His-brace in the active site of the LPMO of AA10, the N-terminal histidine is methylated at the Nε2 nitrogen. The figure was taken from Vaaje-Kolstad et al., 2017, and modified for the purpose of this thesis.

The catalytic center comprises two histidines (one of them being the N-terminal amino acid), which form the His-brace motif. The His-brace is the only fully conserved feature among LPMOs (Bissaro et al., 2018) and is where the essential copper atom binds and contributes to the oxidative properties of LPMOs. In addition, a hydrophobic amino acid, phenylalanine or tyrosine, and in some LPMOs, an alanine contributes to the copper coordinating sphere (**Figure 8**) (Forsberg et al., 2014).

### 1.3.3 Mechanism

LPMOs oxidatively cleave glycosidic bonds in insoluble polysaccharides using either $O_2$ or $H_2O_2$ as co-substrate (Bissaro et al., 2018). This requires a reduction of Cu(II) to Cu(I) in the active site (Quinlan et al., 2011). LPMOs were initially characterized as monooxygenases requiring the delivery of molecular oxygen, two electrons and two protons per reaction cycle ($R\text{-}H + O_2 + 2e^- + 2H+ \rightarrow R\text{-}OH + H_2O$) (**Figure 8**, top) (Vaaje-Kolstad et al., 2010). More recently, hydrogen peroxide, $H_2O_2$, has been described as a co-substrate for LPMOs (Bissaro et al., 2016b; Bissaro et al., 2017) which entails a peroxygenase reaction ($R\text{-}H + H_2O_2 \rightarrow R\text{-}OH + H_2O$) (**Figure 9**, bottom). In a peroxygenase reaction, only one transfer of an electron, to prime the enzyme by reducing Cu(II) to Cu(I), is required, whereas the reaction will follow the cycle shown in **Figure 9** (bottom) until an eventual re-oxidation of the copper ion occurs (Bissaro et al., 2017; Zhou et al., 2020). The peroxygenase activity of LPMOs has been disputed but recent research confirms that hydrogen peroxide is the preferred co-substrate of LPMOs and that catalysis is three orders of magnitude faster with hydrogen peroxide compared to molecular oxygen (Bissaro et al., 2020a; Jones et al., 2020). It has been claimed that the apparent monooxygenase activity of LPMOs may in fact be a peroxygenase reaction that is limited by the *in situ* generation of $H_2O_2$ (Bissaro et al., 2018). $H_2O_2$ may be generated *in situ* by reactions between the reductant and $O_2$ or by a so-called futile LPMO reaction, meaning that the reduced LPMO reduces $O_2$ to generate $H_2O_2$ (Kittl et al., 2012). Importantly, studies have also shown that excessive amounts of $H_2O_2$ leads to inactivation of LPMOs (Bissaro et al., 2017). Thus, optimal LPMO catalysis requires delivery of "appropriate" amounts of $H_2O_2$ (see below).

LPMOs have been reported to cleave glycosidic bond with either $C_1$ or $C_4$ oxidation. A few LPMOs have the ability of both $C_1$ and $C_4$ oxidation (Forsberg et al., 2016; Zhou et al., 2020). $C_1$ oxidation results in a lactone which is spontaneously hydrolyzed to an aldonic acid (**Figure 9**, right), while $C_4$ oxidation results in a 4-ketoaldoses which is hydrolyzed to gemdiols (Phillips et al., 2011; Isaksen et al., 2014; Zhou et al., 2020).

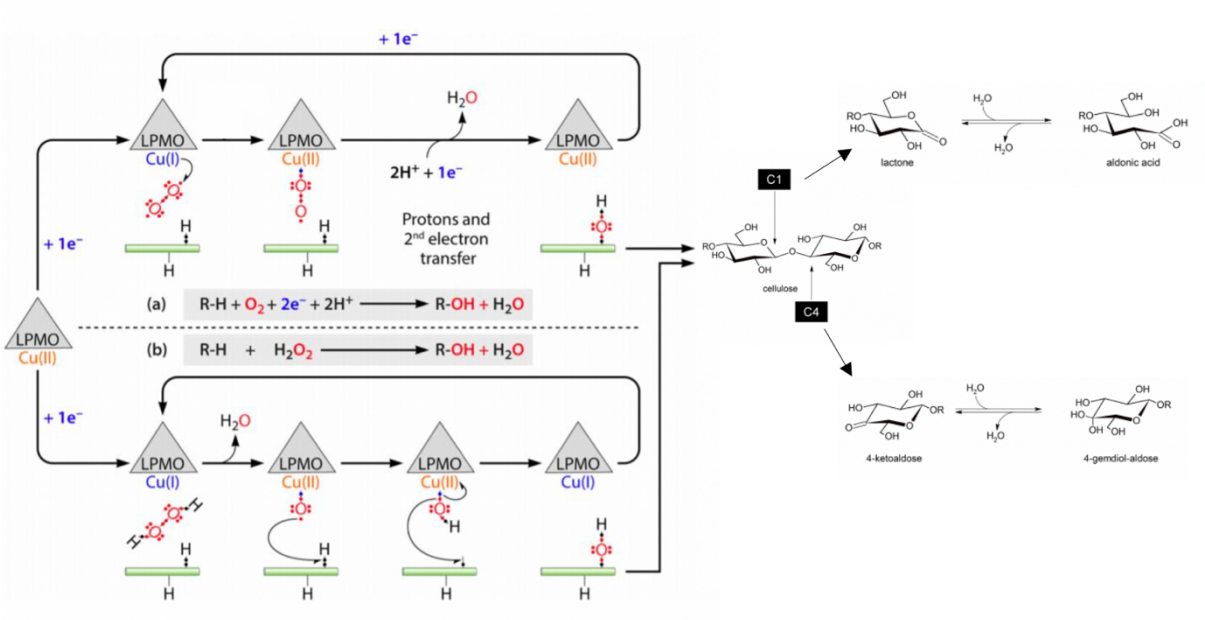


**Figure 9. Schematic comparison of $O_2$-based and $H_2O_2$-based pathways of glycosidic bond cleavage by LPMOs.** The figure illustrates the reaction pathways of glycosidic bond cleavage by an LPMO based on the monooxygenase paradigm (**a**), and the peroxygenase paradigm (**b**). **a:** In the $O_2$-based reaction, the active site is first reduced from Cu(II) to Cu(I). $O_2$ activates the LPMO and the reaction requires two external electron transfers for each reaction cycle to cleave glycosidic bonds. **b:** In the $H_2O_2$-based reaction pathway, the active site is first reduced from Cu(II) to Cu(I). $H_2O_2$ activates the LPMO and this pathway does not require any external electron transfer. The right part of the figure illustrates C1 and C4 oxidation of cellulose to eventually generate an aldonic acid and a 4-gemdiol-aldose, respectively. Figures was taken from Bissaro et al., 2018 and Danneels et al., 2017, and modified for the purpose of this thesis.

### 1.3.4 Traditional LPMO reactions

An improved understanding of the catalytic properties of LPMOs is of major scientific and industrial interest. LPMOs require activation by an electron donor to become catalytically active, and the choice of LPMO reductant has been a topic of intense investigation (Hegnar et al., 2019; Stepnov et al., 2021; Frommhagen et al., 2016; 2017; Kracher et al., 2016). Known reductants include small molecules such as ascorbic acid (AscA), gallic acid (GA), and cysteine, and plant derived flavonoids and lignin building blocks (Hegnar et al., 2019; Stepnov et al., 2021; Frommhagen et al., 2016; 2017; Kracher et al., 2016). AscA is the most commonly used LPMO reductant and is able to fuel LPMOs with reducing equivalents in an apparent monooxygenase reaction, i.e., without exogenous $H_2O_2$ addition (Stepnov et al., 2021). Stepnov et al. (2021) demonstrated that the amount of $H_2O_2$ produced by their model AA10 LPMO is negligible compared to the amount of $H_2O_2$ produced by autooxidation of AscA, and that it is in fact the $H_2O_2$ generated by autooxidation of AscA that most likely fuels the LPMO reaction (Stepnov et al., 2021). Recent studies also highlight the importance of

controlling the amount of free copper in LPMO reactions as free copper can promote to enzyme-independent $H_2O_2$-production (Kommedal et al., 2020; Stepnov et al., 2021).

Some studies have investigated the ability of plant and lignin-derived components to act as LPMO reducing agents (Frommhagen et al., 2016; 2017; Kracher et al., 2016). In one study, three AA9s from the fungus *Myceliophthora thermophila* C1 were assayed using 34 different plant-derived flavonoids and lignin building blocks and it was found that molecules harboring either a 1,2-benzenediol or 1,2,3-benzenetriol moiety were best suited for promoting LPMO activity on cellulose (Frommhagen et al., 2016). Lignin has also been shown to work as electron donor for LPMOs, where insoluble high-molecular weight lignin serves as a reservoir of electrons that are shuttled to the LPMO via low-molecular weight soluble lignin components (Westereng et al., 2015; Muraleedharan et al., 2018).

Another important aspect of LPMO catalysis relates to $H_2O_2$. Although it has been demonstrated that LPMOs favor $H_2O_2$ over $O_2$ as co-substrate (Bissaro et al., 2017; 2020a; Jones et al., 2020), too much $H_2O_2$ results in LPMO inactivation (Bissaro et al., 2017; Loose et al., 2018). Exogenous $H_2O_2$ addition is one way to provide LPMOs with their relevant co-substrate, either initially or by multiple additions at regular intervals (Hegnar et al., 2019), but there are drawbacks to both of these options. Controlled *in situ* $H_2O_2$ generation would be a better option and would allow for a more fine-tuned production to avoid LPMO inactivation. This can be accomplished enzymatically by glucose oxidase (Bissaro et al., 2017) or photocatalytically using a photocatalyst to generate both reducing equivalents and reactive oxygen species (Bissaro et al., 2020; Blossom et al., 2020).

### 1.3.5 Light-driven LPMO catalysis

The aim of photobiocatalysis is to merge the fields of photocatalysis and biocatalysis to harvest the energy from the sun to perform chemical reactions using enyzmes. Photobiocatalysis draws inspiration from the photosynthetic process in green plants and algae where $CO_2$ and $H_2O$ are converted to $O_2$ and carbohydrates. To convert sunlight into chemical energy available for enzymes, photobiocatalytic reactions rely on a photosensitizer or photocatalyst (Macia-Agullo et al., 2015). The photosensitizer absorbs light and excites an electron from its highest occupied molecular orbital to the lowest unoccupied molecular orbital from which the electron can be transferred to a redox enzyme, either indirectly, via a mediator or co-factor, or directly (**Figure 10**) (Schmermund et al., 2019). To facilitate electron transfer and sustain multiple cycles of electron transfer, the photosensitizer depends on sacrificial electron donors or acceptors to return to its ground state **(Figure 10**). Sacrificial electron donors include AscA, ethylenediaminetetraacetate (EDTA), alcohols,

and water depending on the type of photosensitizer (Schmermund et al., 2019). In aerobic conditions, molecular oxygen is an efficient electron acceptor and can undergo a single electron reduction to superoxide ($O_2 + e^- \rightarrow O_2^{\bullet -}$), or two-electron reduction to hydrogen peroxide ($O_2 + 2e^- + 2H+ \rightarrow H_2O_2$) (Macia-Agullo et al., 2015).

The climate change issues have increased the "green" focus on renewable and sustainable energy sources during the twenty-first century. As solar energy is the most accessible energy source on Earth, principles from photosynthetic reaction mechanisms are utilized to transport electrons in biocatalytic reactions (Verma et al., 2020; Lee et al., 2018). In most reported enzymatic reactions involving light, a biocatalyst provides cofactors directly or indirectly via a mediator in an appropriate redox state by excitation of electrons due to exposure of photons (Schmermund et al., 2019). The cofactor will then allow activation of an enzymatic reaction by transporting the additional electron to the active site of a redox enzyme (Maciá-Agulló et al., 2015; Schmermund et al., 2019). With continuous exposure to light and the presence of a sacrificial electron donor (e.g., AscA or ethylenediaminetetraacetate (EDTA)), the mediator and the cofactor can be reused to fuel subsequent reactions (**Figure 10**) (Schmermund et al., 2019).

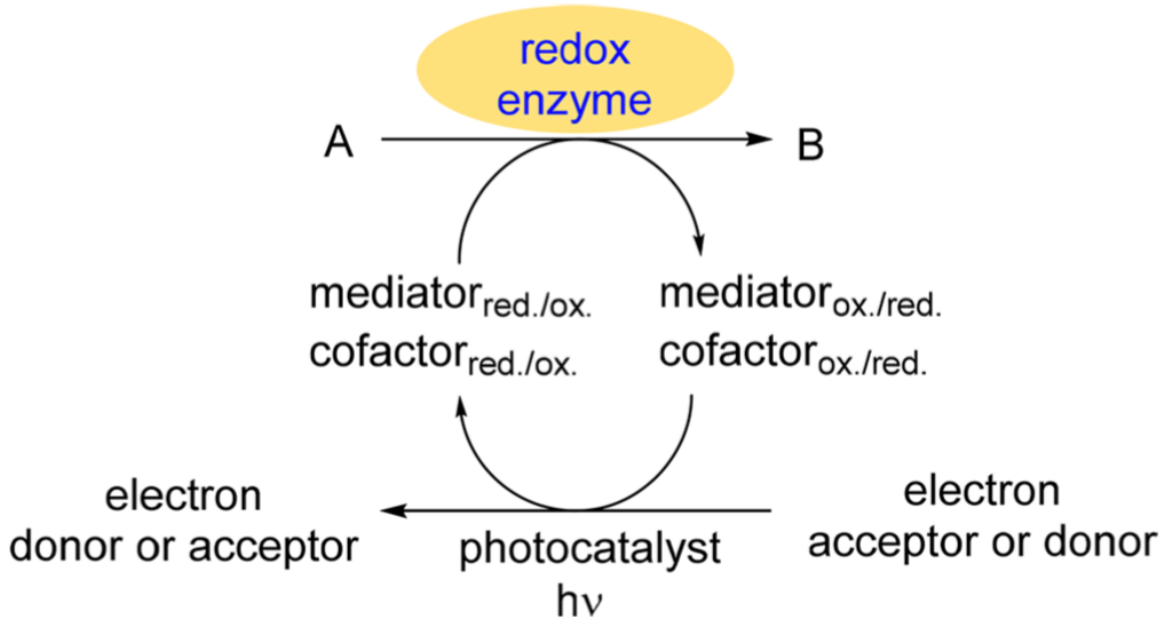


**Figure 10. Schematic reaction pathway of photocatalytic action of a redox enzyme using a photocatalyst/photosensitizer.** The figure illustrates how a photocatalyst/photosensitizer provides a redox enzyme with an electron needed for enzymatic reactions. When the photocatalyst/photosensitizer is exposed to light, an electron excites from its highest occupied orbital to its lowest unoccupied orbital. The excitation leads to either a direct electron transfer between the photocatalyst/photosensitizer and the redox enzyme, or an indirect electron transfer via a mediator or a cofactor. When the redox enzyme is reduced, the enzymatic reaction can occur. The figure is taken from Schmermund et al., 2019.

The first study to demonstrate water as a sacrificial electron donor for biocatalytic redox reactions, employed a titanium dioxide-based photocatalyst to provide the Old Yellow Enzyme from *Thermus scotoductus* SA-01 with reducing equivalents to convert ketoisophorone to (R)-levodione (Mifsud et al., 2014). The activity of this enzyme showed a two-fold increase when vanadium-doped titanium dioxide (V-$TiO_2$) was used as photocatalyst compared to gold doped titanium dioxide (Au-$TiO_2$) indicating that the choice of photocatalyst matters (Mifsud et al., 2014). Light-driven water oxidation by V-$TiO_2$ was later shown to drive oxidation of recalcitrant polysaccharides by LPMOs (families AA9 and AA10) without the need for an external reductant such as AscA, confirming that water could serve as sacrificial electron donor in other photobiocatalytic reactions (Bissaro et al., 2016b). It was clearly shown that LPMO activity was dependent on light intensity and the presence of the photocatalyst; in the absence of either of these reaction components, no oxidized cello-oligosaccharides were observed (Bissaro et al., 2016b).

After discovering that LPMOs prefer $H_2O_2$ as co-substrate, Bissaro and colleagues revisited the study from 2016 using V-$TiO_2$ to promote LPMO activity to investigate a potential role of the reactive oxygen species (ROS) superoxide ($O_2^{\bullet-}$) and hydrogen peroxide. Horseradish peroxidase (HRP) will compete with the LPMO for $H_2O_2$, and it was shown that increased amounts of HRP in a reaction with the LPMO resulted in increasing LPMO inhibition (Bissaro et al., 2020b). This showed that the light-driven LPMO reaction was in fact limited by light-driven *in situ* generation of $H_2O_2$. To determine a potential role for superoxide in reactions with V-$TiO_2$, superoxide dismutase was added to the reactions but did not alter LPMO activity (Bissaro et al., 2020b).

In 2016, Cannella and his research team observed a 100-fold increase in catalytic activity when an LPMO from the AA9 family was incubated with photoexcited pigments, such as chlorophyllin (Chl), combined with AscA or lignin. This observation influenced Möllers et al. to look at the role of ROS when degrading phosphoric acid swollen cellulose (PASC) in the presence of Chl, AscA, and light. When removing $O_2^{\bullet-}$ and $H_2O_2$ by adding superoxide dismutase and catalase, respectively, Möllers et al. did not observe any difference in the amount of generated oxidized products (Möller et al., 2017). Thereby, it was concluded that ROS did not play a role in photocatalytic oxidation of cellulose by LPMOs. However, Bissaro et al. concluded otherwise in their study from 2020, as they studied LPMO activity over time and were able to take LPMO inactivation into account (Bissaro et al., 2020b).

In a recent report, light-exposed lignin was shown to be able to oxidize $H_2O$ and use $H_2O$ as an electron donor in addition to generate $H_2O_2$ by reduction of $O_2$ (Miglbauer et al., 2020). Thus, lignin can function as a photocatalyst in redox reactions (Kim et al., 2021). Insoluble catechols embedded in

the exoskeleton of insects have structural similarities to lignin (Kracher et al., 2016), and by analogy to reported observations regarding the photocatalytic activity of lignin, these insoluble catechols seems like a promising photosensitizer to catalyze LPMO activity towards recalcitrant polysaccharides.

## 1.4 Aim of the study

The aim of this study was to see if insoluble catechols in pupal exuviae from *Hermetia illucens* can provide LPMOs with the necessary reducing equivalents to oxidatively cleave recalcitrant polysaccharides without addition of exogenous reductant and $H_2O_2$, and if exposing reactions to visible light will boost the depolymerization. The study was performed in two steps where the first step includes reaction assays with a cellulose-active model enzyme, *Sc*AA10C, using a microcrystalline cellulose substrate, Avicel. To assess the ability of FMC to provide *Sc*AA10C with the reducing equivalents, reactions were performed with various amounts of FMC, and at varying pH, in the presence or absence of light. Further characterization of the photobiocatalytic system was carried out by varying the enzyme and substrate concentrations and by investigating the effect of the light intensity on the reactions.

The second step of this study aimed at investigating the production of $H_2O_2$ in the photobiocatalytic system. Reactions were performed with and without *Sc*AA10C and with different concentrations of Avicel. Previous studies had shown superoxide ($O_2^{\bullet-}$) to be involved in light-driven LPMO reactions, which led to the hypothesis that $H_2O_2$ is generated from $O_2^{\bullet-}$ in reactions with FMC. To assess the role of $O_2^{\bullet-}$ in the photobiocatalytic system, reactions were supplemented with different concentrations of superoxide dismutase (SOD), which forms $H_2O_2$ from superoxide.

After these studies with cellulose, it was then assessed if chitin in the pupal exuviae of *Hermetia illucens* (FMC) could be directly degraded by either a chitinase, *Sm*ChiA, or by *Sm*AA10A, a chitin-active LPMO and if LPMO action was light-sensitive. Furthermore, reactions were performed to assess if synergy between *Sm*ChiA and *Sm*AA10A can increase the degradation of chitin. This part of the study included reactions with a model chitin substrate, β-chitin. Due to lack of time, these reactions were analyzed in single replica as a proof-of-concept.

# 2. Materials

## 2.1 Laboratory Equipment

Laboratory equipment used in the research described in this thesis is shown in Table 1.

**Table 1: Laboratory equipment**

| Equipment | Specifications | Distributor |
|---|---|---|
| **Affinity chromatography equipment** | BioLogic LP chromatography system<br>Econo-column®, 1.0 x 10 cm<br>Econo-column® flow adapter<br>Chitin resin | BioRad<br>BioRad<br>BioRad<br>New England Biolabs |
| **Baffled shake flask** | 2000 mL | Nalgene |
| **Blue-cap bottles** | 1000 mL, 500 mL, 100 mL | VWR |
| **Centrifugal filters** | Vivaspin 20, 10.000 MWCO PES<br>Amicon® Ultra-15, 10.000 MWCO | Sartorius<br>Merck Millipore |
| **Centrifuges** | Avanti™ J-25 centrifuge<br>Heraeus™ Multifuge™ X1 Centrifuge | Beckman Coulter Inc<br>Thermo Scientific |
| **Centrifuge rotors** | JA-10 | Beckman Coulter Inc |
| **Centrifuge tube** | 500 mL | Nalgene |
| **Eppendorf tubes** | 1.5 mL - Axygen® | VWR |
| **Filters** | Filter upper cup PES membrane 0.20 and 0.45 µm<br>Syringe filters 0.20 and 0.45 µm | VWR<br>Sarstedt |
| **HILIC equipment** | Agilent Infinity 1290 UPLC system<br>Acquity BEH Amide column, 130 Å, 1.7 µm, 2.1x150 mm<br>VanGuard precolumn | Agilent<br>Waters<br>Waters |
| **HPLC equipment** | Dionex™ ICS-5000 system<br>Dionex™ CarboPac™ PA200 column | Thermo Scientific<br>Thermo Scientific |
| **Heating block** | | Thermo Scientific |
| **ICS Eluent flask** | 2 L | VWR |
| **IEX equipment** | ÄKTA Pure™ chromatography system<br>HiTrap® DEAE Sepharose FF, 5 mL column | GE Healthcare<br>GE Healthcare |

| | | |
|---|---|---|
| **LDS-PAGE equipment** | Mini PROTEAN® TGX Stain-Free™ Gels<br>Mini-PROTEAN® Tetra Cell vertical mini gel electrophoresis system<br>PowerPac 300, power supply<br>Stain-Free Sample Tray<br>Gel Doc™ EZ Imager<br>BenchMark™ Protein Ladder | BioRad<br>BioRad<br>BioRad<br>BioRad<br>BioRad<br>Invitrogen |
| **Nunc™ MicroWell™ 96-Well** | Black, Clear | Thermo Scientific |
| **RSLC equipment** | Dionex™ Ultimate™ 3000 RSLC system<br>Rezex™ RFQ-Fast Acid H+(8 %) column, 7.8 x 100 mm | Thermo Scientific<br>Phenomenex |
| **SEC equipment** | ÄKTA™ Purifier chromatography system<br>HiLoad™ 16/600 Superdex™ 75 grep grade column, 120 mL | GE Healthcare<br>GE Healthcare |
| **Serological pipette** | 10 mL | Sarstedt |
| **Snap ring cap** | 11 mm (blue, red) | VWR |
| **Snap ring micro vial** | 0.3 mL | VWR |
| **Spectrophotometer** | BioPhotometer® D30<br>Cary 60 UV-Vis | Eppendorf<br>Agilent Technologies |
| **Spot light source** | Lightning Cure Spotlight source LC8 model L9588 | Hamamatsu |
| **Syringes** | 50 mL, 20 mL, 1 mL<br>5 mL<br>10 mL (12 mL) | BD Plastipak<br>BD Emerald<br>Henke Sass Wolf |
| **Thermomixer** | ThermoMixer® C | Eppendorf |
| **Ultrasonic bath** | Branson 3510 DTH | Sigma-Aldrich |
| **Uvette® disposable cuvettes** | 1x1 cm | Eppendorf |
| **Varioskan™ LUX multimode microplate reader** | | Thermo Scientific |
| **Volumetric flask** | 1 L | VWR |

## 2.2 Chemicals and buffers

Chemicals and buffers used in the research described in this thesis is shown in Table 2.

**Table 2: Chemicals and buffers**

| Compound | Specifications | Distributor |
|---|---|---|
| **Acetonitrile** | ACN | VWR |
| **Ammonium Sulfate** | $(NH_4)_2SO_4$ | Supelco |
| **Amplex® Red** | | Sigma-Aldrich |
| **Bacto™ Tryptone** | | Gibco |
| **Bacto™ Yeast extract** | | Gibco |
| **Copper sulfate** | $Cu(II)SO_4$ | VWR |
| **Ethanol** | EtOH | VWR |
| **Ethylenediaminetetraacetic acid (EDTA)** | $C_{10}H_{16}N_2O_8$ | Merck |
| **Hydrochloric acid, 37 %** | HCl | VWR |
| **Sodium Acetate** | NaOAc | Sigma-Aldrich |
| **Sodium Chloride** | NaCl | VWR |
| **Sodium hydroxide, 50% (w/v)** | NaOH | Sigma-Aldrich |
| **Sodium Phosphate** | $NaH_2PO_4$ | Sigma-Aldrich |
| **Disodiumhydrogenphosphate (dihydrate)** | $Na_2HPO_4 \cdot 2H_2O$ | Sigma-Aldrich |
| **NuPAGE™ LDS Sample Buffer (4x)** | | Thermo Fisher |
| **NuPAGE™ Sample Reducing Agent (10x)** | | Thermo Fisher |
| **Tris-Glycine-SDS buffer (10x)** | | Bio-Rad |

## 2.3 Proteins and enzymes

Proteins and enzymes used in the research described in this thesis is shown in Table 3.

**Table 3: Proteins and enzymes**

| Proteins and enzymes | Supplier |
|---|---|
| **BenchMark™ Protein Ladder** | Thermo scientific |
| ***Sc*AA10C** | Self-made (see sections 3.1-3.6) |
| ***Sm*AA10A** | Self-made (see sections 3.1-3.6) |
| ***Sm*ChiA** | Self-made (see sections 3.1-3.4 & 3.6) |
| ***Tf*Cel6A** | Self-made (a kind gift of Eirik G. Kommedal) |
| **SOD** | Sigma-Aldrich (Prod. nr.: S5639) |
| **HRP** | Sigma-Aldrich (Prod. nr.: P8250) |

## 2.4 Substrates and standards

Substrates and standards used in the research described in this thesis is shown in Table 4.

**Table 4: Substrates and standards**

| Substrates and standards | Specification | Supplier |
|---|---|---|
| **Avicel** | | Sigma-Aldrich |
| **β-chitin** | Extracted from squid pen (batch 20140101) particle size < 0.8 mm | France chitin, Orange, France |
| **Cellotrionic acid (GlcGlc1A)** | $C_{12}H_{22}O_{12}$ | Self-made (a kind gift of Eirik G. Kommedal) |
| **Cellotrionic acid ($Glc_2Glc1A$)** | $C_{18}H3_2O_{17}$ | Self-made (a kind gift of Eirik G. Kommedal) |
| **Cellotriose,**<br>**Cellotetraose,**<br>**Cellopentose** | $C_{18}H_{32}O_{16}$<br>$C_{24}H_{42}O_{21}$<br>$C_{30}H_{52}O_{26}$ | Megazyme |
| **Chitobionic acid,**<br>**Chitotrionic acid,**<br>**Chitotetraonic acid,**<br>**Chitopentaonic acid,**<br>**Chitohexaonic acid** | $C_{16}H_{28}N_2O_{11}$<br>$C_{24}H_{41}N_3O_{16}$<br>$C_{32}H_{54}N_4O_{21}$<br>$C_{40}H_{67}N_5O_{26}$<br>$C_{48}H_{80}N_6O_{31}$ | Self-made (a kind gift of Tina Tuveng) |
| **Glucose**<br>**Cellobiose** | $C_6H_{12}O_6$<br>$C_{12}H_{22}O_{11}$ | Sigma-Aldrich |
| **Hydrogen Peroxide** | $H_2O_2$ | VWR |
| **Pupal exuviae from *Hermetia illucens*** | | Dr. Thomas Hahn, Fraunhofer Institute |
| ***N*-acetylglucosamine,**<br>***N,N'*-diacetylglucosamine** | $C_8H_{15}NO_6$<br>$C_{16}H_{28}N_2O_{11}$ | Megazyme |

## 2.5 Bacterial strains and antibiotics

Bacterial strains and antibiotics used in the research described in this thesis is shown in Table 5.

**Table 5: Bacterial strains and antibiotics**

| Bacterial strains and antibiotics | Supplier |
|---|---|
| **Ampicillin stock solution, 100 mg/mL** | Sigma-Aldrich |
| **E. *coli* One Shot® BL21 Star™ (DE3), containing the expression plasmid pRSET-B_CelS2, coding for *Sc*AA10C** | Self-made (Forsberg et al., 2014) |
| **E. *coli* One Shot® BL21 Star™ (DE3), containing the expression plasmid pRSET-B_CBP21, coding for *Sm*AA10A** | Self-made (Vaaje-Kolstad et al., 2005a) |
| **E. *coli* One Shot® BL21 Star™ (DE3), containing the expression plasmid pRSET-B_ChiA, coding for *Sm*ChiA** | Self-made (ChiA was recloned in pRSET-B for expression; Brurberg et al., 1994) |

## 2.6 Software

Software used in the research described in this thesis is shown in Table 6.

**Table 6: Software**

| Software | Supplier |
|---|---|
| **Chromeleon, version 7.2.9 Software, Chromatography Data Systems** | Chromeleon |
| **Image Lab™ Version 6.0.0 Standard Edition software** | Bio-Rad |
| **SkanIt™ Software for Microplate Readers** | Thermo Scientific |
| **Unicorn™ 6.4 Software** | GE Healthcare |

## 2.7 Self-made buffers and solutions

Self-made buffers and solutions used in the research described in this thesis is shown in Table 7. All buffers and solutions were stored at room temperature unless otherwise specified.

**Table 7: Self-made buffers and solutions**

| Buffers and solutions | Reagents/Preparations | Total volume |
|---|---|---|
| **Acetic acid, pH 3.6, 20mM** | A kind gift of Eirik G. Kommedal | |
| **EDTA solution, pH 8.0, 0.5 M** | 18.6 g EDTA<br>$dH_2O$<br><br>pH was adjusted with 50% NaOH and 1M HCl<br>Filtered through 0.20 μm PES membrane syringe filter | 100 mL |
| **$MgCl_2$ solution, 10 mM** | A kind gift of Eirik G. Kommedal | |
| **$NaH_2PO_4$ solution, 0.5 M** | 30 g $NaH_2PO_4$<br>$dH_2O$<br><br>Filtered through a 0.45 μm PES membrane | 500 mL |
| **$Na_2HPO_4 \cdot 2H_2O$ solution, 0.5 M** | 44.5 g $Na_2HPO_4 \cdot 2H_2O$<br>$dH_2O$<br><br>Filtered through a 0.45 μm PES membrane | 500 mL |
| **Sodium Phosphate buffer, pH 6, 0.5 M** | $NaH_2PO_4$ solution, 0.5 M<br>$Na_2HPO_4 \cdot 2H_2O$ solution, 0.5 M<br><br>$NaH_2PO_4$ solution and $Na_2HPO_4 \cdot 2H_2O$ solution were mixed and adjusted to pH 6 by adjusting the volume of the respective solutions<br>Diluted to the desired concentration with $dH_2O$ | 250 mL |
| **Spheroplast buffer** | 85.5 g Sucrose<br>50 mL Tris-HCl buffer, pH 8.0, 1M<br>0.5 mL EDTA solution, pH 8.0, 0.5M<br>$dH_2O$ | 500mL |

| | | |
|---|---|---|
| | Filtered through a 0.20 μm PES membrane<br>Stored at 4°C | |
| **Tris-HCl buffer, pH 7.5, 1M** | 12.1 g Trisma base<br>$dH_2O$<br><br>pH was adjusted with 37% HCl<br>Filtered through 0.20 μm PES membrane<br>syringe filter | 100 mL |
| **Tris-HCl buffer, pH 8.0, 1M** | 12.1 g Trisma base<br>$dH_2O$<br><br>pH was adjusted with 37% HCl<br>Filtered through 0.20 μm PES membrane<br>syringe filter<br>Diluted to the desired concentration with $dH_2O$ | 100 mL |

### 2.7.1 Cultivation medium

**LB - medium**

- 20 g Bacto™ Tryptone
- 10 g Bacto™ Yeast Extract
- 20 g NaCl
- $dH_2O$

The solids were dissolved in 2 L $dH_2O$ and distributed to two 1 L blue-cap bottles before autoclaving at 121 °C for 20 min. The medium was stored at room temperature.

### 2.7.2 Buffers for ion exchange chromatography

**Buffer A: 50 mM Tris-HCl, pH 7.5**

- 6.06 g Trisma base
- $dH_2O$

**Buffer B: 50 mM Tris-HCl with 1 M NaCl, pH 7.5**

- 6.06 g Trisma base
- 58.55 g NaCl
- $dH_2O$

Buffer A and B were prepared by dissolving the solids in approximately 0.8 L $dH_2O$ using a magnet stirrer. The pH was adjusted to 7.5 by adding 37% HCl. $dH_2O$ was added to a total volume of 1 L before the solutions were filtered through a 0.20 µm PES membrane. The buffers were stored in room temperature.

### 2.7.3 Buffer for size exclusion chromatography

**Running buffer: 50 mM Tris-HCl with 150 mM NaCl, pH 7.5**

- 6.06 g Trisma base
- 8.77 g NaCl
- $dH_2O$

Running buffer was prepared by dissolving the solids in approximately 0.8 L $dH_2O$ using a magnet stirrer. The pH was adjusted to pH 7.5 by adding 37% HCl. $dH_2O$ was added to a total volume of 1 L before the solution was filtered through a 0.20 µm PES membrane. The buffer was stored in room temperature.

### 2.7.4 Buffers for affinity chromatography

**Buffer A: 50 mM Tris-HCl, pH 8.0 with 1M Ammonium sulfate**

- 25 mL Tris-HCl buffer, pH 8.0, 1M
- 66.07 g Ammonium sulfate
- $dH_2O$

**Buffer B: 20 mM acetic acid, pH 3.6**

- A kind gift of Eirik G. Kommedal

Buffer A was prepared by dissolving the solids in approximately 0.4 L $dH_2O$ using a magnet stirrer. The pH was adjusted to pH 8.0 by adding 37 % HCl. $dH_2O$ was added to a total volume of 0.5 L before the solution was filtered through a 0.20 µm PES membrane. The buffer was stored in room temperature.

### 2.7.5 Eluents for High-Performance Anion-Exchange Chromatography with Pulsed Amperometric Detection

**Eluent A: 0.1 M NaOH**

- 10.4 mL 50% (w/v) NaOH
- $dH_2O$

**Eluent B: 1 M NaOAc + 0.1 M NaOH**

- 82.03 g NaOAc
- 5.2 mL 50% (w/v) NaOH
- $dH_2O$

**Eluent C: dH2O**

- 2 L $dH_2O$

Eluents A and C were prepared by adding 2 L $dH_2O$ using a volumetric flask to separate ICS eluent bottles. The eluents were degassed for 20 min prior to adding 10.4 mL 50% (w/v) NaOH to eluent A.

Eluent B was prepared by dissolving 82.03 g NaOAc in 1 L $dH_2O$ using a volumetric flask. The NaOAc solution was filtered through a 0.2 µm PES membrane. 5.2 mL 50% (w/v) NaOH were added to eluent B, before all eluents were placed under $N_2$ gas.

### 2.7.6 Eluents for Hydrophilic Interaction Liquid Chromatography

**Eluent A: 15mM tris-HCl pH 8**

- 15 mL Tris-HCl buffer, pH 8.0, 1M
- $dH_2O$

**Eluent B: 100% acetonitrile**

- 100% acetonitrile, HPLC grade

Eluent A was prepared by mixing 15 mL 1 M Tris-HCl buffer, pH 8.0, with 985 mL $dH_2O$ in a 1000 mL blue-cap bottle. Eluent B was purchased from VWR.

### 2.7.7 Eluents for High Pressure Liquid Chromatography with Rezex Fast Acid H+

**Running buffer: 5 mM $H_2SO_4$**

- A kind gift of Heidi Østby

# 3. Methods

## 3.1 Expression of enzymes in E. *coli*

**Materials**

- LB-medium (see section 3.7.1)
- Ampicillin stock solution (100 mg/mL)
- Glycerol stock of bacterial culture (E. *coli* OneShot® BL21 Star (DE3) with variants of the pRSET-B plasmid) generated for expression of *Sc*AA10C, *Sm*AA10A, or *Sm*ChiA

**Method**

0.5 L LB-medium was added to a sterile 2 L baffled Erlenmeyer flask under sterile conditions. Prior to inoculating the LB-medium with the bacterial glycerol stock coding for the enzyme of interest, ampicillin was aseptically added to a final concentration of 100 µg/mL. The bacterial culture was incubated for ca. 19 h at 37 °C and 200 rpm in a shaking incubator.

## 3.2 Periplasmic extraction

The periplasm is the space between the inner and out membrane in a gram-negative bacterium, and a periplasmic extraction enables isolation of the proteins found in the periplasm. A sequence encoding the enzyme of interest and an N-terminal signal peptide are cloned in a pRSET-B plasmid. The N-terminal signal peptide directs the enzymes to the periplasm, and the signal peptide gets cleaved off. The periplasmic proteins are extracted from the bacterial cells by rupturing the outer membrane of the cell using osmotic shock. Cells are first resuspended in an ice-cold spheroplast buffer causing water to diffuse out of the cell due to the high sugar concentration in the spheroplast buffer. This step is followed by an incubation in room temperature of the pellet before resuspension in ice-cold water to generate the osmotic shock. As a consequence of the rapid change to a lower osmotic pressure, water will rapidly diffuse into the cell causing the outer cell membrane to rupture.

**Materials**

- Overnight culture (see section 3.1)
- Avanti™ J-25 High-Performance Centrifuge, with a JA-10 rotor
- Spheroplast buffer, ice-cold (see section 2.7)
- 10 mM $MgCl_2$ (see section 2.7)
- 1 M Tris-HCl buffer, pH 7.5 (see section 2.7)
- $dH_2O$, ice-cold

**Method**

0.5 L overnight culture (see section 3.2) was equally distributed in two centrifuge tubes and centrifuged by an Avanti™ J-25 High-Performance centrifuge with a JA-10 rotor for 12 min at 6500 rpm and 4 °C. After discarding the supernatant, the pellets were resuspended in 50 mL ice-cold spheroplast buffer each. The spheroplast suspended cells were centrifuged at 8000 rpm for 12 min at 4 °C, and the supernatant was transferred to a 100 mL blue-cap bottle (sugar fraction) and stored at 4 °C. The pellets were resuspended in a total volume of 25 mL ice-cold $dH_2O$ and 700 µl 10mM $MgCl_2$ after 30 min incubation at room temperature. The suspension was centrifuged for 12 min at 8000 rpm and 4 °C, and the supernatant was filtered through a 0.45 µm syringe filter to a 50 mL Falcon tube. The periplasmic extract was adjusted to 10 mM Tris-HCl pH 7.5 by adding 1 M Tris-HCl pH 7.5 prior to storage at 4 °C.

Samples from the sugar fraction, periplasmic extract, and the pellet were analyzed by lithium dodecyl sulfate-polyacrylamide gel electrophoresis (LDS-PAGE) to verify that the enzyme of interest indeed was in the periplasmic extract.

## 3.3 Lithium dodecyl sulfate-polyacrylamide gel electrophoresis (LDS-PAGE)

Lithium dodecyl sulfate-polyacrylamide gel electrophoresis (LDS-PAGE) is a method to separate proteins according to their molecular mass and assess protein purity. Protein separation by LDS-PAGE require denaturing conditions which is achieved by adding a reducing agent, dithiothreitol (DTT), and an anionic detergent, lithium dodecyl sulfate (LDS), to the protein solution and boiling the resulting solution. DTT reduces disulfide bonds and in combination with boiling the protein sample in presence of LDS, the protein becomes denatured and LDS binds to the protein conferring a negative charge that is proportional to the size of the protein. Large proteins have lower mobility through the polyacrylamide pores of the gel and separation occurs as the negatively charged proteins migrate

towards the anode. Protein size is determined by comparing the sample to a marker (BenchMark™ Protein Ladder) with proteins of known size. The gels used in this thesis are stain-free gels containing trihalo components that react with tryptophan residues in the protein and emit fluorescence when exposed to UV-light.

**Materials**

- Samples containing protein
- LDS buffer (2x)
    - 5 mL NuPAGE™ LDS sample buffer (4X)
    - 2 mL NuPAGE™ Sample Reducing Agent (10X)
    - 3 mL $dH_2O$
- Mini PROTEAN® TGX Stain-Free™ Gels
- Mini PROTEAN® Tetra Cell vertical mini gel electrophoresis system
- Tris-Glycine-SDS buffer (10x)
- PowerPac 300, power supply
- Stain-Free Sample Tray
- Gel Doc™ EZ Imager
- BenchMark™ Protein Ladder

**Method**

LDS-PAGE was performed using a Mini PROTEAN® TGX Stain-Free™ Gel mounted in a Mini PROTEAN® Tetra Cell vertical mini gel electrophoresis system. Prior to the analysis, LDS buffer was added, at a ratio of 1:1, to all protein samples before they were incubated at 98 °C for 5 min. A Mini PROTEAN® TGX Stain-Free™ Gel were loaded with 20 µL of boiled protein samples. Depending on how many samples were to be analyzed, one or two wells were loaded with 10 µL Benchmark™ Protein Ladder. The gel was placed in a The Tetra Cell vertical mini gel electrophoresis chamber, which was filled with Tris-Glycine-SDS (TGS) buffer diluted 1:10 with $dH_2O$. The electrophoresis system was connected to a Power Pac 300 power supply set to run for 19 min at 270 V. To image the gel in the Gel Doc™ EZ Imager, the gel was removed from the chamber and transferred to a Stain-free sample tray and inserted to a Gel Doc™ EZ Imager with UV illumination.

## 3.4 Protein Purification

Column chromatography is a commonly used protein purification technique which is based on mobility or affinity of a protein towards the stationary phase. The stationary phase contains polymer beads made of, e.g., agarose or acrylamide to which a functional group is attached. The functional group determines the type of interaction between the protein and the stationary phase, and specific proteins may show high affinity for the stationary phase at specific conditions.

### 3.4.1 Ion-Exchange Chromatography

Ion-Exchange Chromatography (IEX) separates proteins based on their net surface charge and allows separation of proteins with small charge differences providing high-resolution separation. The technique relies on reversible adsorption of charged proteins to a resin of opposite charge. The properties of the functional group determine the type and strength of interaction between the protein and the resin. Ion-exchange resins can be either cation exchangers, binding positively charged cations to a negatively charged resin, or anion exchangers, binding negatively charged anions to a positively charged resin. Depending on the protein's isoelectric point, pI, which is the pH where the net charge of the protein is zero, the conditions can be controlled to favor interaction between the protein and the stationary phase of the column. If the pH of the buffer is higher than the pI, the protein's net surface charge becomes negative and the protein can bind an anion-exchange resin while if the pH is lower than the pI, the protein's net surface charge becomes positive, and the protein will bind to an anionic resin used in cation-exchange. Proteins are separated based on the strength of their interaction with the resin and elution of the bound proteins is done by increasing the salt concentration in the buffer to elute the loosely bound proteins at low salt concentration and tightly bound proteins at high salt concentration.

**Materials**

- Periplasmic extract containing *Sc*AA10C (see section 3.2)
- ÄKTA Pure™ chromatography system
- HiTrap® DEAE Sepharose FF, 5 mL column
- Buffer A: 50 mM Tris-HCl, pH 7.5 (see section 2.7.2)
- Buffer B: 50 mM Tris-HCl with 1 M NaCl, pH 7.5 (see section 2.7.2)
- Fraction collector

**Method**

*Sc*AA10C was purified from the periplasmic extract on a 5 mL HiTrap® DEAE Sepharose FF column using an ÄKTA Pure™ chromatography system. The ÄKTA Pure™ system has a built-in flow cell with UV detection that continuously monitors protein elution at 280 nm. Before connecting the column, the system was washed with water. After connecting the column, it was washed with water and then equilibrated with buffer A to provide *Sc*AA10C with conditions favoring binding to the stationary phase. The protein solution was applied to the column using the system's sample pump at a flow rate of 1 mL/min. After the protein solution had been applied to the column, the system was returned to buffer A at a flow rate of 3 mL/min to elute non-binding proteins. When the UV signal stabilized, a linear gradient of NaCl from 0 M to 0.5 M NaCl over 100 min was applied using buffer B. 3 mL fractions were collected using a fraction collector and analyzed by LDS-PAGE. Fractions containing *Sc*AA10C were pooled and concentrated to less than 1 mL using an Amicon® Ultra-15 Centrifugal Filter with a molecular weight cut-off of 10 kDa, followed by Size-Exclusion chromatography as described in section 3.4.2.

### 3.4.2 Size-Exclusion Chromatography

Size-Exclusion Chromatography (SEC) separates proteins based on their size. The stationary phase is made up by tightly packed spherical beads containing pores of various sizes. The stationary phase provides a porous matrix where small proteins diffuse into small pores which are not accessible to larger proteins and are retained in the stationary phase longer than large proteins. In SEC, large proteins elute first and small proteins elute last.

**Materials**

- Concentrated protein sample from IEX (see section 3.4.1)
- ÄKTA™ Purifier chromatography system
- HiLoad™ 16/600 Superdex™ 75 grep grade column, 120 mL
- Running buffer: 50 mM Tris-HCl pH 7.5 supplemented with 150 mM NaCl (see section 2.7.3)

**Method**

*Sc*AA10C was purified in a second step using an ÄKTA Purifier equipped with a HiLoad™ 16/600 Superdex™ 75 grep grade column. The column was equilibrated with running buffer corresponding to at least two column volumes before loading the concentrated protein solution obtained after IEX onto the column via a 2 mL sample loop using a 1 mL syringe. After applying the protein sample to the

column, the flow of the running buffer was set to 1 mL/min. Protein elution was monitored at 280 nm using the built-in UV detector, and 2 mL fractions were collected using the fraction collector. Eluted fractions were analyzed by LDS-PAGE and fractions containing *Sc*AA10C were pooled and concentrated to less than 2 ml using an Amicon® Ultra-15 Centrifugal Filter MWCO. The solution with purified protein was stored at 4°C.

### 3.4.3 Chitin Affinity Chromatography

Chitin Affinity Chromatography utilizes chitin-binding enzymes to interact with a stationary phase consisting of chitin beads. Prior to purification, the enzyme solutions are treated with ammonium sulfate, which dehydrates the proteins to bind better to the chitin beads. By using acetic acid as elution buffer, the affinity between the chitin-binding proteins and the stationary phase is reduced, and the proteins elute. Affinity chromatography with chitin beads was performed to purify *Sm*AA10A and *Sm*ChiA.

**Materials**

- Periplasmic extract containing *Sm*AA10A or *Sm*ChiA (see section 3.2)
- BioLogic LP chromatography system
- Econo-column®, 1.0 x 10 cm, packed with chitin beads (New England Biolabs, NEB)
- Econo-column® flow adapter
- Ammonium sulfate (see section 2.2)
- Buffer A: 50 mM Tris-HCl, pH 8.0 with 1M Ammonium sulfate (see section 2.7.4)
- Buffer B: 20 mM acetic acid, pH 3.6 (see section 2.7.4)
- Falcon tube

**Method**

Affinity Chromatography was performed using a low-pressure BioLogic LP chromatography system with a Econo-column®, 1.0 x 10 cm, packed with chitin beads connected to a Econo-column® flow adapter. Prior to the separation, the periplasmic extract (see section 3.2) was supplemented with ammonium sulfate corresponding to 1 M. The column was equilibrated with buffer A using a flow rate of 2 ml/min. The flow rate was changed to 1 ml/min while the periplasmic extract was loaded onto the column with buffer A as a mobile phase. As the chromatography system has an inbuilt $A_{280}$ detector, the absorption of flow-through material was measured during the purification. When the detector showed a stable signal, Buffer B was added to elute the proteins and the eluate was collected in a falcon tube. The purified proteins were analyzed by LDS-PAGE (see section 3.3) and

further concentrated to less than 10 ml using an Amicon® Ultra-15 Centrifugal Filter. The concentrated protein solution was buffer exchanged with 20 mM sodium phosphate pH 6.0. The concentrated protein solutions were stored at 4°C.

## 3.5 Copper saturation of *Sc*AA10C and *Sm*AA10A

LPMOs are copper-dependent metalloenzymes with a histidine brace active site which requires a copper co-factor for catalytic activity. To ensure that all active sites harbor a copper atom, LPMOs were copper saturated using Cu(II)$SO_4$ in a three-fold molar excess to the protein. The unbound copper was removed from the protein fraction in a desalting step, using a desalting column.

**Materials**

- Purified *Sc*AA10C or *Sm*AA10A (see section 3.4)
- PD MidiTrap™ column with Sephadex G-25 resin
- Equilibration buffer: 20 mM sodium phosphate, pH 6.0 (see section 2.7)
- 15 mM Cu(II)$SO_4$ (see section 2.2)
- 20% EtOH
- $dH_2O$

**Method**

The copper saturation protocol was performed similarly for *Sc*AA10C and *Sm*AA10A. Cu(II)$SO_4$ was added in a 3:1 molar ration to a 100 µL LPMO solution followed by incubation for 15 min at room temperature. Then, the excess unbound copper was removed by desalting using a PD MidiTrap™ G-25 column. Prior to loading the copper saturated protein solution, the column was washed with three column volumes (CVs) of equilibration buffer (15 mL). After the equilibration buffer had completely entered the column material, the copper saturated protein solution (approximately 110 µL) was applied to the column. Once the protein solution had completely entered the packed bed, 890 µL of the equilibration buffer was applied as the PD MidiTrap™ G-25 columns require a total sample volume of 1 mL. The protein was eluted in 1 mL equilibration buffer and collected in an Eppendorf tube. The protein concentration was determined by $A_{280}$ (see section 3.6).

## 3.6 Protein concentration determination by $A_{280}$

Protein concentration determination by $A_{280}$ is an effective and convenient method for proteins containing tryptophan and tyrosine, as the method utilities the ability of these residues to absorb light at a wavelength of 280 nm. A light source emits light energy through the samples, and further into a detector that calculates the amount of light passing through the sample. Beer-Lambert's law helps determining the protein concentration. This law states that the protein concentration of a sample is proportional to the absorbance and is given in equation 1,

$$A = \varepsilon \cdot l \cdot c \quad (1)$$

where A is referred to as the absorbance, $\varepsilon$ is the extinction coefficient of the solute (proteins in this case; **Table 8)**, l is the optical path length and c is the protein concentration.

**Table 8: Theoretical extinction coefficients for *Sc*AA10C, *Sm*AA10A, and *Sm*ChiA**

| Protein | Extinction coefficient, $M^{-1}cm^{-1}$ |
|---|---|
| *Sc*AA10C | 75775 |
| *Sm*AA10A | 35200 |
| *Sm*ChiA | 107500 |

**Materials**

- BioPhotometer® D30
- Uvette® disposable cuvettes, 1 cm
- Protein solution of interest

**Method**

The protein concentration determining protocol was performed similarly for *Sc*AA10C, *Sm*AA10A, and *Sm*ChiA. Protein solutions were diluted with 20 mM sodium phosphate buffer to ensure an A below 1.0. Then the same buffer was transferred to an Uvette® disposable cuvette and measured as a blank sample by BioPhotometer®. Thereafter, protein samples were transferred to Uvette® disposable cuvettes and inserted into the BioPhotometer®. All samples were measured at $A_{280}$ and the protein concentrations were calculated using equation 1 and the extinction factor for the respective protein shown in **Table 8.**

## 3.7 Photocatalyst preparation

Pupal exuviae obtained from Dr. Thomas Hahn at the Fraunhofer Institute (Stuttgart, Germany) were used as photocatalyst in photobiocatalytic reactions with LPMOs. The raw material contains approximately 1% lipids, 23-25% chitin, 10% catechols, 16% minerals and 23-30% proteins as determined by Dr. Thomas Hahn. The pupal exuviae had been milled and sieved (0.85 mm) by Eirik G. Kommedal prior to the work presented in this thesis and further referred to as FMC, for Fine Milled Cocoon.

To ensure that only the insoluble component of FMC was added to the photobiocatalytic reactions, the FMC was washed to remove soluble components. To determine the amount of washing steps required, the absorbance of the supernatant after washing was measured spectrophotometrically in the range of 240 – 800 nm and washing was determined as sufficient when the absorbance spectra were superposed.

**Materials**

- Cary 60 UV-Vis
- Glass cuvette, 1 cm
- Fine Milled Cocoon (FMC) powder

**Method**

50 g/L FMC was prepared by suspending 50 mg FMC powder in 1 mL $dH_2O$. Then 200 µL 50 g/L FMC was transferred to an Eppendorf tube to which 800 µL 50 mM sodium phosphate pH 6.0 was added before centrifuging at 15000 g for 2 min. The absorbance of the supernatant was measured by Cary 60 UV-Vis in the range of 240 – 800 nm (50 mM sodium phosphate was measured as a blank sample). The remaining pellet was resuspended in 1 mL 50 mM sodium phosphate pH 6.0 and centrifuged at 15000 g for another 2 min. This procedure was repeated until the absorbance spectra of the measurements were superposed, i.e., four times. The pellet obtained after the last centrifugation step was resuspended in $dH_2O$ to 20 g/L. Stock suspensions of FMC were prepared fresh every day.

## 3.8 Activity assays – Degradation of cellulose

Previous studies have used *Sc*AA10C as a model enzyme for photobiocatalytic cellulose degradation. Chlorophyllin, V-$TiO_2$ and lignin have been used as photocatalysts to boost the enzymatic activity of *Sc*AA10C on cellulose (Canella et al., 2016; Bissaro et al., 2016b). In this study, reactions were performed with fine milled cocoon powder (FMC) from pupal exuviae of *Hermetica illucens* to investigate if its content of insoluble catechols could drive *Sc*AA10C activity on Avicel. Reaction conditions were varied to observe the effect of individual reaction parameters on LPMO activity, including the light intensity, and the concentrations of FMC, *Sc*AA10C, and Avicel. Reactions containing superoxide dismutase (SOD) were performed to probe the role of superoxide in these reactions. All reactions were performed in triplicates except for the reactions with SOD which were performed as single replicates.

### 3.8.1 Standard reaction conditions

Hamamatsu Lightning Cure Spotlight source LC8 model L9588, equipped with an L9588-03 filter was used as light source in this work. This filter only allows light between 400 and 700 nm to pass. All reactions, unless otherwise specified, were carried out as 500 µL reactions at 40°C in 1 mL glass vials (Reacti-Vial™) with magnetic stirring and illuminated by visible light from an optic fiber cable positioned approximately 1 cm above the liquid in the reaction vial. Reactions were pre-incubated for 15 min before addition of *Sc*AA10C or turning on the light to start the reactions. The standard conditions used, unless otherwise specified, were 0.5 µM *Sc*AA10C, 50 mM sodium phosphate buffer pH 6.0, 1 g/L FMC, 10 g/L Avicel and a light intensity of 10% $I_{max}$ (approx. 16.8 $mW.cm^{-2}$). 60 µL sample aliquots were taken at regular intervals and filtered, using a 96- well filter plate operated with a vacuum manifold, to stop the reactions. Filtered samples (35 µL) were stored at -20°C prior to High-Performance Anion-Exchange Chromatography with Pulsed Amperometric Detection (HPAEC-PAD) for product analysis (section 3.9).

Before characterizing FMC as photocatalyst in reactions with *Sc*AA10C as model cellulolytic enzyme, reactions at different pH (6.0, 7.0, 8.0) for different FMC concentrations (0.1, 1, 10 g/L) were performed with and without light-exposure (In contrast to all other reactions, the FMC used in reactions for determining pH effect was unwashed). The pH that resulted in the largest increase of produced LPMO products in light-exposed reactions compared to reactions performed in dark, were chosen as the standard pH for further studies. These reactions were carried out in sodium phosphate buffer (50 mM, varying pH) with FMC (varying concentrations), *Sc*AA10C (0.5 µM), and Avicel (10 g/L), and were

exposed to I=10% $I_{max}$ (approx. 16.8 mW.cm$^{-2}$). In addition, negative control reactions without LPMO were performed for the highest photocatalyst concentration, 10 g/L FMC, for each pH condition.

### 3.8.2 The effect of the FMC concentration

To determine the effect of FMC on LPMO activity, reactions with increasing concentrations of FMC (0, 0.5, 1, 2.5, and 5 g/L) were performed in triplicate. 600 µL was used as the total reaction volume, and 60 µL sample aliquots were removed and filtrated after 1, 2, 4, 8, and 24 h. 35 µL filtrate was recovered and stored in Eppendorf tubes at -20°C. Before HPAEC-PAD analysis, the samples were thawed on ice and treated with *Tf*Cel6A to convert soluble oxidized cello-oligosaccharides to a mixture of cellobionic acid and cellotrionic acid. See section 3.9 for details.

### 3.8.3 The effect of the LPMO concentration

To determine the effect of LPMO concentration towards LPMO activity, reactions with increasing concentrations of LPMO (0, 0.05, 0.1, 0.25, and 2.5 µM) were performed in triplicate. 600 µL was used as the total reaction volume, and 60 µL sample aliquots were removed and filtrated after 1, 2, 4, 8, and 24 h. 35 µL filtrate was recovered and stored in Eppendorf tubes at -20°C. Before HPAEC-PAD analysis, the samples were thawed on ice and treated with *Tf*Cel6A to convert soluble oxidized cello-oligosaccharides to a mixture of cellobionic acid and cellotrionic acid. See section 3.9 for details.

### 3.8.4 The effect of the Avicel concentration

To determine the effect of Avicel on LPMO activity, reactions with increasing concentrations of Avicel (0, 5, 20, and 40 g/L) were performed in triplicate. 600 µL was used as the total reaction volume, and 60 µL sample aliquots were removed and filtrated after 1, 2, 4, 8, and 24 h. 35 µL filtrate was recovered and stored in Eppendorf tubes at -20°C. Before HPAEC-PAD analysis, the samples were thawed on ice and treated with *Tf*Cel6A to convert soluble oxidized cello-oligosaccharides to a mixture of cellobionic acid and cellotrionic acid. See section 3.9 for details.

### 3.8.5 The effect of light intensity and SOD

To determine the effect of light on LPMO activity, reactions with increasing light intensities (0, 1, 3, 10, and 30% of $I_{max}$ corresponding to 0, 1.7, 5.0, 16.8, 50.4 W/cm$^2$, respectively.) were performed in triplicate. 600 µL was used as the total reaction volume, and 60 µL sample aliquots were removed and filtrated after 1, 2, 4, 8, and 24 h. 35 µL filtrate was recovered and stored in Eppendorf tubes at -20°C. Before HPAEC-PAD analysis, the samples were thawed on ice and treated with *Tf*Cel6A to

convert soluble oxidized cello-oligosaccharides to a mixture of cellobionic acid and cellotrionic acid. See section 3.9 for details.

To determine the role of superoxide in LPMO reactions, additional reactions including 0.5 µM SOD were performed in single replicas for each light intensity. 600 µL was used as the total reaction volume, and 60 µL sample aliquots were removed and filtrated after 1, 2, 4, 8, and 24 h. 35 µL filtrate was recovered and stored in Eppendorf tubes at -20°C. Before HPAEC-PAD analysis, the samples were thawed on ice and treated with *Tf*Cel6A to convert soluble oxidized cello-oligosaccharides to a mixture of cellobionic acid and cellotrionic acid. See section 3.9 for details.

### 3.8.6 Control reactions

As described in section 3.7, FMC was washed to ensure that oxidized products upon decomposition of cellulose occurred only due to insoluble components from the powder. Triplicate control reactions were performed where the washed FMC was replaced with "washing water" (i.e., the centrifugate) from the first round of centrifugation in step 3.7. The reactions were performed to investigate if any soluble component from the powder possibly could contribute to LPMO activity. Another reaction with the same “wash water” was performed without LPMO as a negative control reaction.

To investigate if the “washing water” from the fourth round of centrifugation would contribute to LPMO activity, an additional reaction using the fourth supernatant was performed in a single replica. Another single reaction with free copper replacing the LPMOs was performed to confirm that free copper alone does not degrade cellulose. 600 µL was used as the total reaction volume for all reactions, and 60 µL sample aliquots were removed and filtrated after 1, 2, 4, 8, and 24 h. 35 µL filtrate was recovered and stored in Eppendorf tubes at -20°C. Before HPAEC-PAD analysis, the samples were thawed on ice and treated with *Tf*Cel6A to convert soluble oxidizedncello-oligosaccharides to a mixture of cellobionic acid and cellotrionic acid. See section 3.9 for details.

## 3.9 High-Performance Anion-Exchange Chromatography with Pulsed Amperometric Detection analysis

### 3.9.1 Preparation of samples

Filtrated samples from *Sc*AA10C reactions were analyzed using High-Performance Anion-Exchange Chromatography with Pulsed Amperometric Detection (HPAEC-PAD) to determine the content of oxidized products. The samples only contained soluble oligosaccharides produced during the reaction time as the reactions were stopped by filtration. To convert the oligosaccharides of various degree of polymerization to di- and trisaccharides, the samples were treated with a solution of an endoglucanase (*Tf*Cel6A). *Tf*Cel6A fragmentates oxidized LPMO products to smaller oxidized oligomers (GlcGlc1A and $Glc_2Glc1A$; Courtade et al., 2018). Peaks of GlcGlc1A and $Glc_2Glc1A$ were analyzed using the Chromeleon® 7 Chromatography Data system software, integrated and converted to concentrations by using a standard curve (see below). The treatment with *Tf*Cel6A produces large amounts of cellobiose, but these will not be detected during the HPAEC-PAD as they do not have the same acidic properties as the oxidized products.

Standard solutions of GlcGlc1A with known concentrations (10, 20, 50, 100, and 200 µM) were used to generate a standard curve needed to calculate and quantify the concentrations of cellobionic acid (GlcGlc1A) in samples from *Sc*AA10C reactions. The concentration of cellotrionic acid ($Glc_2Glc1A$) was quantified by using a single point from a standard solution of $Glc_2Glc1A$ with known concentration (50 µM). A standard solution with $Glc_1$-$Glc_5$ (0.001 g/L) was analyzed to verify that the HPAEC-PAD system separated the products in solution properly. Depending on how many samples were to be analyzed in the same sequence, the standards were analyzed in duplicates or triplicates.

**Materials**

- Filtered samples from *Sc*AA10C reactions (see section 3.8)
- 2 µM *Tf*Cel6A
- 50 mM sodium phosphate, pH 6.0 (see section 2.7)
- $Glc_1$-$Glc_5$ standard solutions (0.001 g/L)
- GlcGlc1A standard solution (10, 20, 50, 100, 200 µM)
- $Glc_2Glc1A$ standard solution (50 µM)

**Method**

Filtrated samples from *Sc*AA10C reactions (see section 3.8) were thawed on ice. *Tf*Cel6A diluted in 50 mM sodium phosphate, pH 6.0 was added to the reaction sample to a final concentration of 1 µM and a total volume of 70 µL. The solutions were centrifuged for 2 min at 15000 g and incubated overnight at 37 °C. The next day, 60 µL of incubated samples were transferred to separate snap ring micro vials. $dH_2O$ and standards with known concentrations of $GlcGlc_1A$ (10, 20, 50, 100 and 200 µM), $Glc_2Glc_1A$ (50 µM) and $Glc_1$-$Glc_5$ (0.001 g/L) were thawed on ice and transferred to snap ring micro vials (120 or 170 µL depending on the number of samples to be run). All vials were sealed with a blue snap ring cap and placed in an ICS tray and inserted to the chromatograph. Samples from 24 h reactions were diluted 1:7 prior to adding the *Tf*Cel6A solution.

### 3.9.2 High-Performance Anion-Exchange Chromatography with Pulsed Amperometric Detection analysis

High-Performance Anion-Exchange Chromatography (HPAEC) was used to analyze oxidized products from LPMOs (see section 3.8). This method is based on the weak acid properties of carbohydrates. Usually, carbohydrates display $pK_a$ values around 12-14. By exposing carbohydrates to a pH in this alkaline range, the carbohydrates achieve a negative charge in that the hydroxyl groups release a proton and become oxyanions. As a negatively charged molecule, the carbohydrate will bind to a positively charged column material. To maintain affinity for the column, HPAEC is usually run in 0.1 M NaOH. Elution is achieved by adding NaOAc, which decreases carbohydrate affinity to the column.

The Pulsed Amperometric Detection (PAD) system can be applied to HPAEC to detect oligosaccharides by size. Detection involves a gold electrode that oxidizes the negatively charged groups on the carbohydrates, while generating a measurable current. The current generated is proportional to the concentration of oxidized polysaccharides. It can thus be directly converted to the concentration of products.

**Materials**

- Dionex™ ICS-5000 system
- Dionex™ CarboPac™ PA200 column
- Eluent A: 0.1 M NaOH (see section 2.7.5)
- Eluent B: 1 M NaOAc + 0.1 M NaOH (see section 2.7.5)
- Eluent C: $dH_2O$ (see section 2.7.5)

**Method**

Oxidized products from *Sc*AA10C reaction samples were analyzed using DionexTM ICS-5000 system coupled to a PAD detection system. Prior to the analysis, the column was washed with eluent C and equilibrated with eluent A. The operating flow rate was set to 0.5 mL/min and the sample injection was set to 50 µL. All runs had a run time of 18 min where oligosaccharides were separated by applying a gradient of eluents A (0.1 M NaOH) and B (1 M NaOAc + 0.1 M NaOH), as follows: After sample injection (at 100 % A), 100 % A was linearly adjusted to 90 % A and 10 % B over 5 min. Over the next 5 min, the eluents were linearly adjusted to 82 % A and 18 % B and further to 70 % A and 30 % B over the next 0.5 min. Then, the eluent was adjusted to 100 % B over 0.5 min, before returning to 100 % A over 0.05 min, after which the gradient was held for 6.95 min, for equilibration prior to the next injection. Eluted products were detected by the PAD detection system and recorded using the Chromeleon® 7 Chromatography Data system software.

## 3.10 Amplex red assay for detection of $H_2O_2$

The amplex red assay, used to measure the amount of $H_2O_2$ generated by light-exposed FMC under various conditions was based on the approach described by Kittl et al. (2012). In the presence of amplex red and hydrogen peroxide, horseradish peroxidase (HRP) converts amplex red to resorufin stoichiometrically (Kittl et al., 2012). Resorufin is a fluorescent molecule and can be monitored spectrophotometrically by fluorescence, with 590 nm as emission wavelength and 530 nm as excitation wavelength.

### 3.10.1 Standard reaction conditions

Hamamatsu Lightning Cure Spotlight source LC8 model L9588, equipped with an L9588-03 filter was used as light source in this work. All reactions, unless otherwise specified, were carried out as 600 µL reactions at 40°C in 1 mL glass vials (Reacti-Vial™) with magnetic stirring and illuminated by visible light from an optic fiber cable positioned approximately 1 cm above the liquid in the reaction vial. Reactions were pre-incubated for 15 min before addition of *Sc*AA10C or turning on the light to start the reactions. The standard conditions used, unless otherwise specified, were 0.5 µM *Sc*AA10C, 50 mM sodium phosphate buffer pH 6.0, 1 g/L FMC, 10 g/L Avicel and a light intensity of 10% $I_{max}$ (approx. 16.8 $mW.cm^{-2}$). The total reaction volume was 600 µL and 125 µL sample aliquots were taken after 0.5 and 1 hour, using a 96-well filter plate operated with a vacuum manifold, to stop the reactions. All reactions were performed in triplicates and in the presence of light.

In addition, one reaction sample for each triplicate was performed with the same content except from the FMC concentration, which was 5 g/L. These reactions were not exposed to any light source, and the whole reaction solution was filtered after 2 min. These samples were used when analyzing the $H_2O_2$ standards to maintain similar conditions as the analyzed reactions.

### 3.10.2 The effect of LPMO, in the presence or absence of Avicel

To determine the effect of LPMO and Avicel on generation of $H_2O_2$, reactions were performed in the presence or absence of Avicel, in triplicate. 600 µL was used as the total reaction volume, and 125 µL sample aliquots were removed and filtrated after 0.5 and 1 h. 100 µL filtrate was directly used to prepare samples for detection of $H_2O_2$ by the amplex red assay, using a Varioskan™ LUX multimode microplate reader for signal detection. See section 3.10.6 for details.

### 3.10.3 The effect of free Cu(II), in the presence or absence of Avicel

To determine the effect of free copper and Avicel on generation of $H_2O_2$, reactions were performed in the presence or absence of Avicel replacing *Sc*AA10C with 0.5 µM Cu(II)$SO_4$, in triplicate. 600 µL was used as the total reaction volume, and 125 µL sample aliquots were removed and filtrated after 0.5 and 1 h. 100 µL filtrate was directly used to prepare samples for detection of $H_2O_2$ by the amplex red assay, using a Varioskan™ LUX multimode microplate reader for signal detection. See section 3.10.6 for details.

### 3.10.4 The effect of the Avicel concentration

To determine the effect of Avicel on generation of $H_2O_2$, reactions were performed with increasing concentrations of Avicel (0, 5, 10, and 20 g/L) in the absence of *Sc*AA10A, n triplicate. 600 µL was used as the total reaction volume, and 125 µL sample aliquots were removed and filtrated after 0.5 and 1 h. 100 µL filtrate was directly used to prepare samples for detection of $H_2O_2$ by the amplex red assay, using a Varioskan™ LUX multimode microplate reader for signal detection. See section 3.10.6 for details.

### 3.10.5 The effect of SOD

To determine the role of SOD on $H_2O_2$ generation, reactions were performed with 0.1 µM and 1 µM SOD in the absence of *Sc*AA10A, in triplicate. 600 µL was used as the total reaction volume, and 125 µL sample aliquots were removed and filtrated after 0.5 and 1 h. 100 µL filtrate was directly used to prepare samples for detection of $H_2O_2$ by the amplex red assay, using a Varioskan™ LUX multimode microplate reader for signal detection. See section 3.10.6 for details.

### 3.10.6 Sample preparation and Amplex red analysis

Filtered samples were immediately mixed, directly in the microtiter plate, with a premix containing HRP and Amplex Red. After the mixing plate was analyzed using Varioskan™ LUX, the concentration of $H_2O_2$ was determined using an $H_2O_2$ standard curve.

**Materials**

- Reaction samples from 3.10.1-3.10.5
- Varioskan™ LUX multimode microplate reader
- Nunc™ MicroWell™ 96-Well, black
- $H_2O_2$ standard solutions (0, 1, 2, 5, and 10 µM)
- Amplex® Red (10 mM stock solution)
- HRP (1 g/L stock solution)
- 0.5 M Sodium Phosphate buffer, pH 6.0 (see section 2.7)

**Method**

Samples were prepared in a black Nunc™ MicroWell™ 96-Well plate. 100 µL of reaction sample filtrate were added to separate wells with 20 µL $dH_2O$. Five wells were prepared by adding 20 µL of filtrated sample with 5 g/L FMC performed in dark (associated to the reaction samples) and 100 µL $H_2O_2$ standard solutions (0, 1, 2, 5, and 10 µM). Finally, 80 µL of a premix of Amplex® Red, HRP and sodium phosphate pH 6.0 were added to all wells to the final concentrations of 0.1 mM, 19 mg/L, and 50 mM, respectively. The Nunc™ MicroWell™ 96-Well was placed in the Varioskan™ LUX multimode microplate reader which was set to measure fluorescence emitted at 590 nm from excitation at 530 nm. Prior to recording fluorescence, the plate was shaken at 600 rpm for 30 s and incubated for 5 min. Each sample was measured every 30 s for 10 min using SkanIt™ Software for Microplate Readers. The $H_2O_2$ standard solutions made the basis of a standard curve, which was used to determine the concentrations of $H_2O_2$ in samples.

## 3.11 Activity assay – Degradation of chitin

Due to limited time, single replicate reactions containing either *Sm*AA10A or *Sm*ChiA were performed using FMC or β-chitin as substrate. In addition, reactions containing both *Sm*AA10A and *Sm*ChiA were set up to investigate a synergy.

### 3.11.1 Standard reaction conditions

Hamamatsu Lightning Cure Spotlight source LC8 model L9588, equipped with an L9588-03 filter was used as light source in this work. This filter only allows light between 400 and 700 nm to pass. All reactions were carried out as 500 µL reactions at 40°C in 1 mL glass vials (Reacti-Vial™) with magnetic stirring and illuminated by visible light from an optic fiber cable positioned approximately 1 cm above the liquid in the reaction vial. The standard conditions used in the reactions were 50 mM sodium phosphate buffer pH 6.0, 5 g/L FMC, 1 µM enzyme (*Sm*AA10A/*Sm*ChiA), 5 g/L β-chitin, and a light intensity of 10% $I_{max}$ (approx. 16.8 $mW.cm^{-2}$). Reactions were pre-incubated for 15 min before addition of *Sm*AA10A and/or *Sm*ChiA and turning on the light to start the reactions. All reactions were carried out in the presence and absence of light.

### 3.11.2 Reactions with *Sm*AA10A

To investigate if FMC is able to drive oxidative degradation of chitin by *Sm*AA10A, four reactions were performed with one replicate. One reaction contained FMC, *Sm*AA10C, and β-chitin. The other three reactions were performed in the absence of *Sm*AA10A, β-chitin, or both. All reactions were carried out in the presence and absence of light. 500 µL was used as the total reaction volume, and 50 µL sample aliquots were removed and filtrated after 1, 2, 3, and 4 h. The filtrates were recovered and stored in Eppendorf tubes at -20°C. Before product analysis by HILIC (see below), the samples were thawed on ice. See section 3.12 for details.

### 3.11.3 Reactions with *Sm*ChiA

To investigate the capability of *Sm*ChiA to degrade chitin, four reactions were performed with one replicate. One reaction contained FMC, *Sm*ChiA, and β-chitin. The other three reactions were performed in the absence of *Sm*ChiA, β-chitin, or both. All reactions were carried out in the presence and absence of light. 500 µL was used as the total reaction volume, and 50 µL sample aliquots were removed and filtrated after 1, 2, 3, and 4 h. 25 µL filtrate were recovered and stored with 25 µL 50mM $H_2SO_4$ in Eppendorf tubes at -20°C. Before product analysis by HPLC (see below), the samples were thawed on ice. See section 3.13 for details.

### 3.11.4 Synergy reactions with *Sm*AA10A and *Sm*ChiA

To investigate the synergetic effect of *Sm*AA10A catalyzed by FMC and *Sm*ChiA to degrade chitin, two reactions were performed with one replicate. One reaction contained FMC, *Sm*AA10C, *Sm*ChiA and β-chitin. The other reaction was performed in the absence of β-chitin. All reactions were carried out in the presence and absence of light. 500 µL was used as the total reaction volume, and 50 µL sample aliquots were removed and filtrated after 1, 2, 3, and 4 h. 25 µL filtrate were recovered and stored with 25 µL 50mM $H_2SO_4$ in Eppendorf tubes at -20°C. Before product analysis by HPLC (see below), the samples were thawed on ice. See section 3.13 for details.

## 3.12 Hydrophilic Interaction Liquid Chromatography

### 3.12.1 Preparation of samples

Samples from the photobiocatalytic reactions containing only *Sm*AA10A (see section 3.11.2) were qualitatively analyzed by Hydrophilic Interaction Liquid Chromatography (HILIC) to analyze oxidized chito-oligosaccharides. Only solubilized oxidized chito-oligosaccharides were analyzed since the reactions were filtrated to stop the reaction. Prior to analysis, the filtered samples were adjusted to 74% acetonitrile. The chromatogram for each sample was compared to a chromatogram containing a mixture of oxidized chito-oligosaccharides with a degree of polymerization ranging from 2 to 6 (kindly provided by Tina Tuveng). A sample containing only the reaction buffer was also prepared to provide baseline subtraction. The chito-oligosaccharide standard and the sodium phosphate buffer were analyzed four times during the HILIC analysis.

**Materials**

- Filtered samples from *Sm*AA10A reactions (see section 3.11.2)
- 100 % Acetonitrile
- $NAG_2^{ox}$-$NAG_6^{ox}$ standard solution (50 µM)

**Method**

Filtered samples from *Sm*AA10A reactions were thawed on ice, and 26 µL sample was mixed with 74 µL 100 % acetonitrile before being transferred to snap ring micro vials. In addition, $dH_2O$, 50 mM sodium phosphate buffer pH 6.0, and a $NAG_2^{ox}$-$NAG_6^{ox}$ standard solution were added to snap ring micro vials and adjusted with 100 % acetonitrile to 74 % acetonitrile, as for the samples containing LPMO reaction products. All vials were sealed with a red snap ring cap, placed in an UPLC tray, and inserted to the chromatograph

### 3.12.2 Hydrophilic Interaction Liquid Chromatography

Hydrophilic Interaction Liquid Chromatography (HILIC) is a method used to separate and identify hydrophilic components in solution. The method is based on the affinity of hydrophilic components to bind to a column and adding a hydrophobic mobile phase. Increased polarity of analytes increases the affinity and the retention time. A UV-detector records the absorbance of the eluting samples, which forms a chromatogram in Chromeleon® 7 Chromatography Data system software. When performing quantitative analysis, peaks from the chromatogram are integrated and solute concentrations are calculated using chromatograms for standard solutions of known concentrations.

**Materials**

- Samples from *Sm*AA10A reactions adjusted to 74 % acetonitrile (See section 3.12.1)
- Agilent Infinity 1290 UPLC system
- Acquity BEH Amide column (130 Å, 1.7 µm, 2.1x150 mm) combined with a VanGuard precolumn
- Eluent A: 15mM Tris-HCl, pH 8.0 (see section 2.7.6)
- Eluent B: 100 % Acetonitrile (see section 2.7.6)

**Method**

Qualitative analysis of LPMO reaction products was performed using an Agilent Infinity 1290 UPLC system equipped with an Acquity BEH Amide column combined with a VanGuard precolumn. The operating flow rate was set to 0.4 mL/min and the sample injection was set to 10 µL. All runs had a run time of 12 min and the oxidized chito-oligosaccharides were separated by size using a gradient of eluents A (15mM Tris-HCl, pH 8.0) and B (100 % acetonitrile) according to the following steps: starting conditions, 26 % A, 74 % of B, for 5 min. For the next 2 mins, eluent B was linearly decreased to 62 % and kept at 62 % for 1 min before increasing back to 74 % B over 2 min. 74 % B was kept for 2 min to prepare the column for the next injection. Eluted products were detected by $A_{205}$ and signals were recorded and analyzed using the Chromeleon® 7 Chromatography Data system software.

## 3.13 High Pressure Liquid Chromatography with Rezex Fast Acid H+

### 3.13.1 Preparation of samples

Filtered samples from *Sm*ChiA and *Sm*ChiA with *Sm*AA10A reactions were analyzed using Rapid Separation Liquid Chromatography (RSLC) with a Rezex Fast Acid H+ column to determine the content of non-oxidized products from chitin degradation. Reactions were stopped at regular intervals by filtration to separate the insoluble fraction from the soluble fraction, and $H_2SO_4$ was added to the filtrate (see section 3.11.3 and 3.11.4). Reactions with *Sm*ChiA yield a mixture of native NAG and $NAG_2$. NAG and $NAG_2$ were injected as separate standards to which the chromatograms from the enzymatic reactions were compared. Peaks corresponding to NAG and $NAG_2$ were integrated and summed up to estimate the total amount of solubilized NAG equivalents. LPMO reactions were performed with one replicate, while the standards used for identifying reaction products were analyzed as triplicates. Samples from reactions containing *Sm*ChiA and β-chitin were diluted ten-fold prior to analysis.

**Materials**

- Filtered samples from *Sm*ChiA / *Sm*ChiA and *Sm*AA10A reactions (see section 3.11.3-3.11.4)
- 10 µM NAG standard solution
- 20 µM $NAG_2$ standard solution

**Method**

Filtered samples from *Sm*ChiA reactions with or without *Sm*AA10A reactions (see section 3.11.3 and 3.11.4) were thawed on ice and transferred to snap ring micro vials. In addition, 60 µL $dH_2O$ and standards containing NAG and $NAG_2$ were thawed on ice and transferred to snap ring micro vials. All vials were sealed with a red snap ring cap and placed in an RSLC tray. Samples containing β-chitin and *Sm*ChiA were diluted in a 1:10 ratio.

### 3.13.2 Rapid Separation Liquid Chromatography with Rezex Fast Acid H+

Rapid Separation Liquid Chromatography (RSLC) with a Rezex column is a fast and suitable method to analyze monomers and dimers of NAG. Ionic and non-ionic analytes in solution are separated as a charged Rezex column repels ionic species, leading to an early elution. Non-ionic components, such as NAG and $NAG_2$, are more retained by the column and will have a higher retention time. The elution of analytes is isocratic, meaning that the mobile phase is constant. In this study, eluted analytes were detected by UV absorption.

**Materials**

- Prepared samples from *Sm*ChiA / *Sm*ChiA and *Sm*AA10A reactions (see section 3.13.1)
- Dionex™ Ultimate™ 3000 RSLC system
- Rezex™ RFQ-Fast Acid H+(8 %) column, 7.8 x 100 mm
- Running buffer: 5 mM $H_2SO_4$ (see section 2.7.7)

**Method**

Native chito-oligosaccharide products from reactions with *Sm*ChiA with or without *Sm*AA10A were analyzed using a Dionex Ultimate 3000 RSLC system equipped with a 7.8 x 100 mm Rezex RFQ-Fast Acid H+(8%) column. The operating flow rate was set to 1 mL/min, the column temperature was set to 85 °C and sample injection was set to 8 µL. All runs had a runtime of 6 min with a constant flow of 5 mM $H_2SO_4$. Eluted products were detected by $A_{194}$ and signals were recorded and analyzed using the Chromeleon® 7 Chromatography Data system software.

# 4. Results

## 4.1 Periplasmic extraction

LB-medium supplemented with 100 µg/ml ampicillin was inoculated with bacterial strains expressing either *Sc*AA10C, *Sm*AA10A, or *Sm*ChiA and incubated overnight at 37 °C with shaking in a baffled Erlenmeyer flask. The cells were harvested by centrifugation and the resulting cell pellet was subject to a periplasmatic extraction resulting in a periplasmic extract and a pellet. The periplasmic extract and the associated pellet were analyzed by LDS-PAGE to verify that the enzymes were primarily present in the periplasmic extract. **Figure 11 A** and **B** display marked protein bands at approximately 40 kDa for *Sc*AA10C, 18 kDa for *Sm*AA10A, and 60 kDa for *Sm*ChiA in the periplasmic extracts, while these bands are absent in the pellet fraction, indicating a successful protein extraction.

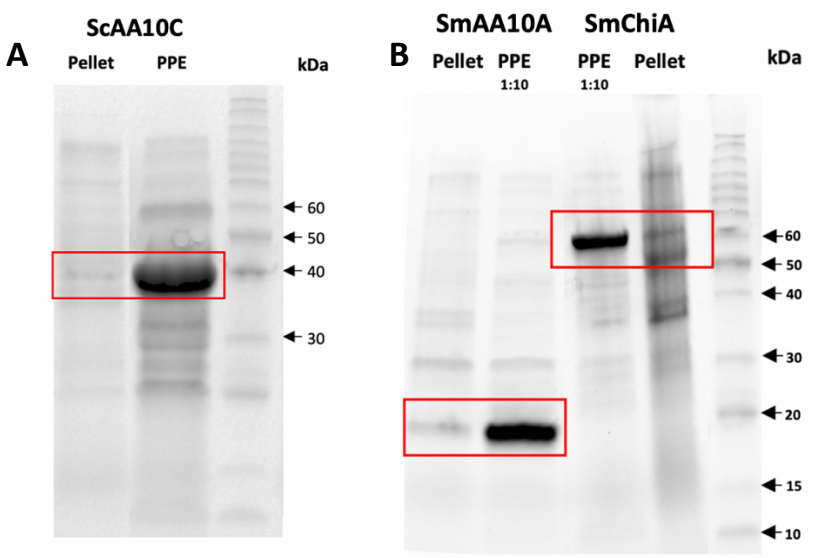


**Figure 11. LDS-PAGE analysis of periplasmic extracts.** The right lane in both gel images contains the Benchmark™ Protein Ladder, which helps estimate protein size in other samples from the same gel. **A:** the well with PPE represents the supernatant obtained after periplasmic extraction and displays a clear protein band around 40 kDa, which corresponds to *Sc*AA10C, and is indicated by a red square. **B:** PPE from *Sm*ChiA and *Sm*AA10A represent the supernatants from the respective periplasmatic extractions and display clear bands around 60 kDa and 18 kDa, respectively, as indicated by red squares. The PPE from both *Sm*ChiA and *Sm*AA10A were diluted 10 times. Sample buffer was added to all samples before application to the gel.

## 4.2 Purification of *Sc*AA10C

After periplasmic extraction, *Sc*AA10C was purified in two steps, using Ion-Exchange Chromatography (IEX), followed by Size-Exclusion Chromatography (SEC). During IEX proteins were eluted by applying an NaCl gradient from 0 to 50 % over 100 min. Protein elution was monitored continuously, and fractions were collected. A selection of fractions from the second peak, indicated by a blue arrow in **Figure 12A** were analyzed by LDS-PAGE (**Figure 12B**). The collected fractions all contained *Sc*AA10C but co-eluting impurities were also present (**Figure 12B**). Based on the chromatogram (**Figure 12A**) and the LDS-PAGE analysis (**Figure 12B**), fractions 12-18 were pooled and concentrated by ultrafiltration to a final volume of approximately 1 mL prior to the second purification step, SEC.

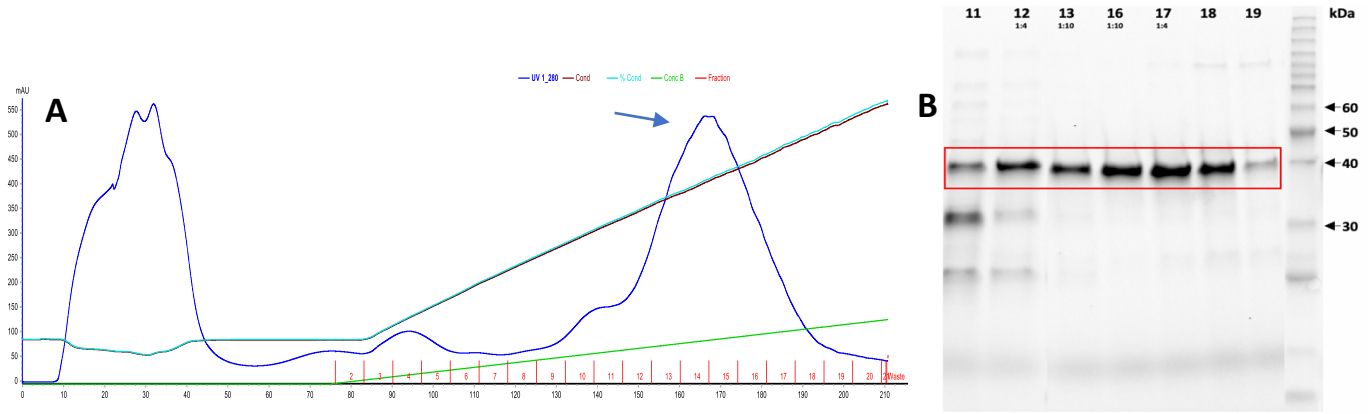


**Figure 12. Purification of *Sc*AA10C by Ion-Exchange Chromatography.** Panel **A** shows the chromatogram for *Sc*AA10C monitored by $A_{280}$.The x-axis represents the number of mL solution passed through the column and shows fraction number, and the y-axis covers absorbance measured at $A_{280}$ (blue graph). The blue arrow indicates the peak containing *Sc*AA10C. The red numbered lines refer to collected fractions. The light green line represents the gradient of NaCl that is gradually added (with 0-50% buffer B over 100 min with a 3 mL/min flow). The dark green line refers to the conductivity of the etute. The chromatogram was recorded and exported using Unicorn™ 6.4 Software. Panel **B** Shows the gel image from LDS-PAGE analysis of fractions collected during IEX. The right lane contains Benchmark™ Protein Ladder, which helps estimate protein size in other samples from the same gel. All fractions contain a clear protein band at about 40 kDa, which corresponds to *Sc*AA10C. The bands are marked with a red square. Fractions 12 and 17 were diluted 4 times, and fractions 13 and 16 were diluted 10 times. Sample buffer was added to all samples prior to application to the gel.

The concentrated *Sc*AA10C solution obtained after IEX purification was loaded onto the SEC column and eluted within one column volume of running buffer (**Figure 13A**). Fractions were collected continuously and analyzed by LDS-PAGE (**Figure 13B**), and fractions 5-9 were pooled and concentrated by ultrafiltration to a final volume of approximately 1 mL, before storing at 4°C.

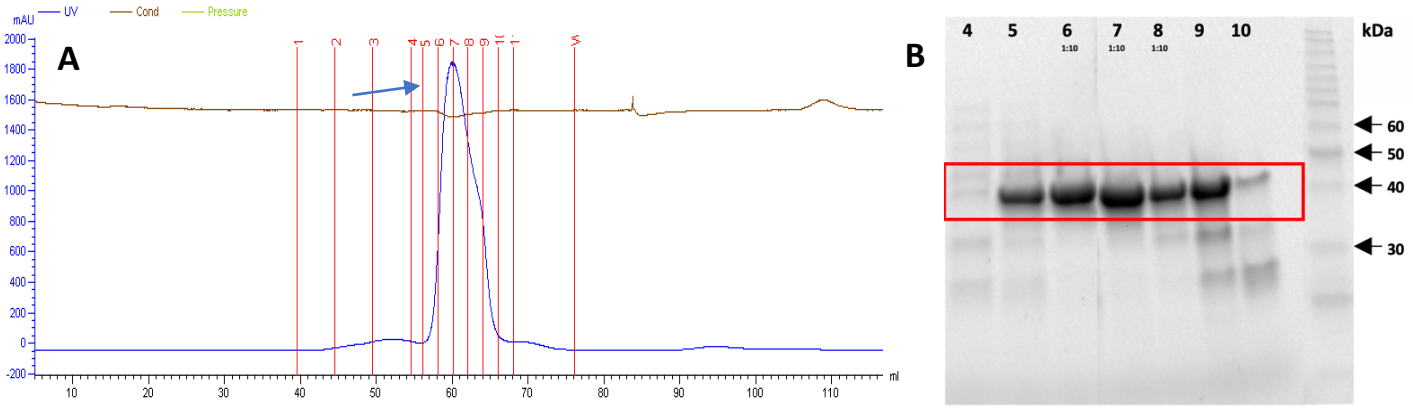


**Figure 13. Purification of *Sc*AA10C by Size-Exclusion Chromatography.** Panel **A** shows the chromatogram for *Sc*AA10C monitored by $A_{280}$. The x-axis represents the number of mL solution passed through the column and shows fraction numbers. The y-axis covers absorbance measured at $A_{280}$ (blue graph) The blue arrow indicates the peak containing *Sc*AA10C. The red numbered lines refer to collected fractions. The brown line refers to the conductivity of the eluate. The chromatogram was recorded and exported using Unicorn™ 6.4 Software. Panel **B** shows the gel image from LDS-PAGE analysis of fractions collected during SEC. The right lane contains Benchmark™ Protein Ladder, which helps estimate protein size in other samples from the same gel. All fractions contain a clear protein band at about 40 kDa, which corresponds to *Sc*AA10C. The bands are marked with a red square. Fractions 6-8 were diluted 10 times. Sample buffer was added to all samples before application to the gel.

## 4.3 Purification of *Sm*AA10A and *Sm*ChiA

After periplasmic extraction, affinity chromatography was used to purify both *Sm*AA10A and *Sm*ChiA separately. The periplasmic extract was applied to a column of chitin beads, and proteins were eluted by applying diluted acetic acid to the column. Eluted *Sm*AA10A and *Sm*ChiA indicated by peaks pointed by a blue arrow in the **Figures 14A and 15A**, respectively, were collected in a falcon tube (two with *Sm*ChiA) and analyzed by LDS-PAGE (**Figures 14B and 15B**). The sample containing purified *Sm*AA10A displays a protein band at 18 kDa, and both fractions with purified *Sm*ChiA display a band at 60 kDa, as indicated by the red squares in **Figures 14B and 15B**. Both protein solutions were buffer exchanged with 20 mM sodium phosphate pH 6.0 and concentrated to a final volume of less than 10 mL, before storing at 4°C.

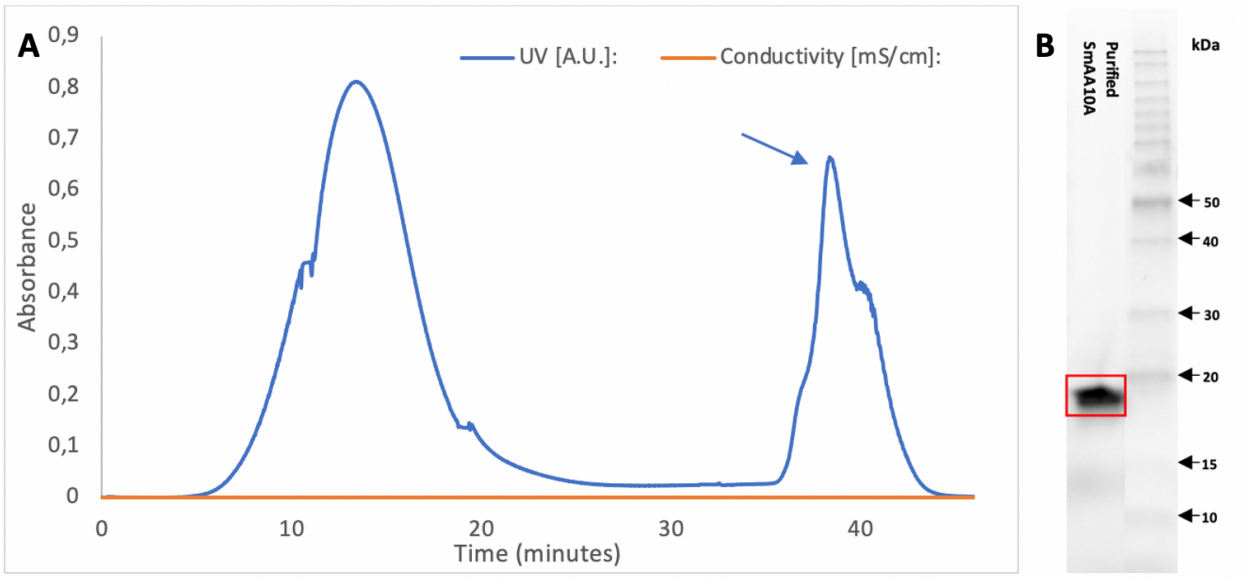


**Figure 14. Purification of *Sm*AA10A using Affinity Chromatography.** Panel **A** show the chromatogram for *Sm*AA10A monitored by $A_{280}$. The x-axis represents the time of solution passing through the column, and the y-axis covers absorbance measured at $A_{280}$ (blue graph). The blue arrow indicates the peak containing *Sm*AA10A. The orange line refers to the conductivity of the eluate. The chromatogram was recorded and exported using Unicorn™ 6.4 Software. Panel **B** shows the gel image from LDS-PAGE analysis of the eluted protein solution. The right lane contains Benchmark™ Protein Ladder, which helps estimate protein size in other samples from the same gel. The purified protein solution contains a clear protein band at about 18 kDa, which corresponds to *Sm*AA10A. The band is marked with a red square. Sample buffer was added to the sample before application to the gel.

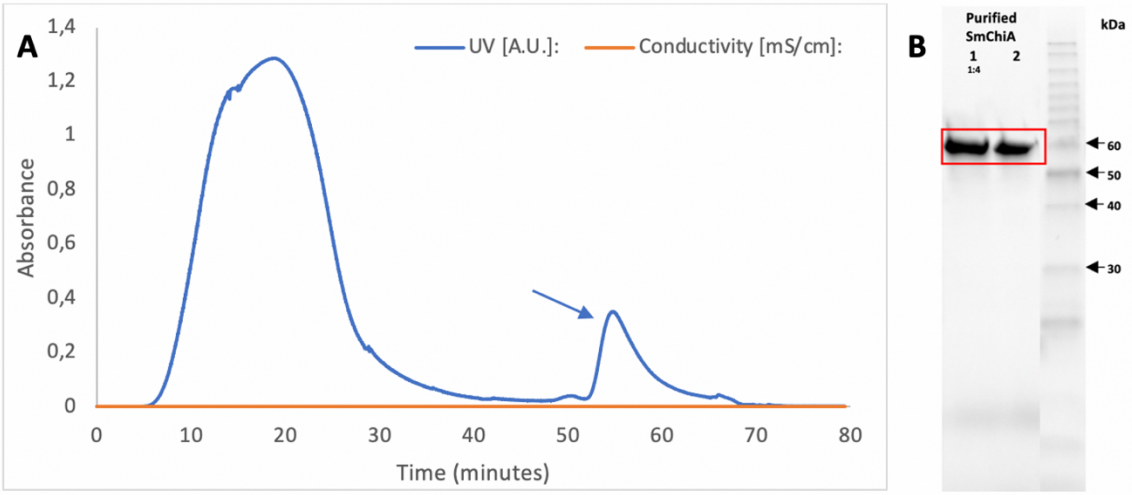


**Figure 15. Purification of *Sm*ChiA using Affinity Chromatography.** Panel **A** show the chromatogram for *Sm*ChiA monitored by $A_{280}$. The x-axis represents the time of solution passing through the column, and the y-axis covers absorbance measured at $A_{280}$ (blue graph). The blue arrow indicates the peak containing *Sm*ChiA. The orange line refers to the conductivity of the eluate. The chromatogram was recorded and exported using Unicorn™ 6.4 Software. Panel **B s**hows the gel image from LDS-PAGE analysis of the eluted protein solution. The right lane contains Benchmark™ Protein Ladder, which helps estimate protein size in other samples from the same gel. The purified protein solution contains a clear protein band at about 60 kDa, which corresponds to *Sm*ChiA. The bands are marked with a red square. Fraction 1 were diluted 4 times. Sample buffer was added to both samples before application to the gel.

### 4.4 Determination of protein concentrations by optimeasuring $A_{280}$

All the purified and concentrated protein solutions were analyzed spectrophotometrically to determine the absorbance of ultraviolet light at a wavelength of 280 nm ($A_{280}$) which was used to calculate the protein concentrations (see section 3.6). As *Sc*AA10C and *Sm*AA10A are copper-dependent LPMOs, these enzymes were subjected to a copper saturating and desalting step (see section 3.5), before the measurement. Two batches of *Sc*AA10C were analyzed, and the concentrations were determined to 25 µM and 19 µM. For *Sm*AA10A, the concentration was determined to 14 µM. The concentration of the concentrated *Sm*ChiA solution was measured directly after purification and determined to be 39 µM.

### 4.5 Photocatalyst preparation

Prior to use in enzymatic reactions, FMC was washed five times with 50 mM sodium phosphate buffer, pH 6.0, to remove soluble components. The UV-Vis absorption spectra of the washing buffer were measured after each centrifugation step (**Figure 16**). These spectra indicated that four washing steps were required to remove the soluble compounds in FMC, since the superposed absorption spectra of the supernatants obtained after the fourth and the fifth washing step were very similar (**Figure 16**).

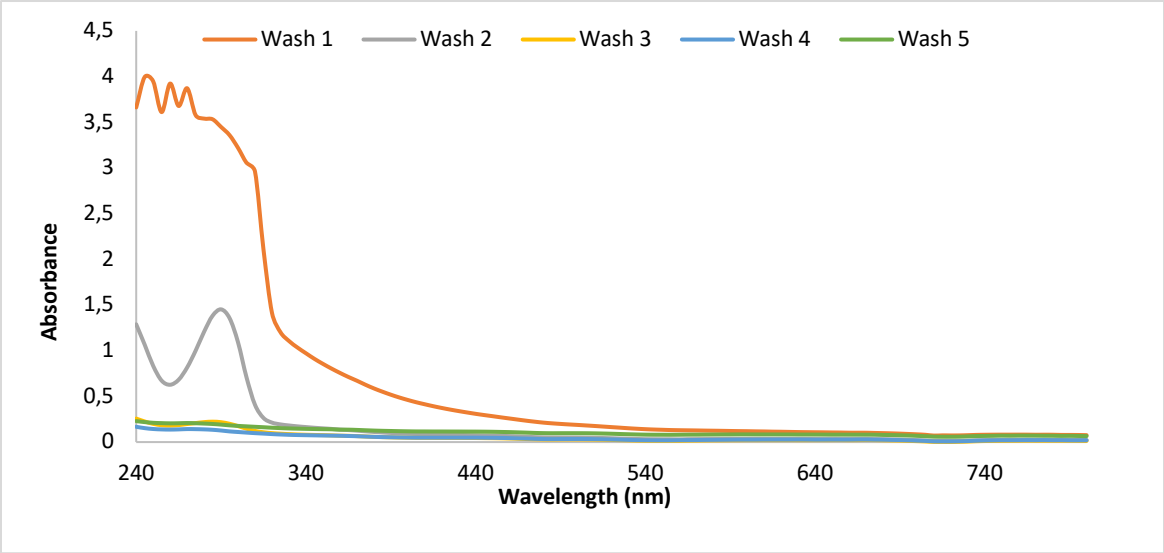


**Figure 16. Removal of soluble compounds from FMC.** The figure shows the UV-Vis absorption spectra of supernatants obtained from successive washing steps of FMC. The absorbance of light was measured with wavelengths in the range 240 - 800 nm. 50 mM sodium phosphate pH 6.0 solution was initially measured as a blank. Each line represents a round of washing in which 20 g/L FMC was suspended in 50 mM sodium phosphate pH 6.0 and centrifuged for 2 min at 15000 g. The supernatant was transferred to a quartz cuvette and measured spectrophotometrically. The remaining pellet was then re-suspended in 1 mL 50 mM sodium phosphate pH 6.0 for the next washing step.

## 4.6 Photocatalytic reactions with *Sc*AA10C

### 4.6.1 The effect of the FMC concentration and the pH, in the presence and absence of light

Photocatalytic reactions with *Sc*AA10C and Avicel were performed with different concentrations of FMC (0.1, 1, and 10 g/L), in the presence and absence of light, and at various pH 6.0, 7.0, and 8.0 to assess the effect of pH and FMC concentration on LPMO catalysis. **Figure 17** shows a clear effect of the FMC concentration on LPMO performance, both in the presence (**Figure 17B, D, and F**) and absence of light (**Figure 17A, C, and E**). Reactions in the dark showed similar LPMO activity at pH 7.0 and 8.0, which was much higher than the activity at pH 6.0 for all FMC concentrations (0.1, 1, and 10 g/L) (**Figure 17A, C, and E**). For the reactions with the two lowest FMC concentrations, exposure of light resulted in an increase in product formation by one order of magnitude, while the dose-response effect was maintained (i.e., product formation at 1 g/L FMC was higher compared to 0.1 g/L FMC). In this case reactions at pH 7.0 showed the lower product formation rates. For the reactions at 0.1 g/L FMC, no oxidized products were detected for the reaction at pH 7.0 (**Figure 17B and D**). At pH 8.0, LPMO activity was approximately two-fold higher compared pH 6.0 (**Figure 17B**). For reactions containing 1 g/L FMC, the effect of pH became smaller and product formation was also observed at pH 7.0 (**Figure 17D**). Interestingly, the reactions carried out with 10 g/L FMC and light showed non-linear progress curve, with a rapid initial product formation phase followed by almost complete cessation of product formation after 3 – 6 h (the slight increase in product levels between 6 h and 24 h is most likely due to evaporation from the reaction vial). In this case, the effect of light on the initial rate of product formation was limited (compare **Figures 17E and 17F**) and the effects of the pH were small (**Figure 17F**). The apparent enzyme inactivation observed in this experiment may indicate that the LPMO suffers from autocatalytic inactivation, as has been observed when LPMOs are exposed to (too) high concentrations of reductant of $H_2O_2$ (Bissaro et al., 2017; Loose et al., 2018). All control reactions in the absence of LPMO show no formation of oxidized products (**Figure 17**).

Overall, the results depicted in **Figure 17** show that LPMO activity is clearly dependent on FMC dosage and on light. The effect of pH varies between the conditions, but the overarching picture is that the effect of light is most prominent for reactions at pH 6.0. In other words, the ratio of the level of oxidized products when the reaction is exposed to visible light compared to reactions in the dark is highest at pH 6.0 (**Figure 17**). Therefore, pH 6.0 was used in further experiments.

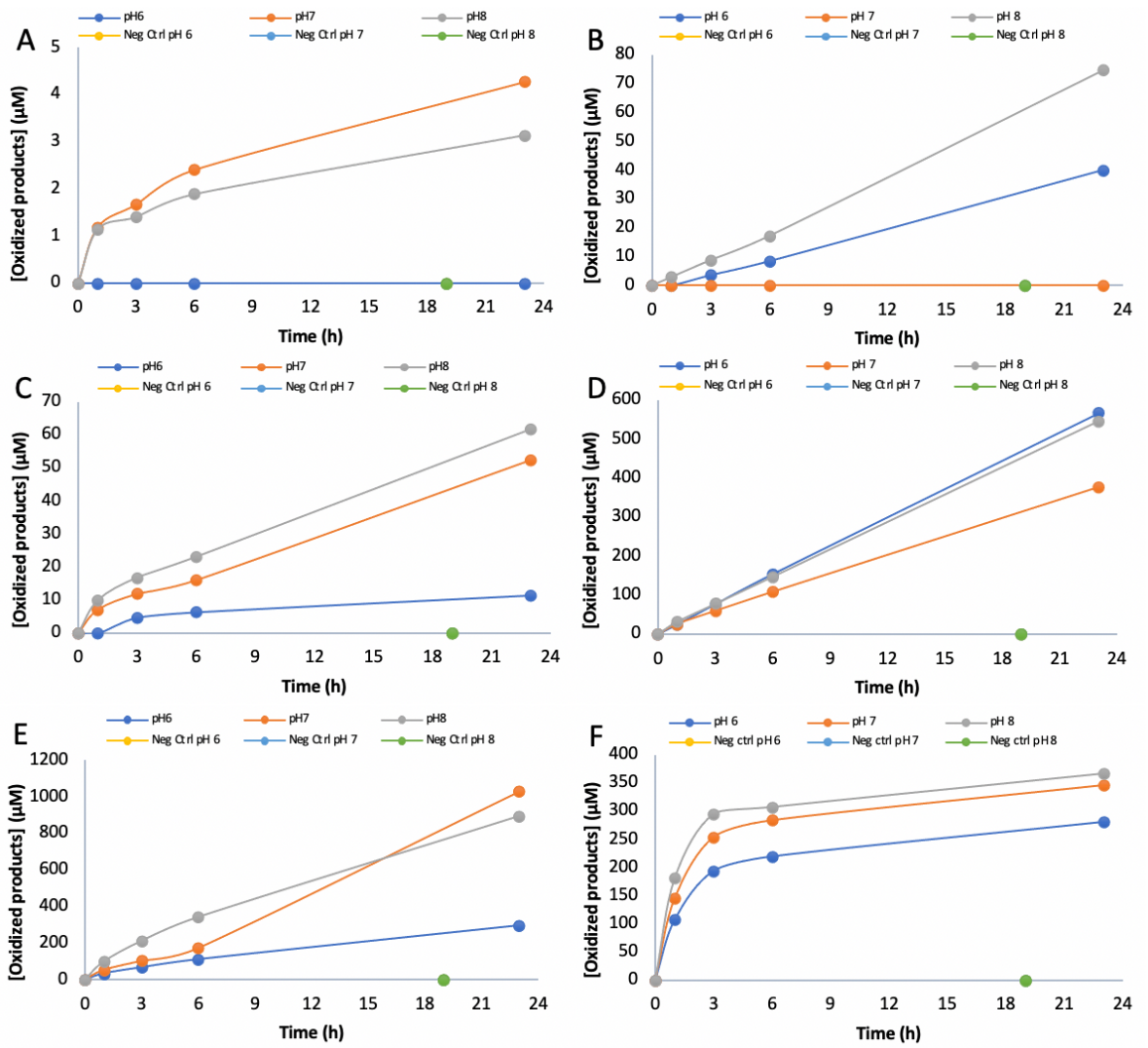


**Figure 17. The effect of pH and FMC concentration on photocatalytic activity of *Sc*AA10C**. The figure shows how the photocatalytic reaction with *Sc*AA10C and Avicel is influenced by different concentrations of FMC (0.1 (**A and B**), 1 (**C and D**), and 10 g/L (**E and F**)) and pH (6.0, 7.0, and 8.0) in the presence (**B, D, and F**) and absence (**A, C, and E**) of visible light (I= 10 % of $I_{max}$, approximately 16.8 W·cm$^{-2}$). All reactions were performed with 10 g/L Avicel in 50 mM sodium phosphate pH 6.0. During the total reaction time of 23 h, all reactions were incubated at 40 °C with magnet stirring. Samples were taken after 1, 3, 6, and 23 h and filtrated before treatment with *Tf*Cel6A to convert oxidized oligosaccharides to oxidized oligomers with a degree of polymerization of 2 (GlcGlc1A) and 3 ($Glc_2Glc1A$). The graphs show the sum of the total amounts of GlcGlc1A and $Glc_2Glc1A$. Neg ctrl. indicates product formation in control reactions lacking light-exposure. For these reactions sampling was only done at 19 hours and all samples showed no products. Thus, the green point are in fact three overlapping points (green, yellow, light blue). Note the variation in the values on the Y-axes.

### 4.6.2 Further analysis of the effect of the FMC concentration

To further investigate whether the amount of a photosensitizer was limiting the reactions, the impact of the FMC concentration on the production of oxidized products was studied. Thus, reactions with various concentrations of FMC (0, 0.5, 1, 2.5, and 5 g/L) were performed in the presence of light. The generation of oxidized products over time in each reaction in presented in **Figure 18**, which shows linear progress curves for all reactions. The results confirm that increased concentrations of FMC increase the generation of oxidized products (**Figure 18**). Of note, **Figure 18** also shows that a control reaction with no FMC did not yield any oxidized products.

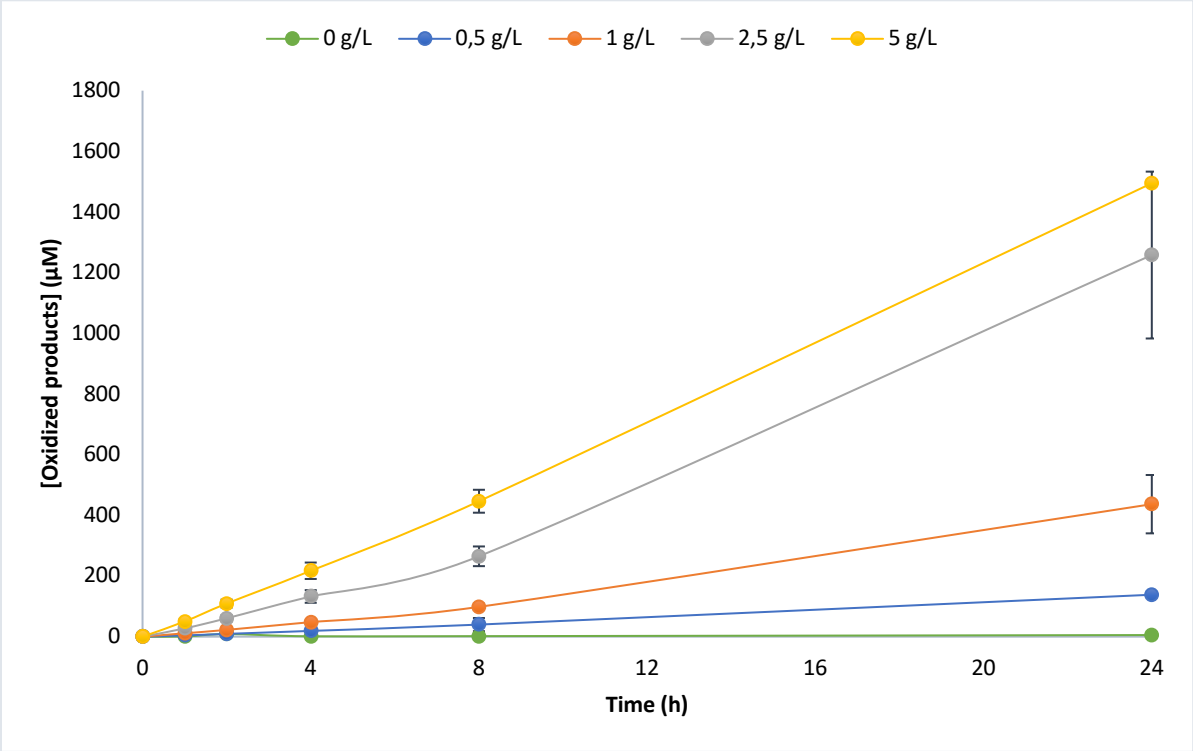


**Figure 18. The effect of the FMC concentration on photocatalytic activity of *Sc*AA10C.** The figure shows how the photocatalytic reaction with *Sc*AA10C and Avicel is influenced by different concentrations of FMC (0, 0.5, 1, 2.5, and 5 g/L). 0.5 µM *Sc*AA10C was added to all reactions and the reactions were exposed to visible light (I= 10 % of $I_{max}$, approximately 16.8 W·cm$^{-2}$). All reactions were performed with 10 g/L Avicel in 50 mM sodium phosphate pH 6.0. All reactions were incubated at 40 °C with magnet stirring. Samples were taken after 1, 2, 4, 8, and 24 h and filtrated before treatment with *Tf*Cel6A to convert oxidized oligosaccharides to oxidized oligomers with a degree of polymerization of 2 (GlcGlc1A) and 3 ($Glc_2Glc1A$). The graphs show the sum of the total amounts of GlcGlc1A and $Glc_2Glc1A$.

### 4.6.3 The effect of the LPMO concentration

To study whether the amount of enzyme was limiting the reactions, the impact of the LMPO concentration on the production of oxidized products was studied. Thus, reactions with various concentrations of *Sc*AA10C (0, 0.5, 1, 2.5, and 5 g/L) were performed in the presence of light. The results (**Figure 19**) show that the generation of oxidized products increased approximately linearly over time in all reactions. Reactions containing LPMO produced the same number of oxidized products in the initial phase (0 – 8 h) of the reaction regardless of the LPMO concentration (**Figure 19**). The data indicated more variation between the various reactions at the later timepoint (24 h). These differences were not statistically significant and did not show a clear trend in terms of LPMO concentration-dependency (**Figure 19**). The initial rates depicted in **Figure 19** clearly show that under the conditions used here, the LPMO reaction is limited by one of the reactants and not by the enzyme.

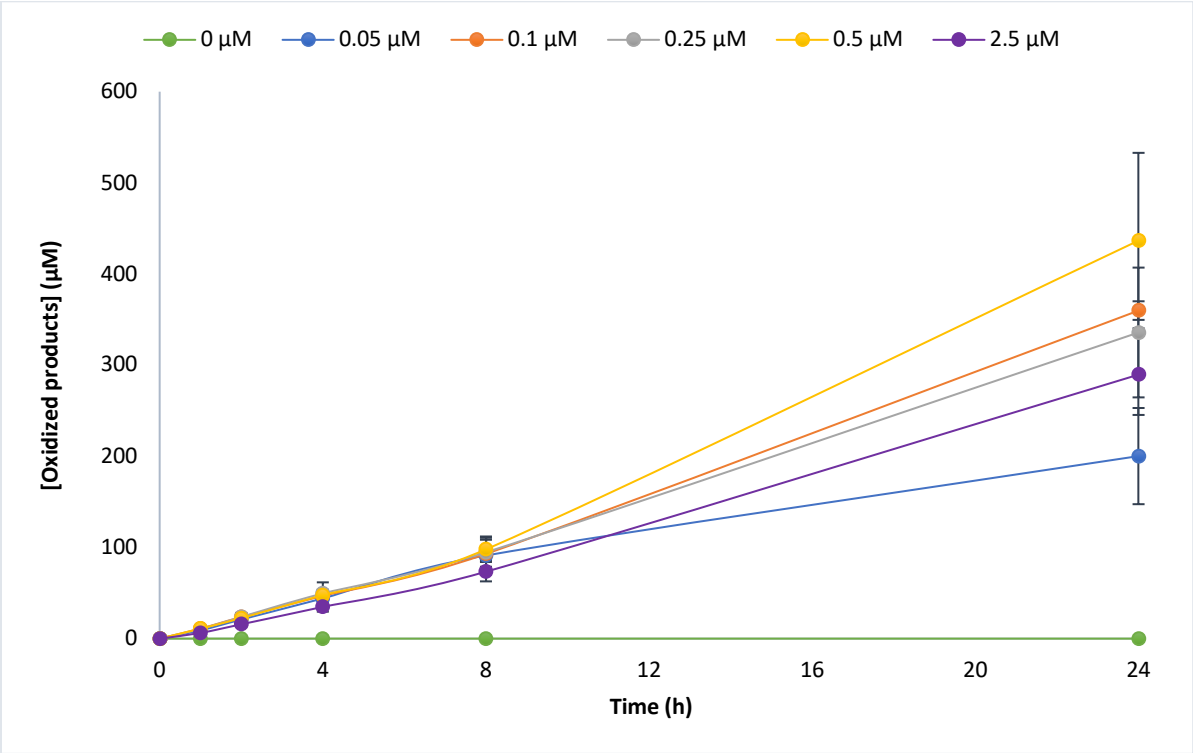


**Figure 19. The effect of the LPMO concentration on photocatalytic activity of *Sc*AA10C.** The figure shows how the photocatalytic reaction with *Sc*AA10C and Avicel is influenced by different concentrations of *Sc*AA10C (0, 0.5, 0.1, 0.25, 0.5, and 2.5 µM). *Sc*AA10C was added to all reactions and the reactions were exposed to visible light (I= 10 % of $I_{max}$, approximately 16.8 $W \cdot cm^{-2}$). All reactions were performed with 10 g/L Avicel and 1 g/L FMC in 50 mM sodium phosphate pH 6.0. All reactions were incubated at 40 °C with magnet stirring. Samples were taken after 1, 2, 4, 8, and 24 h and filtrated before treatment with *Tf*Cel6A to convert oxidized oligosaccharides to oxidized oligomers with a degree of polymerization of 2 (GlcGlc1A) and 3 ($Glc_2Glc1A$). The graphs show the sum of the total amounts of GlcGlc1A and $Glc_2Glc1A$.

### 4.6.4 The effect of Avicel concentration

To study whether the amount of substrate was limiting the reactions, the impact of the Avicel concentration on the production of oxidized products was studied. Thus, reactions with various concentrations of Avicel (0, 5, 10, 20, and 40 g/L) were performed in the presence of light. The results, depicted in **Figure 20,** show that the progress curve for LPMO reactions with 5 and 10 g/L Avicel were very similar. A further increase in the concentration of Avicel decreased the production of oxidized products (**Figure 20**). Thus, it would seem that with the substrate concentration (10 g/L) used above, and further below, the substrate concentration is not limiting the reaction.

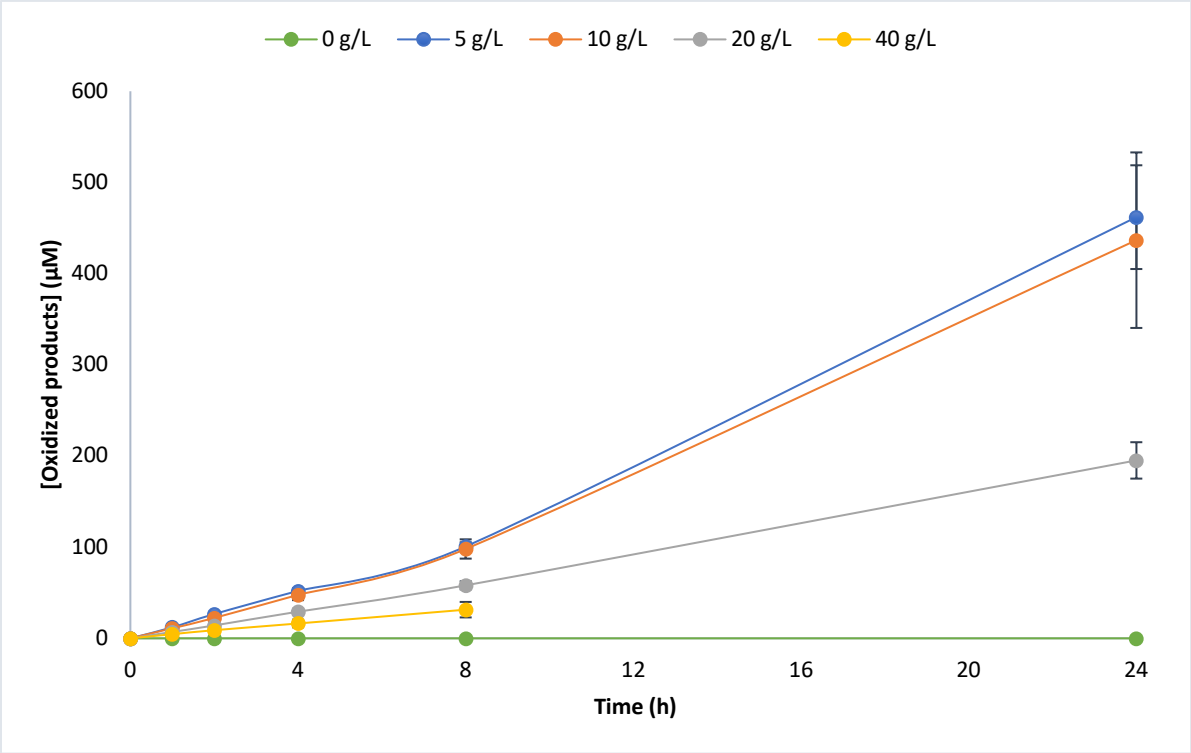


**Figure 20. The effect of the Avicel concentration on photocatalytic activity of *Sc*AA10C.** The figure shows how the photocatalytic reaction with *Sc*AA10C and Avicel is influenced by different concentrations of Avicel (0, 5, 10, 20, and 40 g/L). 0.5 µM *Sc*AA10C was added to all reactions and the reactions were exposed to visible light (I= 10 % of $I_{max}$, approximately 16.8 W·cm$^{-2}$). All reactions were performed with 1 g/L FMC in 50 mM sodium phosphate pH 6.0. All reactions were incubated at 40 °C with magnet stirring. Samples were taken after 1, 2, 4, 8, and 24 h and filtrated before treatment with *Tf*Cel6A to convert oxidized oligosaccharides to oxidized oligomers with a degree of polymerization of 2 (GlcGlc1A) and 3 ($Glc_2Glc1A$). The graphs show the sum of the total amounts of GlcGlc1A and $Glc_2Glc1A$. There is no data point for reactions containing 40 g/L Avicel after 24 hours as the reaction sample had evaporated almos completely.

### 4.6.5 The effect of light intensity and SOD

Light-driven ScAA10C catalyzed depolymerization of Avicel was performed with different light intensities (0, 1, 3, 10, and 30% of $I_{max}$ corresponding to 0, 1.7, 5.0, 16.8, 50.4 W/cm$^2$, respectively) in the presence and absence of SOD to assess the effect of light and SOD on the production of oxidized products. The production of oxidized products in reactions without SOD is illustrated in **Figure 21A**. The results show that increased light intensity increases the production of oxidized products, and all reactions exposed to light show a linear progress curve. Thus, the LPMO activity is limited by the light. Reactions with SOD are depicted in **Figure 21B**. These reactions have very similar progress curves compared to reactions without SOD (**Figure 21A**).

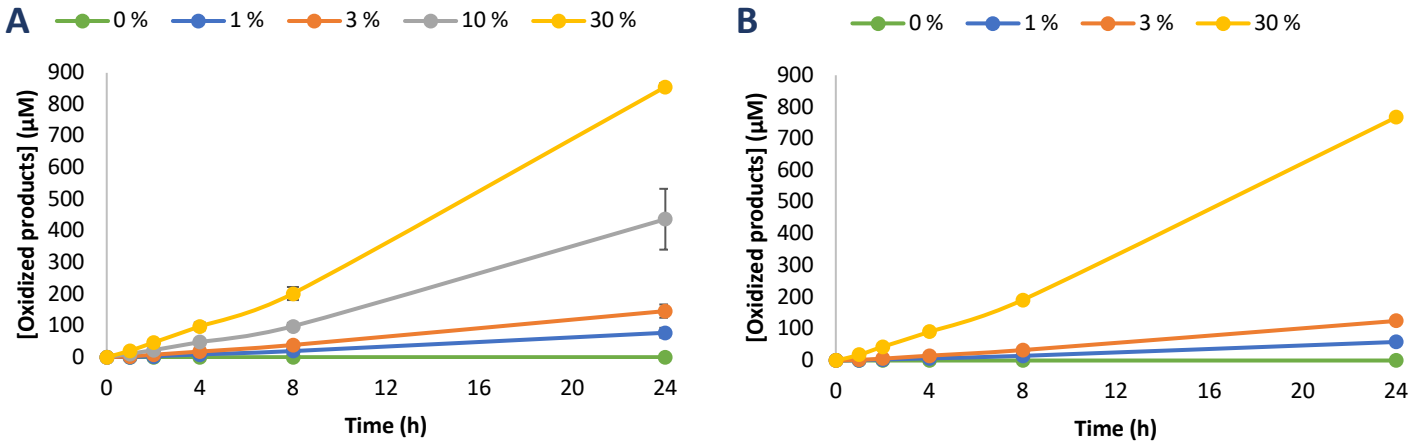


**Figure 21. The effect of the light intensity and SOD on photocatalytic activity of *Sc*AA10C.** The figure shows how the photocatalytic reaction with *Sc*AA10C and Avicel is influenced by different light intensities (0, 1, 3, 10, and 30% of $I_{max}$ corresponding to 0, 1.7, 5.0, 16.8, 50.4 W/cm$^2$, respectively) with (**B**) and without SOD (**A**). 0.5 µM *Sc*AA10C was added to all reactions and exposed to visible light. All reactions were performed with 10 g/L Avicel and 1 g/L FMC in 50 mM sodium phosphate pH 6.0. All reactions were incubated at 40 °C with magnet stirring. Samples were taken after 1, 2, 4, 8, and 24 h and filtrated before treatment with *Tf*Cel6A to convert oxidized oligosaccharides to oxidized oligomers with a degree of polymerization of 2 (GlcGlc1A) and 3 ($Glc_2Glc1A$). Reactions without SOD were performed in triplicates, and the standard deviations are referred to as error bars.

### 4.6.6 Control reactions

As FMC powder was suspended in $dH_2O$ and may contain soluble components that affect the photocatalytic activity, the FMC was washed prior to use (see section 3.7). To investigate if the soluble components would lead to activity, the supernatant from the first washing step was added to a single standard reaction replacing FMC. An additional reaction with the same supernatant was performed with no *Sc*AA10C as a negative control. The results are illustrated in **Figure 22** and show activity in the reaction containing the supernatant and *Sc*AA10C. The reaction with no *Sc*AA10C had

no activity. The same procedure was done with the supernatant from the fourth round of washing and *Sc*AA10A. This reaction had some activity, approximately ten times lower than the reaction from the first wash. The amount of supernatant added corresponded to an FMC concentration of 7.8 g/L. This means that product formation after 19 h in the reaction with the supernatant from the first wash was about one magnitude times lower than the corresponding reaction with FMC (**Figure 18**). Note that the highest FMC concentration in **Figure 18** is 5 g/L.

Another control reaction was performed with free copper (Cu(II)) replacing *Sc*AA10C. The purpose was to demonstrate that *Sc*AA10A is necessary to achieve photocatalytic activity and that product formation is not due to the possible presence of free copper itself. As **Figure 22** shows, reactions with free copper did not show formation of oxidized products.

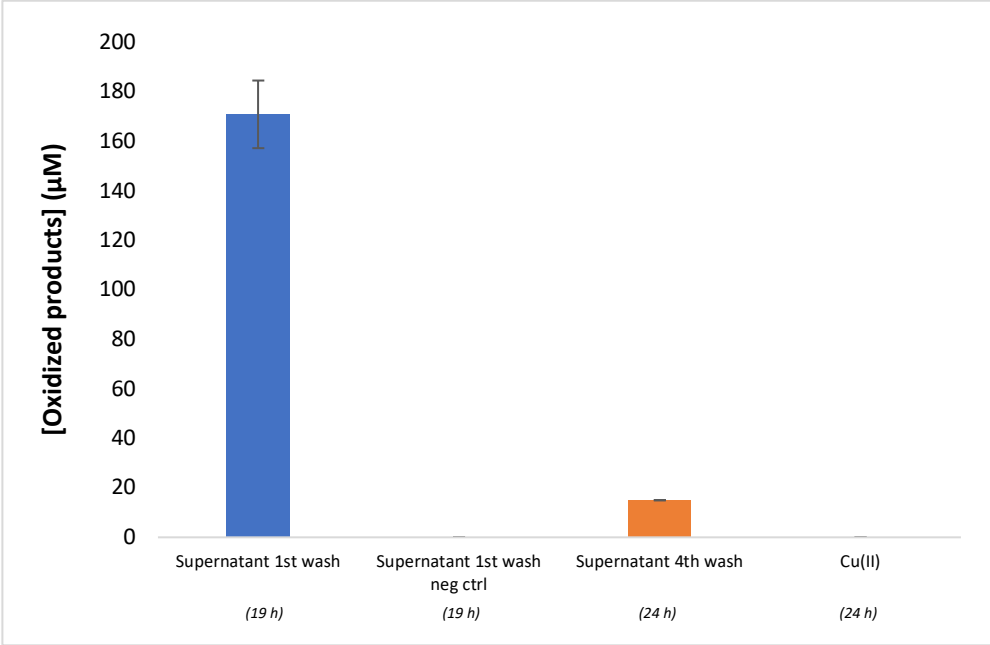


**Figure 22. Photocatalytic activity in control reactions.** The figure shows how the photocatalytic reaction with *Sc*AA10C and Avicel are influenced by the supernatant from the first and the fourth washing step of FMC preparation (see section 3.7), and in reaction with free Cu(II) in the lack of *Sc*AA10C. 0.5 µM *Sc*AA10C were added to reactions with the first and the fourth supernatant, while 0.5 µM free Cu(II) and 5 g/L FMC was added to the reaction with Cu(II). One reaction with supernatant from the first washing step was performed without *Sc*AA10C as a negative control. All reactions were exposed to visible light (I= 10 % of $I_{max}$, approximately 16.8 $W \cdot cm^{-2}$) and performed with 10 g/L Avicel in 50 mM sodium phosphate pH 6.0. All reactions were incubated at 40 °C with magnet stirring. Sample were taken after 19 or 24 h (indicated for each sample) and filtrated before treatment with *Tf*Cel6A to convert oxidized oligosaccharides to oxidized oligomers with a degree of polymerization of 2 (GlcGlc1A) and 3 ($Glc_2Glc1A$).

## 4.7 Assessing $H_2O_2$ production using the Amplex red assay

### 4.7.1 The effect of LPMO and free copper, in the presence or absence of Avicel

To investigate $H_2O_2$ accumulation by 1 g/L FMC in the experimental setup used for *Sc*AA10C catalyzed oxidation of Avicel, similar reactions with and without Avicel were performed in the presence of either *Sc*AA10C or free copper. Measurements were performed after 30 and 60 min of incubation time. The highest amount of $H_2O_2$ was observed in the reaction without LPMO, free copper, and Avicel (**Figure 23**). In the same reaction with Avicel present, the accumulation of $H_2O_2$ was slightly lower. In reactions with the LPMO and Avicel, accumulation of $H_2O_2$ was not observed, but in absence of Avicel, low levels of $H_2O_2$ were detected (**Figure 23**). In the last set of experiments, *Sc*AA10C was replaced by free copper and the amount of accumulated $H_2O_2$ was slightly lower compared to the reaction without LPMO and copper, but $H_2O_2$ levels were still much higher compared to the reaction with LPMO present (**Figure 23**). Also in this case, $H_2O_2$ levels were lower in reactions with Avicel. Taken together, these results show redox activity of FMC producing $H_2O_2$ in the photobiocatalytic reaction system, and that the production of $H_2O_2$ is higher in reactions lacking substrate (Avicel). It must be noted that no control reactions were performed in this part of the research.

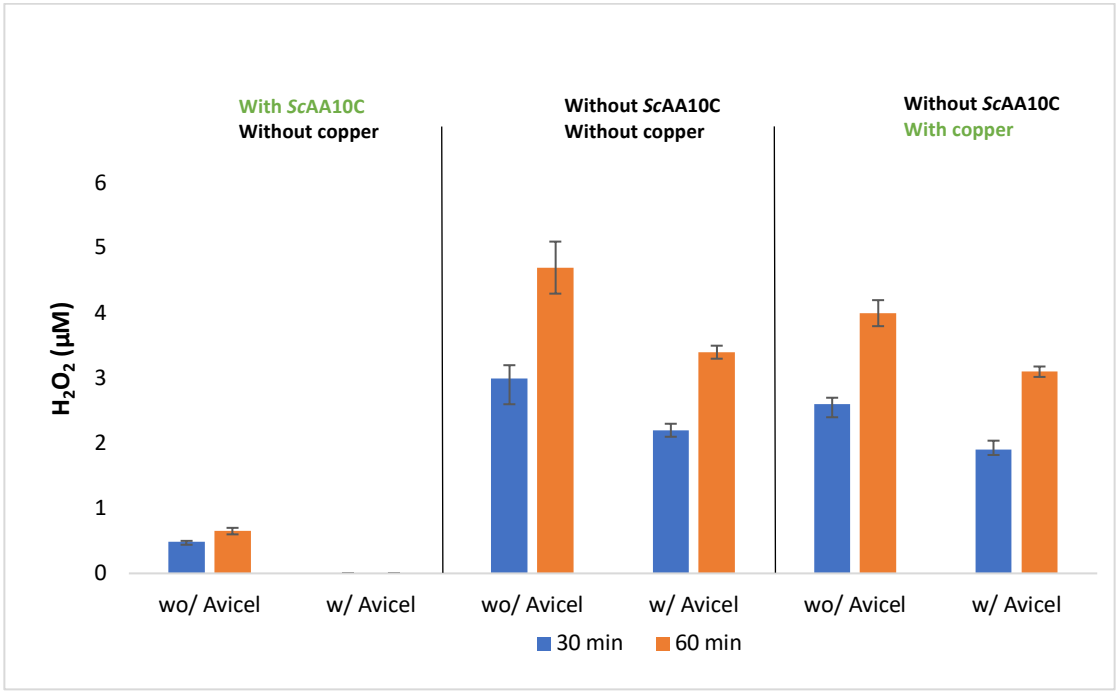


**Figure 23. Accumulation of $H_2O_2$ in photocatalytic reactions with *Sc*AA10C or free copper in the presence and absence of Avicel.** The reactions contained 0.5 µM *Sc*AA10C or free copper and all reactions were exposed to visible light (I= 10 % of $I_{max}$, approximately 16.8 W·cm$^{-2}$). 10 g/L Avicel was added to some of the reactions, as indicated ("w/Avicel"). All reactions were performed with 1 g/L FMC and 50 mM sodium phosphate pH 6.0 and incubated at 40 °C with magnet stirring. Sample aliquots were taken after 0.5 and 1 h, filtrated and added to a premix containing HRP and Amplex Red. $H_2O_2$-driven formation of resorufin was detected using a Varioskan™ LUX multimode microplate reader.

### 4.7.2 The effect of the Avicel concentration

To investigate how the Avicel affects $H_2O_2$ production in the reaction system, reactions with various concentrations of Avicel (0, 5, 10, and 20 g/L) were performed in the presence of light and the absence of *Sc*AA10C. The results, illustrated in **Figure 24**, show that increasing the Avicel concentration decreases the generation of $H_2O_2$ (**Figure 24**).

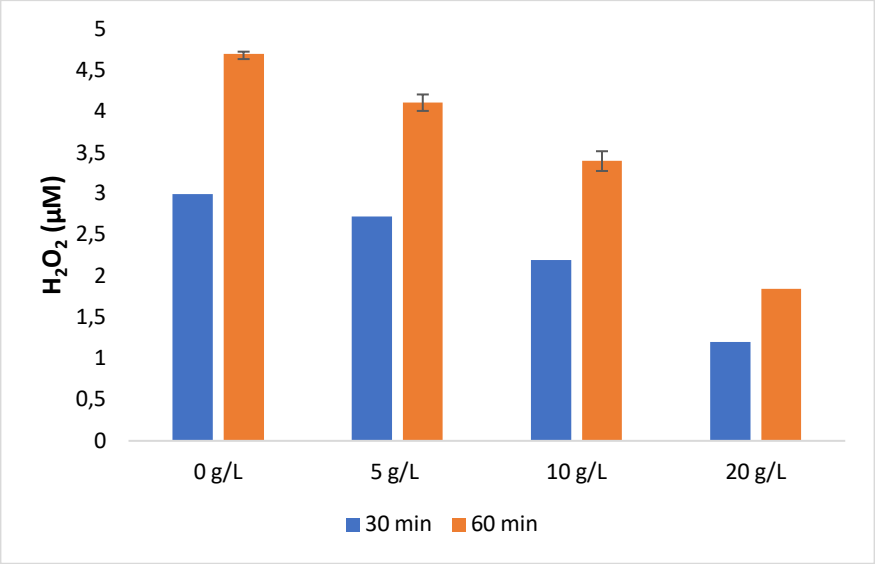


**Figure 24. Accumulation of $H_2O_2$ in photocatalytic reactions with different concentrations of Avicel.** The reactions contained different concentrations of Avicel (0, 5, 10, and 20 g/L) and all reactions were exposed to visible light (I= 10 % of $I_{max}$, approximately 16.8 W·cm$^{-2}$). All reactions were performed with 1 g/L FMC and 50 mM sodium phosphate pH 6.0 and incubated at 40 °C with magnet stirring. Sample aliquots were taken after 0.5 and 1 h, filtrated and added to a premix containing HRP and Amplex Red. $H_2O_2$-driven formation of resorufin was detected using a Varioskan™ LUX multimode microplate reader.

### 4.7.3 The effect of SOD

Different concentrations of superoxide dismutase (0, 0.1, and 1 µM) were added to standard reactions without *Sc*AA10C to investigate if the presence of this enzyme would lead to generation of additional $H_2O_2$ in the reaction system. **Figure 25** shows that slightly less $H_2O_2$ was generated in the reactions containing SOD compared to the reaction without SOD. The figure also tells that the concentration of SOD does not influence any difference in $H_2O_2$ concentration.

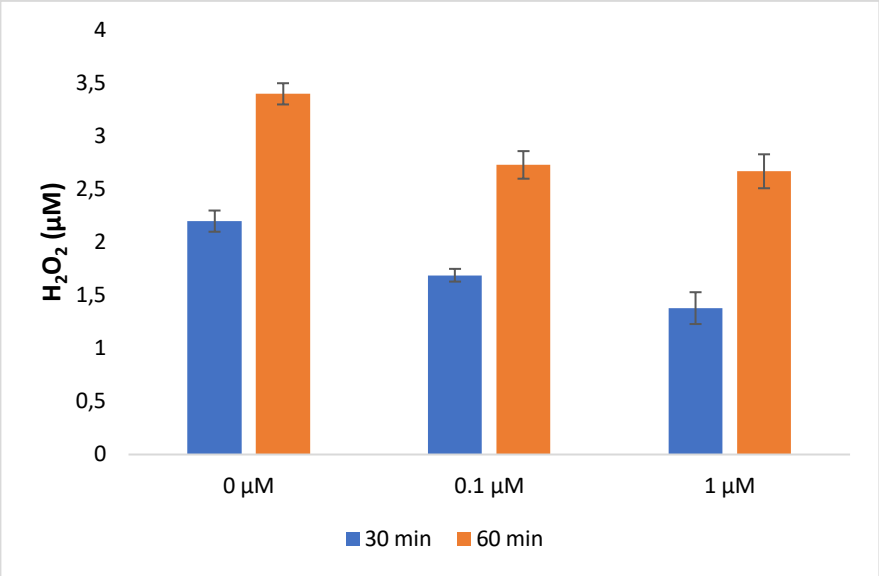


**Figure 25. Accumulation of $H_2O_2$ in photocatalytic reactions with different concentrations of SOD.** The reactions contained different concentrations of SOD (0, 0.1, and 1 µM) and all reactions were exposed to visible light (I= 10 % of $I_{max}$, approximately 16.8 W·cm$^{-2}$). All reactions were performed with 1 g/L FMC, 10 g/L Avicel, and 50 mM sodium phosphate pH 6.0 and incubated at 40 °C with magnet stirring. Sample aliquots were taken after 0.5 and 1 h, filtrated and added to a premix containing HRP and Amplex Red. $H_2O_2$-driven formation of resorufin was detected using a Varioskan™ LUX multimode microplate reader.

## 4.8 Photocatalytic reactions with *Sm*AA10A and *Sm*ChiA

Photocatalytic reactions with chitin-active *Sm*AA10A were performed with (chitin-containing) FMC, with or without β-chitin, and the presence or absence of visible light. The purpose of the experiment was to qualitatively demonstrate the ability of light-exposed FMC to catalyze a chitin-active LPMO, *Sm*AA10A, which would be expected to depolymerize the chitin in FMC as well as β-chitin. The results showed no generation of oxidized products in reactions where *Sm*AA10A (**Figure 26A and B**) or visible light were absent (**Figure 26**). In the light-exposed sample containing FMC in the presence of *Sm*AA10A, the chromatograms clearly show production of oxidized chito-oligosaccharides (**Figure 26C**). Generation of oxidized chito-oligosaccharides was also observed for light-exposed reactions containing both FMC and β-chitin in the presence of *Sm*AA10A (**Figure 26D**).

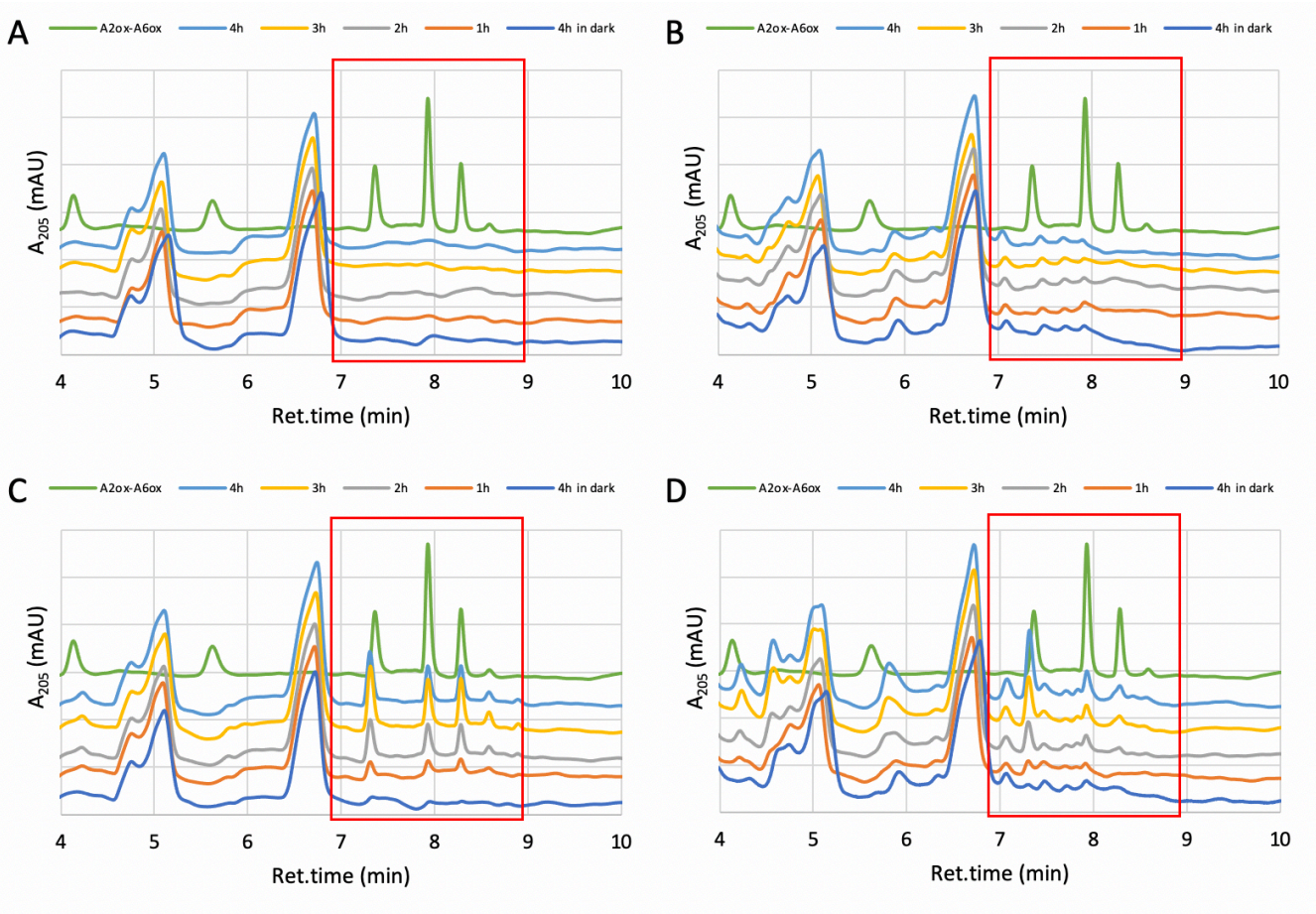


**Figure 26. photocatalytic activity of *Sm*AA10A**. The figure shows chromatograms of photocatalytic reactions containing FMC (**A**), FMC and β-chitin (**B**), FMC and SmAA10A (**C**), and FMC, β-chitin and *Sm*AA10A (**D**) in the presence or absence (dark blue line) of visible light. 1 µM *Sm*AA10A were added to reactions shown in panel **C and D** and 5 g/L β-chitin were added to reactions shown in panel **B and D**. All reactions were performed with 5 g/L FMC in 50 mM sodium phosphate pH 6.0. All reactions were incubated at 40 °C with magnet stirring. Samples were taken after 1, 2, 3, and 4 h and filtrated. The green line in all panels illustrates the chromatogram of a standard solution containing $NAG_2^{ox}$-$NAG_6^{ox}$. The peaks of $NAG_2^{ox}$-$NAG_6^{ox}$ are indicated by red squares.

Further photobiocatalytic reactions with *Sm*ChiA with and without *Sm*AA10A were performed to investigate the synergy between the two enzymes when degrading the chitin in FMC in the presence and absence of visible light. In this case, chitin degradation was assessed by measuring native products, *N*-acetylglucosamine (NAG) and *N,N'*-diacetylglucosamine ($NAG_2$) , as described in section 3.13. Reactions without enzymes were performed as control reactions and did not yield any chitin degradation products regardless of the presence of light (**Figure 27**, FMC). While product formation in reactions with FMC and *Sm*ChiA was not affected by light (**Figure 27**, FMC + *Sm*ChiA), light increased product formation in reactions with FMC, *Sm*ChiA and *Sm*AA10A, (**Figure 27**, FMC + *Sm*ChiA + *Sm*AA10A). The boosting effect of the LPMO, *Sm*AA10A, on chitin degradation by SmChiA, was not noticeable in reactions in the dark (**Figure 27**, - Light), when the LPMO is hardly active (**Figure 26**), whereas the LPMO affect was clear when applying light (**Figure 27**, + Light).

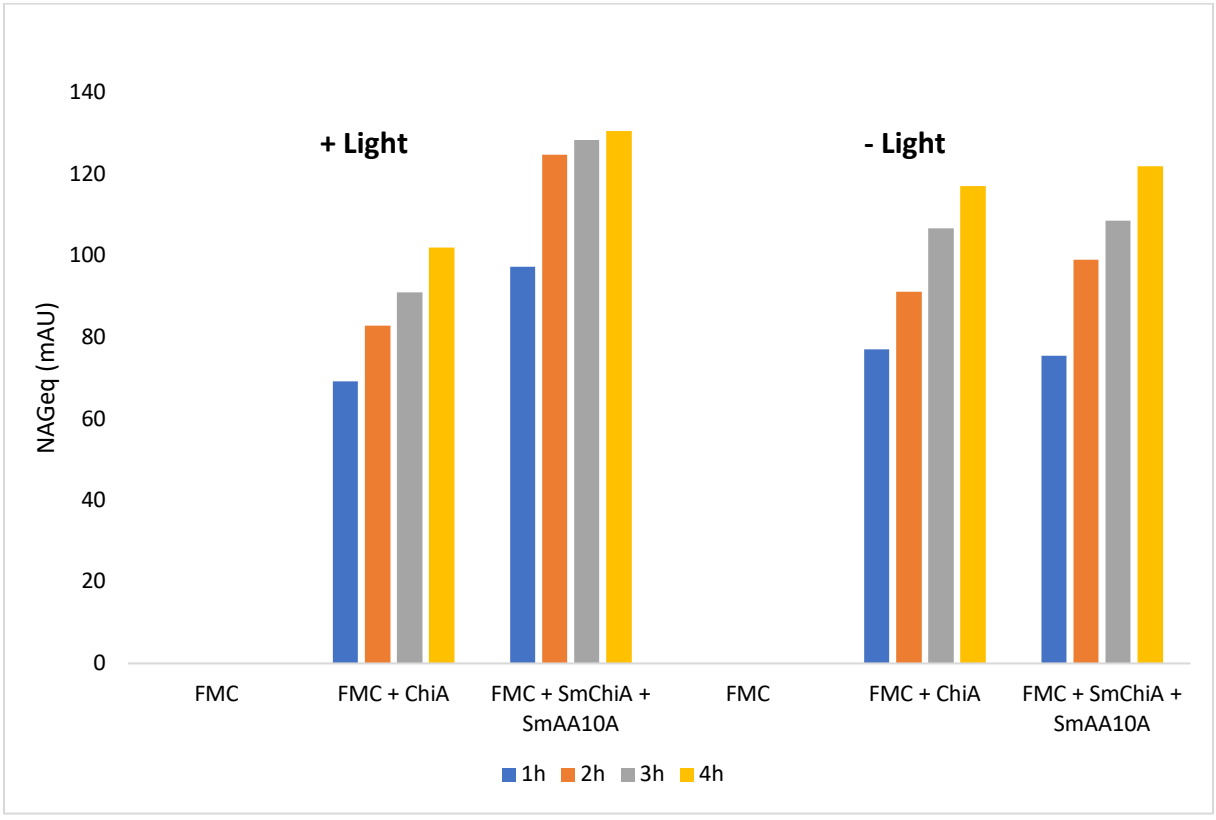


**Figure 27. The synergy between *Sm*ChiA and *Sm*AA10A to produce native products from FMC in the presence or absence of visible light.** The figure shows how chitin in FMC are depolymerized by *Sm*ChiA with and without the addition of *Sm*AA10A in the presence or absence of visible light. 1 µM enzyme (*Sm*ChiA/*Sm*AA10A) were added to the associated reactions and samples exposed to visible light were exposed by I= 10 % of $I_{max}$, approximately 16.8 $W \cdot cm^{-2}$. All reactions were performed with 5 g/L FMC in 50 mM sodium phosphate pH 6.0. All reactions were incubated at 40 °C with magnet stirring. Samples were taken after 1, 2, 3, and 4 h and filtrated before addition of 25 µL 50mM $H_2SO_4$ to ensure the reaction to stop. The graphs show the sum of the total amounts of NAG and $NAG_2$.

Corresponding photobiocatalytic reactions with *Sm*ChiA with and without *Sm*AA10A were performed with FMC and the addition of β-chitin**.** The results show a low content of native products in reactions with only FMC and β-chitin in the presence and absence of light (**Figure 28**, FMC + β-chitin). As for reactions with only FMC (**Figure 27**), there are also here observed the same production of native products in reactions with FMC, β-chitin, *Sm*ChiA, and *Sm*AA10A compared to reaction containing FMC, β-chitin, and *Sm*ChiA performed in darkness (**Figure 28**, - Light). There is also an increase of produced native products between the corresponding reactions performed in visible light (**Figure 28**, + Light). The reactions with FMC and β-chitin (**Figure 28**) show a 10-fold increase in production of native products compared to the reactions with only FMC as a chitin source (**Figure 27**).

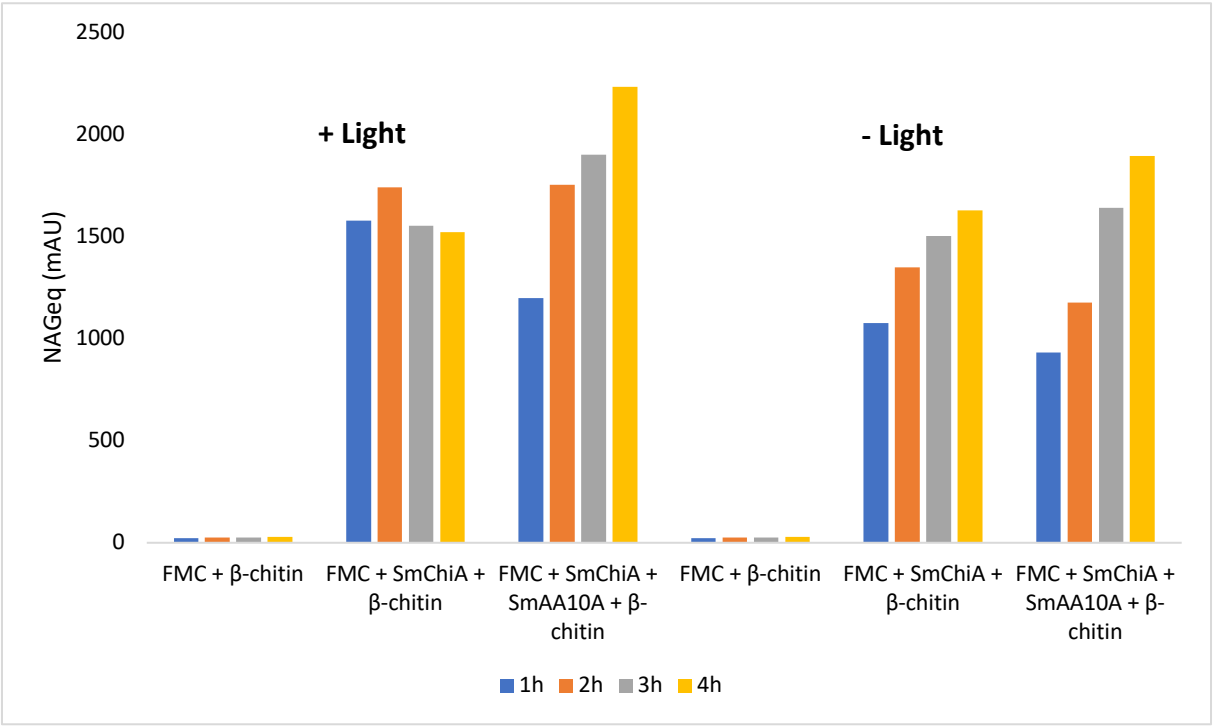


**Figure 28. The synergy between *Sm*ChiA and *Sm*AA10A to produce native products from FMC and β-chitin in the presence or absence of visible light.** The figure shows how chitin from FMC and β-chitin are degraded by *Sm*ChiA with and without the addition of *Sm*AA10A in the presence and absence of visible light. 1 µM enzyme (*Sm*ChiA/*Sm*AA10A) were added to the associated reactions and samples exposed to visible light were exposed by I= 10 % of $I_{max}$, approximately 16.8 W·cm$^{-2}$. All reactions were performed with 5 g/L FMC and 5 g/L β-chitin in 50 mM sodium phosphate pH 6.0. All reactions were incubated at 40 °C with magnet stirring. Samples were taken after 1, 2, 3, and 4 h and filtrated before addition of 25 µL 50mM $H_2SO_4$ to ensure the reaction to stop. The graphs show the sum of the total amounts of NAG and $NAG_2$.

# 5. Discussion

The main purpose of the work described in this thesis was to investigate if pupal exuviae from *Hermetia illucens* (FMC) can provide LPMOs with reducing equivalents and be used as a photosensitizer for *in situ* generation of $H_2O_2$ when irradiated by visible light due to its content of insoluble catechols. During the last decade, after $H_2O_2$ was discovered to be the preferred co-substrate to LPMOs, scientists have intensively studied various combinations of light and photosensitizers to drive LPMO reactions. The most used reductant is AscA, which is able to provide the LPMOs with reducing equivalent and may also generate $H_2O_2$ (Stepnov et al., 2021). Other studies have shown LPMO activity by addition of chlorophyllin (Bissaro et al., 2020b; Cannella et al., 2016) and V-$TiO_2$ (Bissaro et al., 2016b) as photocatalysts, and recent studies have demonstrated lignin's ability to reduce $O_2$ to $H_2O_2$ in the presence of light (Miglbauer et al., 2020; Kim et al., 2021). Lignin-derived compounds have been shown to be good reductants for LPMOs due to their high content of hydroxyl groups (Frommhagen et al., 2016; Muraleedharan et al., 2018). It is important to note that most studies of LPMO reductants have not explicitly taken into account that these reductants may have two functions. Originally, reductants were thought to act by supplying electrons to the LPMO, fueling a monooxygenase reaction. It is however very likely that the reductants promote LPMO-independent production of $H_2O_2$ to drive enzymatic activity. This "mixed effect" of reductants complicates the interpretation of experimental results.

As insoluble catechols are chemical structures comparable to lignin (Kracher et al., 2016), it was hypothesized that FMC, which contains ca. 10 % insoluble catechols, can reduce and catalyze activity of LPMOs. The first experiments performed in this thesis aimed at investigating if FMC could provide a model enzyme, *Sc*AA10C, with the necessary reducing equivalents to oxidize cellulose. Single reactions were performed with different pH and FMC concentrations in the presence and absence of visible light. The combination of pH and FMC concentration that resulted in the highest increase by light-exposure compared to the equivalent reactions in dark (i.e., the reaction conditions where light had the most limiting effect), was chosen as standards for use in further reactions. After having determined the pH to use for characterizing FMC as a photosensitizer in LPMO reactions, the effect of the following reaction parameters was investigated: FMC concentration, light intensity, LPMO concentration, Avicel concentration and the addition of SOD. As chitin represents a renewable source of polysaccharides, experiments were also conducted to assess the depolymerization of the chitin content in the pupal exuviae using either *Sm*ChiA or *Sm*AA10A or a combination of both.

## 5.1 FMC acts as a photosensitizer towards *Sc*AA10C

To investigate if FMC was able to drive LPMO reactions, reactions were performed with FMC, a cellulose active LPMO, *Sc*AA10C, and Avicel in the presence or absence of visible light. The overall findings presented in **Figure 17** clearly show production of oxidized products, confirming FMC´s ability to promote *Sc*AA10C activity on Avicel. **Figure 17** show a clear observation of that the production of oxidized products is higher when visible light is present compared to reactions performed in dark. This observation occurs at all pH and FMC concentrations tested.

The theoretical explanation of how FMC contributes to LPMO activity, is that photons hit insoluble catechols where an electron excites from its highest occupied orbital to its lowest unoccupied orbital (Schmermund et al., 2019). The excitation may result in an electron transfer between the catechols in FMC and the active site of LPMOs. When the active-site Cu(II) is reduced to Cu(I), a co-substrate, either $O_2$ or $H_2O_2$, is needed to activate cleaving of glycosidic bonds. The use of $H_2O_2$ as a co-substrate have shown a 2000-fold more efficient LPMO activity compared to reactions with $O_2$ (Bissaro et al., 2020a), thus, $H_2O_2$ is considered the preferred co-substrate towards LPMO activity. Recent studies have demonstrated lignin-based reduction of $O_2$ to $H_2O_2$ ($O_2 + 2H^+ + 2e^- \rightarrow H_2O_2$) (Miglbauer et al., 2020; Kim et al., 2021) and it was hypothesized that FMC could do the same (meaning that FMC would reduce the LPMO and produce its preferred co-substrate). Indeed light-driven generation of $H_2O_2$ in a reaction with FMC was observed in this study (**Figure 23**).

When the LPMO reaction occurs in a more acidic environment, the hydroxyl groups of the catechols get deprotonated and followingly become better reductants to reduce $O_2$ to $H_2O_2$. When more $H_2O_2$ is available in a reaction solution with reduced LPMOs, it will boost the degradation of polysaccharides, or even lead to inactivation due to oxidative damage to the active-site histidines (Bissaro et al., 2017). This might explain the observation from **Figure 17**, showing that the reactions performed in dark have a higher production of oxidized products at pH 8.0 and 7.0 compared to the reactions in pH 6.0. In the corresponding reactions performed in visible light, progress curves of reactions in pH 6.0 show more similarity to reactions in pH 7.0 and 8.0. Thus, the light is a more limiting parameter in reactions with pH 6.0. **Figure 17** show a higher generation of oxidized products in reactions with 1 g/L FMC (**Figure 17D**) compared to 0.1 g/L FMC (**Figure 17B**). However, the total generation of oxidized products in the light-exposed reaction with 10 g/L FMC (**Figure 17F**) did not reach the same levels as the reaction with 1 g/L FMC (**Figure 17D**). Nor is the progress curve linear, as it stagnates somewhere between 3 and 6 h (**Figure 17D**). This is most likely due to an overproduction and accumulation of $H_2O_2$ which has led to oxidative damage and inactivation of the LPMOs. This

may be verified by adding more LPMO to the reactions and observe if that would lead to additional production of oxidized products.

In the reactions with 10 g/L FMC, showing enzyme inactivation, the progress curve after 6 h still shows a slight increase between 6 h and 24 h which is an unexpected observation considering the LPMO inactivation (**Figure 17F**). This apparent increase is most likely caused by evaporation from the sample (increasing the apparent product concentration) and not by degradation of Avicel by *Sc*AA10C.

FMCs effect on LPMO activity was further investigated as reactions were performed with various concentrations of FMC. The results clearly show a correlation between the progress curve of oxidized products and the FMC concentration, where increased concentrations of FMC increase the total generation of oxidized products (**Figure 18**). This is the same observation as shown in **Figure 17B and D**. Higher concentrations of FMC will most likely lead to more formation of $H_2O_2$ and may also lead to more efficient reduction of the LPMO. The latter factor was likely not limiting, since reactions with varying LPMO concentrations showed that product formation was independent of the enzyme concentration. Thus, it seems safe to assume that the dose-response effects observed for FMC relate to $H_2O_2$ production. As the formation of $H_2O_2$ most likely is limiting the LPMO activity, more production of oxidized products is expected when increasing the FMC concentration, which was the case presented in **Figure 17B and D** and **Figure 18**. When the level of accumulated $H_2O_2$ gets too high, LPMOs become inactivated, which was observed in the reaction illustrated by **Figure 17F**. The light-exposed reactions with varying concentrations of FMC (**Figures 17 (B, D, and F) and 18**), indicate that the combination of FMC concentrations up to at least 5 g/L and light intensity corresponding to 10 % of $I_{max}$ leads to a level of $H_2O_2$ formation which the LPMOs are able to use without getting inactivated. When increasing the FMC concertation to somewhere between 5 g/L and 10 g/L, the high level of $H_2O_2$ will lead to oxidative damage and inactivation of the LPMO.

To study the effect of light exposure, reactions were performed with different light intensities from 1 % to 30 % of $I_{max}$. When increasing the light intensity, more photons will interact with the insoluble catechols in solution and lead to more reduction of the active-site copper and of $O_2$ to form $H_2O_2$. More efficient reduction of $O_2$ to $H_2O_2$ will lead to more efficient LPMO activity, which was the case in **Figure 21A,** showing a clear correlation between increased light intensities and increased progress curves of oxidized products. The generation of oxidized products in light exposed reactions (**Figure 21A**) is clearly higher compared to reactions performed in dark (**Figure 17A, C, and E**), indicating light exposure as a limiting parameter towards *Sc*AA10C activity. There were no signs of inactivation due

to overproduction of $H_2O_2$, not even in reactions exposed to 30 % of $I_{max}$ (**Figure 21A, yellow line**). Given the standard parameters set for light-driven Sc*AA10C reactions toward Avicel catalyzed by FMC, it would be interesting to further investigate if there is any upper limit in light intensity before occurrence of LPMO inactivation.

As noted above, the experiment with different concentrations of *Sc*AA10C showed that LPMO activity was independent of the LPMO concentration (**Figure 19**), which can be taken to show that $H_2O_2$ production is limiting the enzymatic activity. A study performed by Kittl et al. in 2012 demonstrated that $H_2O_2$ indeed may be generated by LPMOs. However, the unaffected progress curves shown in **Figure 19** may be explained by that the same amount of generated $H_2O_2$ are used as a co-substrate to activate LPMOs, which prevent accumulation and further increased production of oxidized products. The lack of effect indicates that the LPMO concentration are not a limiting parameter to LPMO efficiency towards degradation of Avicel.

The effect of substrate on LPMO activity was investigated by adding different concentrations of Avicel to light exposed reactions with *Sc*AA10C. Here, the progress curve and total generation of oxidized products decreased by increasing the Avicel concentration (**Figure 20**). The Avicel particles make the reaction solution less transparent, which most likely will decrease the access of interactions between the insoluble catechols in FMC and the light. A further discussion of how Avicel particles may affect the LPMO activity is provided in section 5.2.

The overall findings from the experiments described above, are that $H_2O_2$ generation by light exposed FMC is limiting the *Sc*AA10C activity towards Avicel. Increased FMC concentration and light intensity led to increased progress curves of oxidized products. Thus, the limiting parameters detected in this study are the concentration of FMC and the light intensity. In contrast, the enzyme concentration did not affect the progress curve, or the total generation of oxidized products. Avicel seems to limit the interaction between photons and the photosensitizing molecules, which hampers the formation of $H_2O_2$ to boost LPMO activity.

## 5.2 $H_2O_2$ generation from light-exposed FMC fuels LPMO activity

Amplex red assays were performed to assess the accumulation of $H_2O_2$ in the photobiocatalytic reaction system. The purpose of the first reactions performed, shown in **Figure 23**, was to compare the accumulation of $H_2O_2$ in reactions with FMC in the presence and absence of Avicel. Furtherly, the effects of *Sc*AA10C and free copper were assessed in separate reactions. Free copper can catalyze Fenton chemistry and convert $H_2O_2$ into hydroxyl radicals (Bissaro et al., 2018), while reduced LPMOs use $H_2O_2$ as a co-substrate when depolymerizing sugars (Bissaro et el., 2017) and may also react with $H_2O_2$ in futile turnover reactions, possibly leading to enzyme inactivation. The overall results show that $H_2O_2$ accumulates over time in reactions with FMC and light and that the presence of Avicel decreases the level of $H_2O_2$ (**Figure 23**). There was a slight decrease in $H_2O_2$ levels in reactions with free copper compared to the reaction without free copper and *Sc*AA10C, indicating occurrence of Fenton chemistry (**Figure 23**). In reactions containing *Sc*AA10C and Avicel, $H_2O_2$ was not detected, which likely reflects that *Sc*AA10C use $H_2O_2$ as a co-substrate to promote degradation of cellulose. The reaction with *Sc*AA10C in the absence of substrate (Avicel) generated amounts of $H_2O_2$ that were lower compared to reactions without *Sc*AA10C (**Figure 23**).

When LPMOs were first discovered, it was thought that molecular oxygen was the relevant co-substrate for catalytic activity, hence the name monooxygenase (Vaaje-Kolstad et al., 2010). However, in 2017, LPMOs were shown to prefer $H_2O_2$ over $O_2$ in competition experiments and it became clear that LPMOs are more efficient when using $H_2O_2$ (Bissaro et el., 2017). A reduced LPMO can react with $H_2O_2$ in the absence of substrate, and this may lead to inactivation of the enzyme by reactive oxygen species (Hegnar et al., 2019), which is the likely explanation for why there is less $H_2O_2$ in the reaction with *Sc*AA10C and FMC in absence of substrate, compared to the reaction with only FMC (**Figure 23**).

To elucidate the effect of Avicel on $H_2O_2$ accumulation, further experiments were performed with different concentrations of Avicel. The observations illustrated in **Figure 24**, show that the level of $H_2O_2$ decreases at higher concentrations of Avicel. This explains the observations shown in **Figure 20**, where increased Avicel concentrations led to decreased generation of oxidized products. A recent study has shown that light is attenuated by Avicel particles (Blossom et al., 2020), where increased concentrations of Avicel in solution led to decreased amounts of light being transmitted. This explains the decreased enzymatic activity shown in **Figure 20**, as the Avicel particles scatters the light, which leads to less photons, or photons with lower energy levels, to interact with FMC and generate $H_2O_2$.

## 5.3 No apparent production of superoxide from light-exposed FMC

To assess the role of superoxide in the photobiocatalytic reaction system, reactions with superoxide dismutase (SOD) were performed. If $O_2^{\bullet-}$ is produced when FMC is exposed to visible light, SOD will convert $O_2^{\bullet-}$ to $H_2O_2$ and boost the LPMO activity. There was no significant difference in the generation of oxidized products observed in reactions with SOD compared to the reactions where SOD was absent (**Figure 21**). This observation is supported by the observations depicted in **Figure 25**, which show no significant change in accumulated $H_2O_2$ (regardless of the SOD concentration) compared to the reaction without SOD. Thus, there is no $O_2^{\bullet-}$ for SOD to convert to provide *Sc*AA10C with more $H_2O_2$ to boost LPMO activity.

A recent study performed by Kim et al. described lignin as a photocatalyst to form $H_2O_2$ by reduction of $O_2$ through two single-electron reductions: ($O_2 + 2H^+ + 2e^- \rightarrow O_2^{\bullet-} + 2H^+ + e^- \rightarrow H_2O_2$) (Kim et al., 2021). The same study further described how this reduction could proceed in one step (i.e., $O_2 + 2H^+ + 2e^- \rightarrow H_2O_2$). Based on experiments with a $O_2^{\bullet-}$ scavenger, Kim et al. concluded that the one-step reduction of $O_2$ into $H_2O_2$ rarely occurred in reactions photocatalyzed by lignin. As lignin has structural similarities to catechols (Kracher et al., 2016), the lack of effect when adding SOD is unexpected. However, the one-step reduction route of $O_2$ into $H_2O_2$ is most likely the reason why the reactions fueled by light-exposed FMC were unaffected by SOD. It must be noted that the LPMO reactions containing SOD were performed in single replicas and that more investigation is needed to completely exclude the role of superoxide in *Sc*AA10C reactions photocatalyzed by FMC.

## 5.4 Light-exposed FMC can drive *Sm*AA10A activity towards its own chitin content

To demonstrate FMCs ability to drive enzymatic activity of a chitin active LPMO (i.e., *Sm*AA10A), additional experiments were performed. The main purpose of these experiments was to investigate if *Sm*AA10A could contribute to direct degradation of the chitin content in FMC, and if synergy between *Sm*ChiA and *Sm*AA10A would increase production of native products compared to reactions with only *Sm*ChiA. Due to limited time, these experiments were only performed in single replicas.

The experiments were performed qualitatively, first through HILIC analysis, to demonstrate chitin degradation of both FMC and FMC with β-chitin in light-exposed *Sm*AA10A reactions with FMC as a photosensitizer. As expected, the results showed light-dependent generation of oxidized products in form of absorbance tops in the chromatogram corresponding to $NAG_2^{ox}$ – $NAG_6^{ox}$ in both samples where *Sm*AA10A was added (**Figure 26C and D**), while no absorbance of oxidized products were detected in samples without *Sm*AA10A (**Figure 26A and B**).The results indicate that FMC can be used

as a photosensitizer to degrade its own chitin (in addition to β-chitin), meaning that the chitin in FMC is available for LPMOs to bind.

Further experiments were performed to investigate the effect of *Sm*ChiA and the synergy between *Sm*AA10A and *Sm*ChiA when degrading chitin. These experiments were performed with and without β-chitin added to the reactions. **Figures 27 and 28** display the generation of native products in reactions without (**Figure 27**) and with (**Figure 28**) β-chitin. Both figures show that *Sm*ChiA is necessary to produce native products, as native products are not detected in any samples only containing FMC (**Figures 27 and 28**). Both figures display a higher generation of native products in samples with *Sm*ChiA and *Sm*AA10A in the presence of visible light compared to the reaction only containing *Sm*ChiA, which confirms that the synergy between the two enzymes requires (in this case light-driven) activation of LPMO. Comparison of **Figures 27 and 28** shows a 10-fold higher production of native products in samples containing β-chitin and FMC (**Figure 28**) compared to samples with only FMC (**Figure 27**). This observation makes sense, as there is more available chitin for the enzymes to degrade when β-chitin is added. As there is available chitin in FMC for LPMOs to bind, it would be interesting to see if any kind of pretreatment of the pupal exuviae would lead to more chitin degradation when using *Sm*AA10A and *Sm*ChiA.

# 6. Conclusion and further perspectives

The aim of this study was to investigate if fine-milled cocoon powder from *Hermetia illucens* could provide LPMOs with reducing equivalents to drive enzymatic degradation of recalcitrant polysaccharides. Light-driven *Sc*AA10C reactions were performed with different concentrations of FMC, *Sc*AA10C, and Avicel and exposed to various light intensities to characterize the effects of these parameters on LPMO activity towards Avicel. To assess the role of superoxide ($O_2^{\bullet-}$) in the photobiocatalytic reaction system, superoxide dismutase was added and the activity of ScAA10C towards Avicel was measured. Amplex red assays was used to investigate the accumulation of $H_2O_2$ in the presence of *Sc*AA10C and free copper in separate reactions. In addition, the accumulation of $H_2O_2$ were measured in reactions with different concentrations of Avicel and SOD in the absence of *Sc*AA10C. Furthermore, this thesis aimed to investigate if *Sm*ChiA could produce native products from chitin in FMC with and without β-chitin and if FMC could drive *Sm*AA10A activity on its own chitin content. Finally, reactions with both *Sm*ChiA and *Sm*AA10A were performed to investigate possible synergistic effects when degrading chitin.

In conclusion, FMC can fuel *Sc*AA10C and *Sm*AA10A reactions towards cellulose and chitin, respectively, and this effect is drastically enhanced by light, especially at low pH. In light-driven *Sc*AA10C reactions on Avicel with FMC as a photosensitizer, the FMC concentration and the light intensity are the parameters that limits the generation of oxidized products, most likely explained by their effect on the production of $H_2O_2$. Increased concentrations of Avicel had a negative effect on reaction efficiency, likely because the Avicel prevents interactions between the insoluble catechols in FMC and photons. The experiments with SOD indicated that $O_2^{\bullet-}$ plays no role in this photobiocatalytic reaction system, suggesting that reduction of $O_2$ to $H_2O_2$ happens in one step. However, further research is necessary to rule out the reduction of $O_2$ to $H_2O_2$ in two steps.

*Sc*AA10C reactions combining 10 g/L FMC and light intensity corresponding to 10 % of $I_{max}$ led to oxidative damage and inactivation of the enzymatic activity, most likely caused by overproduction of $H_2O_2$. To investigate if $H_2O_2$ accumulation inactivates the LPMO activity, further experiments should focus on corresponding reactions with addition of more *Sc*AA10C after the inactivation to observe any increase in generation of oxidized products. Overall, the results indicate that the generation of oxidized products in *Sc*AA10C reactions towards Avicel with light-exposed FMC as a photosensitizer is related to the generation of $H_2O_2$.

The experimental degradation of chitin in FMC with and without β-chitin in *Sm*AA10A reactions, showed generation of oxidized product in samples when *Sm*AA10A and visible light were present. Native products were produced by SmChiA in reactions with FMC with and without the addition of β-chitin. There was also a clear synergetic effect between *Sm*ChiA and *Sm*AA10A in the sample exposed to light, as more native products were detected compared to the reactions with only *Sm*ChiA. This observation occurred both in the sample with only FMC and in the sample with FMC and β-chitin. In conclusion, the results indicate that light-exposed FMC can drive *Sm*AA10A activity on its own content of chitin. Reactions with both *Sm*ChiA and *Sm*AA10A indicateed a synergistically increase in the generation of native products from FMC and β-chitin when light was present. Further work should qualitatively confirm the *Sm*AA10A efficiency towards chitin in FMC and investigate if any pretreatment of the pupal exuviae from *Hermetia illucens* can increase the production of native products. The fact that a chitin rich waste material (i.e., FMC) can catalyze degradation of itself is promising to the focus of a "greener" use of resources and inspiring towards further research on other chitin rich waste materials.

In a broader perspective, the current findings add to the notion that the presence of large amounts of redox active compounds in biomass (lignin, catechols) may make the degradation of such biomass light-dependent in Nature. The interplay between light-exposed lignin and LPMOs isolated from the soil bacteria *Streptomyces coelicolor* might explain how plant biomass in Nature are degraded more efficiently upon solar radiation (Austin et al., 2006; 2015)

# References


Agger, J. W., T. Isaksen, A. Várnai, S. Vidal-Melgosa, W. G. T. Willats, R. Ludwig, S. J. Horn, V. G. H. Eijsink, & B. Westereng. 2014. Discovery of LPMO activity on hemicelluloses shows the importance of oxidative processes in plant cell wall degradation. *PNAS, 111 (17).* 6287-6292. https://doi.org/10.1073/pnas.1323629111

Akil, H. M., M. F. Omar, A. A. M. Mazuki, S. Safiee, Z. A. M. Ishak, & A. A. Bakar. 2011. Kenaf fiber reinforced composites: A review. *Materials and Design, 32(8–9).* 4107-21.

Andersen, S. O. 2010. Insect cuticular sclerotization: A review. *Insect Biochemistry and Molecular Biology, 40.* 166-178. https://doi.org/10.1016/j.ibmb.2009.10.007

Arantes, V., & J. N. Saddler. 2010. Access to cellulose limits the efficiency of enzymatic hydrolysis: the role of amorphogenesis. *Biotechnology for Biofuels, 3 (4).* https://doi.org/10.1186/1754-6834-3-4

Austin, A. T., & L. Vivanco. 2006. Plant litter decomposition in a semi-arid ecosystem controlled by photodegradation. *Nature, 442*. 555-558. https://doi.org/10.1038/nature05038

Austin, A. T., M. S. Méndez, & C. L. Ballaré. 2015. Photodegradation alleviates the lignin bottleneck for carbon turnover in terrestrial ecosystems. PNAS, 113 (16). 4392-4397. https://doi.org/10.1073/pnas.1516157113

Beier, S., & S. Bertilsson. 2013. Bacterial chitin degradation – mechanisms and ecophysiological strategies. *Frontiers in Microbiology, 4*. https://doi.org/10.3389/fmicb.2013.00149

Bissaro, B., Å. K. Røhr, M. Skaugen, Z. Forsberg, S. J. Horn, G. Vaaje-Kolstad, & V. G. H. Eijsink. 2016a. Fenton-type chemistry by a copper enzyme; molecular mechanism of polysaccharide oxidative cleavage. *BioRxiv, 097022*. https://doi.org/10.1101/097022

Bissaro, B., Z. Forsberg, Y. Ni, F. Hollmann, G. Vaaje-Kolstad, & V. G. H. Eijsink. 2016b. Fueling biomass-degrading oxidative enzymes by light-driven water oxidation. Green Chemistry, 18 (19). 5357-5366. https://doi.org/10.1039/C6GC01666A

Bissaro, B., Å. K. Røhr, G. Müller, P. Chylenski, M. Skaugen, Z. Forsberg, S. J. Horn, G. Vaaje-Kolstad, & V. G. H. Eijsink. 2017. Oxidative cleavage of polysaccharides by monocopper enzymes depends on $H_2O_2$. *Nature Chemical Biology, 13*. 1123-1128. https://doi.org/10.1038/nchembio.2470

Bissaro, B., A. Várnai, Å. K. Røhr, V. G. H. Eijsink. 2018. Oxidoreductases and Reactive Oxygen Species in Conversion of Lignocellulosic Biomass. *Microbiology and Molecular Biology Reviews, 82 (4).* https://doi.org/10.1128/MMBR.00029-18

Bissaro, B., B. Streit, I. Isaksen, V. G. H. Eijsink, G. T. Beckham, J. L. DuBois, & Å. K. Røhr. 2020a. Molecular mechanism of the chitonolytic peroxygenase reaction. PNAS, 117 (3). 1504-1513. https://doi.org/10.1073/pnas.1904889117

Bissaro, B., E. Kommedal, Å. K. Røhr, & V. G. H. Eijsink. 2020b. Controlled depolymerization of cellulose by light-driven lytic polysaccharide oxygenase. *Nature Communications, 11 (890).* https://doi.org/10.1038/s41467-020-14744-9

Blossom, B. M., D. A. Russo, R. K. Singh, B. Van Oort, M. B. Keller, T. I. Simonsen, A. Perzon, L. F. Gamon, M. J. Davies, D. Cannella, R. Croce, P. E. Jensen, M. J. Bjerrum, & C. Felby. 2020. Photobiocatalysis by a Lytic

Polysaccharide Monooxygenase Using Intermittent Illumination. *ACS Sustainable Chemistry & Engineering, 8(25)*. 9301-9310. https://doi.org/10.1021/acsseschemeng.0c00702

Brurberg, M. B., V. G. H. Eijsink, & I. F. Nes. 1994. Characterization of a chitinase gene (chiA) from Serratia marcescens BJL200 and one-step purification of the geneproduct. *FEMS Microbiology Letters, 124 (3)*. 399-404. https://doi.org/10.1111/j.1574-6968.1994.tb07315.x

Cannella, D., K. Möller, N. U. Frigaard, P. E. Jensen, M. J. Bjerrum, K. S Johansen & C. Felby. 2016. Light-driven oxidation of polysaccharides by photosynthetic pigments and a metalloenzyme. *Nature communications, 7 (11134).* https://doi.org/10.1038/ncomms11134

Cantarel, B. L., P. M. Coutinho, C. Rancurel, T. Bernard, V. Lombard, & B. Henrissat. 2009. The Carbohydrate-Active EnZymes database (CAZy): an expert resource for Glycogenomics. *Nucleic Acids Research, 37 (1).* D233-D238. https://doi.org/10.1093/nar/gkn663

Costa, T. F. H., A. Kadic, P. Chylenski, A. Várnai, O. Bengtsson, G. Lidén, V. G. H. Eijsink, & S. J. Horn. 2020. Demontration-scale enzymatic saccharification of sulfite-pulped spruce with addition of hydrogen peroxide for LPMO activation. *Biofuels Bioproducts & Biorefining, 14*. 734-745. https://doi.org/10.1002/bbb.2103

Courtade, G., Z. Forsberg, E. B. Heggset, V. G. H. Eijsink, & F. L. Aachmann. 2018. The carbohydrate-binding module and linker of a modular lytic polysaccharide monooxygenase promote localized cellulose oxidation. *Journal of Biological Chemistry, 293 (34).* 13006-13015. https://doi.org/10.1074/jbc.RA118.004269

Danneels, B., M. Tanghe, H.-J. Joosten, T. Gundinger, O. Spadiut, I. Stals, & T. Desmet. 2017. A quantitative indicator diagram for lytic polysaccharide monooxygenases reveals the role of aromatic surface residues in *Hj*LPMO9A regioselectivity. *PLoS ONE, 12 (5*). https://doi.org/10.1371/journal.pone.0178446

Dimarogona, M., E. Topakas, & P. Christakopoulos. 2012. Cellulose degradation by oxidative enzymes. *Computational and Structural Biotechnology Journal, 2 (3*). http://dx.doi.org/10.5936/csbj.201209015

Elumalai S., B. Agarwal, T.M. Runge, & R.S. Sangwan. 2018 Advances in Transformation of Lignocellulosic Biomass to Carbohydrate-Derived Fuel Precursors. *Biorefining of Biomass to Biofuels*. 87-116. https://doi.org/10.1007/978-3-319-67678-4_4

Ezeilo, U. R., I. I. Zakaria, F. Huyop, & R. A. Wahab. 2017. Enzymatic breakdown of lignocellulosic biomass: the role of glycosyl hydrolases and lytic polysaccharide monooxygenases. *Biotechnology & Biotechnological Equipment, 31 (4).* 647-662. https://doi.org/10.1080/13102818.2017.1330124

Forsberg, Z., G. Vaaje-Kolstad, B. Westereng, A. C. Bunæs, Y. Stenstrøm, A. Mackenzie., & V. G. H. Eijsink. 2011. Cleavage of cellulose by a CBM33 protein. Protein science: a publication of the Protein Society, 20(9), 1479–1483. https://doi.org/10.1002/pro.689

Forsberg, Z., A. K. Mackenzie, M. Sørlie, Å. K. Røhr, R. Helland, A. S. Arvai, G. Vaaje-Kolstad, & V. G. H. Eijsink. 2014. Structural and functional characterization of a conserved pair of bacterial cellulose-oxidizing lytic polysaccharide monooxygenases. *PNAS, 111 (23).* 8556-8451. https://doi.org/10.1073/pnas.1402771111

Forsberg, Z., C. E. Nelson, B. Dalhus, S. Mekasha, J. S. M. Loose, L. I. Crouch, Å. K. Røhr, J. G. Gardner, V. G. H. Eijsink, & G. Vaaje-Kolstad. 2016. Structural and Functional Analysis of a Lytic Polysaccharide Monooxygenase Important to Efficient Utilization of Chitin in Cellvibrio japonicus. *Journal of Biological Chemistry, 291 (14).* 7300-7312. https://doi.org/10.1074/jbc.M115.700161

Frommhagen, M., M. J. Koetsier, A. H. Westphal, J. Visser, S. W. A. Hinz, J.-P. Vincken, W. J. H. van Berkel, M. A. Kabel, & H. Gruppen. 2016. Lytic polysaccharide monooxygenases from Myceliophthora thermophila C1 differ in substrate preference and reducing agent specificity. *Biotechnology for Biofuels, 9 (186).* https://doi.org/10.1186/s13068-016-0594-y

Frommhagen, M., S. K. Mutte, A. H. Westphal, M. J. Koetsier, S. W. A. Hinz, J. Visser, J.-P. Vincken, D. Weijers, W. J. H. van Berkel, H. Gruppen, & M. A. Kabel. 2017. Boosting LPMO-driven lignocellulose degradation by polyphenol oxidase-activated lignin building blocks. *Biotechnology for Biofuels, 10 (121)*. https://doi.org/10.1186/s13068-017-0810-4

Fuchs, R. L., S. A. McPherson, D. J. Drahos. 1986. Cloning of a Serratia marcescens Gene Encoding Chitinase. *Applied and Environmental Microbiology, 51 (3*). 504-509.

Goldberg, R. N., J. Schlesser, A. Mittal, S. R. Decker, A. F. L. O. M. Santos, V. L. S. Freitas, A. Urbas, B. E. Lang, C. Heiss, M. D. M. C. Ribiero da Silva, B. F. Woodfield, R. Katahira, W. Wang, & D. K. Johnson. 2015. A thermodynamic investigation of the cellulose allomorphs: Cellulose (am), cellulose Iβ (cr), cellulose II (cr), and cellulose III (cr). *J. Chem. Thermodynamics, 81.* 184-226. https://doi.org/10.1016/j.jct.2014.09.006

Hahn, T. & Zibek, S. 2018. Sewage Polluted Water Treatment via Chitosan: A Review. Chitin - Chitosan Myriad Functionalities in Science and Technology. Edited by Rajendra Dongre. 119-142. http://dx.doi.org/10.5772/intechopen.75395

Hahn, T., Roth, A. Ji, R. Schmitt, E. & Zibek, S. 2020. Chitosan production with larval exoskeletons derived from the insect protein production. *Journal of Biotechnology, 310.* 62-67. https://doi.org/10.1016/j.jbiotec.2019.12.015

Hajji, S., I. Younes, O. Ghorbel-Bellaaj, R. Hajji, M. Rinaudo, M. Nasri, & K. Jellouli. 2014. Structural differences between chitin and chitosan extracted from three different marine sources. *International Journal of Biological Macromolecules, 65.* 298-306.

Hasanov I., M. Raud, & T. Kikas. 2020. The Role of Ionic Liquids in the Lignin Separation from Lignocellulosic Biomass. *Energies, 13 (18).* https://doi.org/10.3390/en13184864

Hegnar, O. A., D. M. Petrovic, B. Bissaro, G. Alfredsen, A. Várnai, V. G. H. Eijsink. 2019. pH-Dependent Relationship between Catalytic Activity and Hydrogen Peroxide Production Shown via Characetrization of a Lytic Polysaccharide Monooxygenase from *Gleophyllum trabeum. Applied and Envirmental Microbiology, 85 (5).* https://doi.org/10.1128/AEM.02612-18

Himmel, M.E., S-Y. Ding, D. K. Johnson, W. S. Adney, M. R. Nimlos, J. W Brady, & T. D. Foust. 2007. Biomass Recalcitrance: Engeneering Plants and Enzymes for Biofuels Production. *Science, 314 (5813).* 804-807. https://doi.org/10.1126/science.1137016

Horn, S. J., G. Vaaje-Kolstad, B. Westereng, & V. G. H. Eijsink. 2012. Novel enzymes for the degradation of cellulose. *Biotechnology for Biofuels, 5 (45).* https://doi.org/10.1186/1754-6834-5-45

Hülsey, M. J. 2018. Shell biorefinery: A comprehensive introduction*. Green Energy & Environment, 3.* 318-327. https://doi.org/10.1016/j.gee.2018.07.007

Isaksen, T., B. Westereng, F. L. Aachmann, J. W. Agger, D. Kracher, R. Kittl, R. Ludwig, D. Haltrich, V. G. H. Eijsink, & S. J. Horn. 2014. A C4-oxidizing Lytic Polysaccharide Monooxygenase Gleaving Both Cellulose and Cello-

oligosaccharides. *The Journal of Biological Chemistry, 289 (5).* 2632-2642. https://doi.org/10.1074/jbc.M113.530196

Jang, M-K., B-G. Kong, Y-I. Jeong, C. H. Lee, & J-W. Nah. 2004. Physiochemical Characterization of α-Chitin, β-Chitin, and γ-Chitin Separated from Natural Resources. *Wilet Interscience, 42*. 3423-3432. https://doi.org/10.1002/pola.20176

Jones, S. M., W. J. Transue, K. K. Meier, B. Kelemen, & E. I. Solomon. 2020. Kinetic analysis of amino acid radicals formed in $H_2O_2$-driven Cu´ LPMO reoxidation implicates dominant homolytic reactivity. *PNAS, 117(22).* 11916-11922. https://doi.org/10.1073/pnas.1922499117

Kim, J., F. Hollmann, & C. B. Park. 2021. Lignin as a multifunctional photocatalyst for solar-powered biocatalytic oxyfunctionalization of C-H bonds. *ChemRxiv.* https://doi.org/10.26434/chemrxiv.13650383.v1

Kittl, R., D. Kracher, D. Burgstaller, D. Haltrich, & R. Ludwig. 2012. Production of four *Neurospora crassa* lytic polysaccharide monooxygenases in *Pichia pastoris* monitored by a fluorimetric assay. *Biotechnology for biofuels, 5(79).* https://doi.org/10.1186/1754-6834-5-79

Kramer, K. J., T. L. Hopkins, & J. Schaefer. 1995. Applications of Solids NMR to the Analysis of Insect Sclerotized Structures. *Insect Biochemistry and Molecular Biology, 25 (10).* 1067-1080.

Kracher, D., S. Scheiblbradner, A. K. G. Felice, E. Breslmayr, M. Preims, K. Ludwicka, D. Haltrich, V. G. H. Eijsink, & R. Ludwig. 2016. Extracellular electron transfer systems fuel cellulose oxidative degradation. *Science, 352 (6289).* 1098-1101. https://doi.org/10.1126/science.aaf3165

Kramer, K. J., M. R. Kanost, T. L. Hopkins, H. Jiang, Y. C. Zhu, R. Xu, J. L. Kerwin, & F. Turecek. 2000. Oxidative conjugation of catechols with proteins in insect skeletal systems. *Tetrahedron, 57*. 385-392.

Langner, T., & V. Göhre. 2016. Fungal chitinases: function, regulation, and potential roles in plant/pathogen interactions. *Current Genetics, 62*. 243-254. https://doi.org/10.1007/s00294-015-0530-x

Lee, H. V. S. B. A. Hamid, & S. K. Zain. 2014. Conversion of Licnocellulosic Biomass to Nanocellulose: Structure and Chemical Process. *The Scientific World Journal, 631013*. https://doi.org/10.1155/2014/631013

Lee, S. H., S. D. Choi, S. K. Kuk, & C. B. Park. 2018. Photobiocatalysis: Activating redox enzymes by direct or indirect transfer of photoinduced electrons. *Angewandte Chemie International Edition, 57 (27).* 7958-7985. https://doi.org/10.1002/anie.201710070

Levasseur, A., E. Drula, V. Lombard, P. M. Coutinho, & B. Henrissat. 2013. Expansion of the enzymatic repertoire of the CAZy database to integrate auxiliary redox enzymes. *Biotechnology for Biofuels, 6(41).* https://doi.org/10.1186/1754-6834-6-41

Li, Q., Dunn E. T. Grandmaison E. W. & Goosen M. F. A. 1992. Applications and Properties of Chitosan. Journal of Bioactive and Compatible Polymers, 7 (4). 370-397. https://doi.org/10.1177/088391159200700406

Lindman, B., G. Karlström, & L. Stigsson. 2010. On the mechanism of dissolution of cellulose. *Journal of Molecular Liquids, 156 (2010), 76-81.* https://doi.org/10.1016/j.molliq.2010.04.016

Loose, J. S. M., M. Ø. Arntzen, B. Bissaro, R. Ludwig, V. G. H. Eijsink, & G. Vaaje-Kolstad. 2018. Multipoint Precision Binding of Substrate Protects Lytic Polysaccharide Monooxygenases from Self-Destruction Off-Pathway Processes. *Biochemistry, 57(28).* 4114-4124. https://doi.org/10.1021/acs.biochem.8b00484

Maciá-Agulló, J. A., A. Corma, & H. Garcia. 2015. Photobiocatalysis: the power of combining photocatalysis and enzymes. Chemistry-A European Journal, 21 (31). 10940-10959. https://doi.org/10.1002/chem.201406437

Mifsud, M., S. Gargiulo, S. Iborra, I. W. C. E. Arends, F. Hollmann, & A. Corma. 2014. Photobiocatalytic chemistry of oxidoreductases using water as the electron donor. *Nature Communications, 5 (1)*. 1-6. https://doi.org/10.1038/ncomms4145

Miglbauer, E., M. Gryszel, & E. D. Głowachi. 2020. Photochemical evolution of hydrogen peroxide on lignins. *Green Chemistry, 22.* 673-677. https://doi.org/10.1039/C9GC04324A

Muraleedharan, M. N., D. Zouraris, A. Karantonis, E. Topakas, M. Sandgren, U. Rova, P. Christakopoulos, & A. Karnaouri. 2018. Effect of lignin fractions isolated from different biomass sources on cellulose oxidation by fungal lytic polysaccharide monooxygenases. *Biotechnology for Biofuels, 11 (1*). 1-15. https://doi.org/10.1186/s13068-018-1294-6

Müller, G., P. Chylenski, B. Bissaro, V. G. H. Eijsink, & S. J. Horn. 2018. The impact of hydrogen peroxide supply on LPMO activity and overall saccharification efficiency of a commercial cellulase cocktail. *Biotechnology for Biofuels, 11 (209).* https://doi.org/10.1186/s13068-018-1199-4

Möller, K. B., H. Mikkelsen, T. I. Simonsen, D. Canella, K. S. Johansen, M. J. Bjerrum, & C. Felby. 2017. On the formation and role of reactive oxygen species in light-driven LPMO oxidation of phosphoric acid swollen cellulose. *Carbohydrate Research, 448 (7).* 182-186. https://doi.org/10.1016/j.carres.2017.03.013

O'Sullivan, A. C. 1997. Cellulose: the structure slowly unravels. *Cellulose, 4 (3).* 173-207. https://doi.org/10.1023/A:1018431705579

Phillips, C. M., W. T. Beeson, J. H. Cate, & M. A. Marletta. 2011. Cellobiose Dehydrogenase and a Copper-Dependent Polysaccharide Monooxygenase Potentiate Cellulose Degradation by *Neurospora crassa*. *ACS Chemical Biology. 6(12).* 1399-1406. https://doi.org/10.1021/cb200351y

Quinlan, R. J., M. D. Sweedney, L. L. Leggio, H. Otten, J.-C. N. Poulsen, K. S. Johansen, K. B. R. M. Krogh, C. I. Jørgensen, M. Tovborg, A. Anthonsen, T. Tryfona, C. P Walter, P. Dupree, F. Xu, G. J. Davies, & P. H. Walton. 2011. Insights into the oxidative degradation of cellulose by a copper metalloenzyme that exploits biomass components. *PNAS, 108 (37).* 15079-15084. https://doi.org/10.1073/pnas.1105776108

Reese, E. T., Siu, R. G. H., & Levinson, H. S. 1950. The Biological Degradation of Soluble Cellulose Derivatives and its Relationship to the Mechanism of Cellulose Hydrolysis. *Journal of Bacteriology, 59(4),* 485-497.

Rinaudo, M. 2006. Chitin and chitosan: Properties and applications. *Progress in Polymer Science, 31 (7).* 603-632. https://doi.org/10.1016/j.progpolymsci.2006.06.001

Roberts, G. A. F. 1992. Chitin Chemistry (1st ed.). The Macmillan Press Ltd. https://doi.org/10.1007/978-1-349-11545-7

Schmermund, L., V. Jurkaš, F. F. Özgen, G. D. Barone, H. C. Büchsenschütz, C. K. Winkler, S. Schmidt, R. Kourist, & W. Kroutil. 2019. Photo-Biocatalysis: Biotransformations in the Presence of Light. ACS Catalysis, 9. 4115-4144. https://doi.org/10.1021/acscatal.9b00656

Selig, J. M., T. V. Vuong, M. Gudmundsson, Z. Forsberg, B. Westereng, C. Felby, & E. R. Master. 2015. Modified cellobiohydrolase–cellulose interactions following treatment with lytic polysaccharide monooxygenase

CelS2 (*Sc*LPMO10C*)* observed by QCM-D. *Cellulose, 22*. 2263-2270. https://doi.org/10.1007/s10570-015-0635-x

Shoseyov, O., Z. Shani, & I. Levy. 2006. Carbohydrate Binding Module: Biochemical Properties and Novel Applications. *Microbiology and Molecular Biology Reviews, 70(2).* 283-295. https://doi.org/10.1128/MMBR.00028-05

Stepnov, A. A., Z. Forsberg, M. Sørlie, G.-S. Nguyen, A. Wentzel, Å. K. Røhr, & V. G. H. Eijsink. 2021. Unraveling the roles of the reductant and free copper ions in LPMO kinetics. *Biotechnology for Biofuels, 14 (28).* https://doi.org/10.1186/s13068-021-01879-0

Suzuki, K., M. Suzuki, M. Taiyoji, N. Nikaidou, & T. Watanabe. 1998. Chitin Binding Protein (CBP21) in the Culture Supernatant of *Serretia marcescens* 2170. *Bioscience, Biotechnology, and Biochemistry, 62 (1).* 128-135. https://doi.org/10.1271/bbb.62.128

Sygmund, C., P. Santner, I. Krondorfer, C. K. Peterbauer, M. Alcalde, G. S. Nyanhongo, G. M. Guebitz, & R. Ludwig. 2013. Semi-rational engineering of cellulbiose dehydrogenase of improved hydrogen peroxide production. Microbial Cell Factories 12(38). https://doi.org/10.1186/1475-2859-12-38

Vaaje-Kolstad, G., D. R. Houston, A. H. K. Riemen, V. G. H. Eijsink, & D. M. F. van Aalten. 2005a. Crystal Structure and Binding Properties of the *Serratia marcescens* Chitin-binding Protein CBP21. *The Journal of Biological Chemistry, 280 (12).* 11313-11319. https://doi.org/10.1074/jbc.M407175200

Vaaje-Kolstad, G., S. J. Horn, D. M. F. Van Aalten, B. Synstad, & V. G. H. Eijsink. 2005b. The Non-catalytic Chitin-binding Protein CBP21 from *Serratia marcescens* Is Essential for Chitin Degradation. *The Journal of Biological Chemistry, 280 (31).* 28492-28497. https://doi.org/10.1074/jbc.M504468200

Vaaje-Kolstad, G., B. Westereng, S. J. Horn, Z. Liu, H. Zhai, M. Sørlie, & V. G. H. Eijsink. 2010. An oxidative enzyme boosting the enzymatic conversion of recalcitrant polysaccharides. *Science*, *330 (6001):* 219-222. https://doi.org/10.1126/science.1192231

Vaaje-Kolstad, G., S. J. Horn, M. Sørlie, & V. G. H. Eijsink. 2013. The chitinolytic machinery of *Serratia marcescens* – a model system for enzymatic degradation of recalcitrant polysaccharides. *The FEBS Journal, 280 (13).* 3028-3049. https://doi.org/10.1111/febs.12181

Vaaje-Kolstad, G., Z. Forsberg, J. S. M. Loose, B. Bissaro, & V. G. H. Eijsink. 2017. Structural diversity of lytic polysaccharide monooxygenases. *Current Opinion In Structural Biology, 44*. 67-76. https://dx.doi.org/10.1016/j.sbi.2016.12.012

Verma, M. L., S. Devi, & M. Mathesh. 2020. Photobiocatalysis: At the interface of Photocatalysis and Biocatalysts. In:Rajendran S., M. Naushad, L. Ponce, & E. Lichtfouse (eds) Green Photocatalysts for Energy and Enviromental Process. *Enviromental Chemistry for a Sustainable World, 36*. 187-209. https://doi.org/10.1007/978-3-030-17638-9_7

Westereng, B. D. Canella, J. W. Agger, H. Jørgensen, M. L. Andersen, V. G. H. Eijsink, & C. Felby. 2015. Enzymatic cellulose oxidation is linked to lignin by long-range electron transfer. *Scientific Reports, 5(18561).* https://doi.org/10.1038/srep18561

Zhao, D., Y. Zhu, W. Cheng, W. Chen, Y. Wu, & H. Yu. 2020. Cellulose-Based Flexible Functional Materials for Emerging Intelligent Electronics. *Advanced materials: 2000619*. https://doi.org/10.1002/adma.202000619

Zhou, X., & H. Zhu. 2020. Current understanding of substrate specificity and regioselectivity of LPMOs. *Bioresources and Bioprocessing, 7 (11).* https://doi.org/10.1186/s40643-020-0300-6

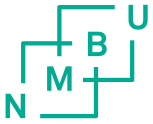


**Norges miljø- og biovitenskapelige universitet**
Noregs miljø- og biovitskapelege universitet
Norwegian University of Life Sciences

Postboks 5003
NO-1432 Ås
Norway